UNIVERSITY OF SOUTHAMPTON

Fabrication and Characterization of Nanostructured Palladium Hydride Microelectrode pH Sensors

by Toru Imokawa

A thesis submitted for the degree of

Doctor of Philosophy

August 2003

Department of Chemistry

Faculty of Science

UNIVERSITY OF SOUTHAMPTON

ABSTRACT

FACULTY OF SCIENCE

CHEMISTRY

Doctor of Philosophy

Fabrication and Characterization of Nanostructured Palladium Hydride Microelectrode pH Sensors

by Toru Imokawa

A reliable micro pH sensor with a wide effective pH range is of interest to many fields. In the present study, an attempt was made to fabricate such a reliable sensor with nanostructured Pd-hydride microelectrodes. Thorough investigation of the fabrication of nanostructured Pd films, their hydrogen absorption behaviour and the potentiometric response of the sensors are presented.

Nanostructured Pd films (H_I-e Pd films) were electrodeposited on Pt microdisc electrodes using a molecular template created by a hexagonal lyotropic crystalline phase. While retaining micrometer dimensions these electrodes possess huge electroactive surface areas; ie. roughness factors of H_I-e Pd films were estimated to be typically 300. Hydrogen absorption was shown to be very fast for H_I-e Pd films and the films were readily loaded with hydrogen to β phase. It was found to be possible to obtain the Pd-hydride with the desired H/Pd ratio by controlling the potential and the time of electrolysis.

The nanostructured Pd-hydride microelectrodes showed excellent potentiometric response over a wide rage of pH (2 ~ 12). The potentiometric pH response was rapid, stable, reproducible and almost theoretical in deaerated solutions. These properties, clearly superior to conventional micro pH sensors, were thought to be achieved by the combination of (1) the α+β Pd-hydride phase which was known to show almost theoretical potential with normal size electrodes and (2) a nanostructured film with a huge surface area and a rapid potential determining process ($H^+ + e \rightleftarrows H(Pd\text{-}H)$). H_I-e Pd-hydride microelectrodes had limited lifetime (typically 1 ~ 3 hours in deaerated solutions) because of the continuous removal of hydrogen under open circuit conditions. Although the lifetime is too short for continuous process monitoring, it is sufficient for many analytical applications. The electrode can be reloaded with hydrogen quickly, which makes it possible to perform pH measurements repeatedly.

ACKNOWLEDGEMENTS

First and foremost, I am deeply grateful to my supervisor Dr. Guy Denuault for his guidance and encouragement throughout this research. I would like to thank him for the helpful discussions we have had and valuable advice he has given me.

I would like to acknowledge the assistance of other people who have contributed their time and expertise. I would especially like to thank Prof. Derek Pletcher and Prof. Phil Bartlett for precious discussions and advice. Particular thanks also go to Dr. Stuart Evans, who has helped and encouraged me since the first day of my PhD.

I would also like to thank the Denuault group members that have made my time in Southampton such a great experience. My thanks go to Stuart, Henrique and Maciek for being so friendly and helpful to me. My thanks also go to the Bartlett group members especially Mamdouh, Mohamed, Ibrahim, Jan, Enass, Dave, Rob, Romaric, Alex, Joe and Tim. Special thanks go to Sergio for his remarkable contribution in the lab and in the kitchen. Thanks to the members of both groups, I enjoyed jokes from all over the world.

I would like to express my appreciation to JFE Steel Corporation, which gave me the valuable opportunity to study at the university of Southampton.

I would like to take this opportunity to thank my family in Japan especially my parents for their constant emotional support.

Finally, I would like to thank Hiromi for her understanding and encouragement.

Contents

Chapter 1. Introduction 1
1-1. Measurement of pH 1
1-1-1. pH-sensing electrodes 2
1-1-2. Measurement of local pH 5
1-2. Palladium / hydrogen system 13
1-2-1. Palladium-hydride phases 13
1-2-2. Potential of palladium hydride 16
1-2-3. Palladium hydride electrodes 22
1-2-4. Hydrogen reactions on palladium electrodes 23
1-3. Nanostructured films deposited from liquid crystalline phases 26
1-3-1. Principle of fabrication 26
1-3-2. Application 28
1-3-3. H_I-e Pd films 29
1-4. Summary 31
Chapter 2. Experimental 35
2-1. Generalities 35
2-1-1. Reagents 35
2-1-2. Purified water 35
2-1-3. Glassware 35
2-2. Electrochemical measurements 37
2-2-1. Electrochemical cells 37
2-2-2. Reference electrodes 37
2-2-3. Experimental set-up 38
2-3. Preparation of microelectrodes 41
2-3-1. Pt and Pd microdisc electrodes 41
2-3-2. Deposition of H_I-e Pd films 43
2-3-3. Deposition of plain Pd films 44
2-4. pH measurements with a combination pH electrode 45
2-5. Scanning electron microscopy 46
Chapter 3. Deposition and characterization of Pd films 48
3-1. Deposition of Pd films 48

3-1-1. Plating mixtures 48
3-1-2. H_1-e Pd (A) film deposition 49
3-1-3. H_1-e Pd (B) film deposition 54
3-1-4. 'Plain' Pd film deposition 56
3-2. Characterization of Pd films 59
3-2-1. Electroactive surface area 59
3-2-2. Geometric diameter 65
3-2-3. Roughness factor and thickness 68
3-3. Hydrogen reactions in 1 M H_2SO_4 solution 70
3-3-1. H_1-e Pd film on Pt microdisc 70
3-3-2. H_1-e Pd film on Pd microdisc 73
3-4. Summary 75
Chapter 4. Hydrogen absorption behaviour of H1-e Pd films 78
4-1. H absorption behaviour in 0.5 M Na_2SO_4 + H_2SO_4 (pH ≈ 2) solutions 78
4-1-1. Cyclic Voltammetry 78
4-1-2. Potentiostatic loading of H 87
4-2. Hydrogen absorption behaviour in solutions containing other supporting electrolytes (pH ≈ 2) 97
4-2-1. Fundamental electrochemical behaviour 97
4-2-2. Hydrogen absorption behaviour 102
4-3. Effect of pH on H absorption behaviour 104
4-4. Summary 106
Chapter 5. Potentiometric response of H1-e Pd-hydride microelectrodes 109
5-1. Potential – time curves after hydrogen loading 109
5-1-1. 0.5 M Na_2SO_4 + H_2SO_4 (pH ≈ 2) solution 109
5-1-2. Solutions containing other supporting electrolytes 117
5-2. Potential in solutions with different pH 120
5-2-1. Calibration curves 120
5-2-2. Response Time 129
5-3. Influence of dissolved oxygen 130
5-3-1. Current transient while loading hydrogen in an aerated solution . 130
5-3-2. Potential in an aerated solution 131
5-3-3. Oxygen reduction on H_1-e Pd (-hydride) electrodes 133
5-3-4. Influence of other oxidizing agents 136
5-4. Summary 137

Chapter 6. Advantage of the nanostructure 140
6-1. Properties of plain Pd films on Pt microdisc electrodes 140
6-1-1. H absorption behaviour 140
6-1-2. Potentiometric response 144
6-1-3. Surface blockage 150
6-2. Properties of polished Pd microdisc electrodes 153
6-2-1. H absorption behaviour 154
6-2-2. Potentiometric response 158
6-3. Advantage of the nanostructure 159
6-3-1. Advantage to hydrogen loading 160
6-3-2. Advantage to potentiometric response 160
6-4. Summary 167
Chapter 7. Conclusions and further work 170
7-1. Conclusions 170
7-2. Further work 173
Chapter 8. References 176

ABBREVIATIONS

$C_{16}EO_8$	octaethylene glycol monohexadecyl ether
f.c.c.	face centred cubic structure
FET	field effect transistor
GSED	gaseous secondary electron detector
H_1	hexagonal liquid crystalline phase
H_1-e Pd	nanostructured Pd formed by electrochemical deposition from H_1 liquid crystalline phase
H_1-e Pd (A)	H_1-e Pd deposited from plating mixture containing $C_{16}EO_8$
H_1-e Pd (B)	H_1-e Pd deposited from plating mixture containing Brij®56
H_2Q	hydroquinone (HOC_6H_4OH)
ISFET	ion-selective field effect transistor
Q	benzoquinone (OC_6H_4O)
SCE	Hg / Hg_2Cl_2, KCl (saturated) reference electrode
SECM	scanning electrochemical microscopy
SEM	scanning electron microscopy
SMSE	Hg / Hg_2SO_4, K_2SO_4 (saturated) reference electrode
TLCT	true liquid crystal templating mechanism
TEM	transmission electron microscopy
XRD	X-ray diffraction analysis

SYMBOLS

Symbol	Description	Units
a	radius of electrode	μm
a_i	activity of species i	–
c_i	concentration of species i	M
D	diffusion coefficient	$cm^2\ s^{-1}$

d	diameter of electrode	μm
E	potential vs a reference electrode	V
E°	standard potential	V
E_{C_Lim}	cathodic limit potential of cyclic voltammetry	V
E_{A_Lim}	anodic limit potential of cyclic voltammetry	V
E_{Dep}	potential of Pd film deposition	V
E_L	hydrogen loading potential	V
E_{LJ}	liquid junction potential	V
$E_{Pd\text{-}H}$	open circuit potential of Pd-hydride electrode	V
E_{PL}	plateau potential for α+β phase	V
F	the Faraday constant	F mol^{-1}
I	current density	A m^{-2}
I_0	exchange current density	A m^{-2}
i	current	A, mA or μA
i_L	limiting current	A, mA or μA
n	number of electrons transferred in electrode reaction	–
Q_{Dep}	charge passed during Pd film deposition	μC
$Q_{Str(H)}$	charge for stripping adsorbed and absorbed hydrogen from Pd film	μC
R	gas constant	J $K^{-1}mol^{-1}$
R_F	roughness factor (electroactive area/geometric area)	–
T	temperature	K
t	time from commencement of experiment	s
t_1	time at which $E_{Pd\text{-}H} - E_{PL} = -0.0012$ V	s or min
t_2	time at which $E_{Pd\text{-}H} - E_{PL} = +0.0012$ V	s or min
t_L	hydrogen loading time	s
η	overpotential	V
μ_i	chemical potential of species i	kJ mol^{-1}
μ_i°	standard chemical potential of species i	kJ mol^{-1}

Chapter 1. Introduction

The measurement of the pH of aqueous solutions is vital in many diverse areas such as environmental monitoring, wastewater treatment, industrial processes, and clinical chemistry. The pH is an important parameter in so many fields because the stability of compounds, the rate and pathways of reactions, and the selectivity of reactions versus competing reactions all depend on the pH.

Important electrochemical reactions are often associated with pH changes. For example, protons are produced or consumed during corrosion processes, metal deposition, electropainting, etc. The pH close to an active region on the surface can be significantly different from the bulk pH. The knowledge of pH distribution in such chemical processes can further our understanding of the mechanism of these processes and thus it is of great scientific and technical importance. Although pH is readily measured in the bulk of solutions, pH measurement with high spatial resolution at or near the interface is not an easy task.

In this research, a novel potentiometric micro pH sensor was studied. This thesis will describe the preparation of nanostructured Pd-hydride microelectrodes and demonstrate that they show excellent potentiometric pH response. In this chapter, the background relating to the following topics will be presented: conventional methods of the pH measurement including local pH measurements, the palladium / hydrogen system, and a recently developed method for the preparation of nanostructured films.

1-1. Measurement of pH

The degree of acidity (or basicity) of aqueous solutions may be expressed as pH, which is defined formally by the equation:

$$\mathrm{pH} = -\log a_{\mathrm{H^+}}$$

where a_{H+} is the activity of protons in the solution.

1-1-1. pH-sensing electrodes

An electrochemical cell, which can be represented by:

Reference electrode | | pH sensing electrode, Test solution

is commonly used for measurements of pH. Several pH sensing electrodes will be reviewed and discussed in this section. Among them, Pd-hydride electrodes will be considered in section 1-2.

1-1-1-(1). Hydrogen electrodes

A hydrogen electrode[1-3] consists of freshly platinized platinum immersed in the test solution with a constant supply of pure hydrogen bubbling. The electrode process occurring at the platinum surface of the hydrogen electrode is:

$$H^+ + e \rightleftarrows 1/2\ H_2$$

For the sake of simplicity, the partial pressure of H_2 is assumed to be 1 atm, the customary standard state for a gaseous component. Since the standard potential for the hydrogen electrode reaction is zero at all temperatures by convention, the Nernst equation yields the following relationship between the equilibrium potential and pH:

$$E = \frac{RT}{F} \ln a_{H^+} = -\frac{2.303RT}{F} \mathrm{pH}$$

The potential of the hydrogen electrode is the fundamental basis for the establishment of all values for pH.

The pH of a solution can be measured by determining the potential of a hydrogen electrode with respect to a reference electrode. However, it is often inconvenient to use hydrogen electrodes since the hydrogen gas has to be vented and the platinum electrodes have to be freshly plated with platinum black before use. Hence, in practice, indirect methods are often used rather than one based on the hydrogen electrode.

1-1-1-(2). Glass electrodes

The far-reaching application of pH measurements in modern commerce and industry was made possible by the discovery of the hydrogen ion function of glass membranes which led to the development of convenient, practical glass electrodes[1-3].

In one of the most common forms, the glass electrode consists of a thin glass membrane bulb inside which is mounted an internal reference electrode immersed in an internal solution of constant pH containing the ion to which the inner reference electrode is reversible. Normally for an internal reference electrode and an internal solution, a Ag/AgCl electrode and a buffered chloride solution are used. When dipped into an external solution (of unknown pH) containing a suitable reference electrode, the potential difference recorded between the two reference electrodes reflects a potential developed across the thin glass membrane. This arises since the glass functions as an ion-exchange material and an equilibrium is established between Na^+ cations in the surface of the glass matrix and protons in the solution.

The potential difference between the internal and external reference electrodes is given by:

$$E = \text{Constant} - \frac{2.303RT}{F}\text{pH}$$

The glass electrode is known to behave almost theoretically in solutions with pH 1 ~ 9, ie. its E/ pH slope is about 59 mV / pH.

In highly basic solutions, particularly those containing a high concentration of Na^+ cations, the glass electrode shows more positive potentials than expected from the behaviour at pH 1 ~ 9, since Na^+ cations inhibit the Na^+ / H^+ exchange reaction. Such alkali errors are well known and lead to unreliable pH readings in test solutions with pH > 9. However the use of special glasses, for example lithium glass, minimizes this problem and can extend the reliable range of pH measurements to beyond 12.

The mechanism through which the glass membrane alters its potential with a change of pH is not an electron transfer process; hence, the glass electrode is almost completely unaffected by oxidizing and reducing agents and not poisoned by heavy metals.

1-1-1-(3). Other pH-sensing electrodes

Of the several electrodes sensitive to pH, the glass electrode is by far the most convenient and versatile. The use of other methods is limited to specific fields where the glass electrode is not suitable: ie. under a high temperature and pressure condition, in fluoride solutions, use in food industry (fragility is a major concern), local pH measurements, etc.

(a) Antimony electrodes[1, 2]

The potential of antimony electrodes is thought to arise from an oxidation-reduction process involving antimony and the thin layer of oxide on the surface. Assuming the oxide as Sb_2O_3, the electrochemical process can be formulated as follows:

$$Sb_2O_3\,(s) + 6\,H^+ + 6\,e \rightleftarrows 2\,Sb\,(s) + 3\,H_2O$$

$$E_{Sb} = E^{\circ}_{Sb} + \frac{RT}{F}\ln a_{H^+}$$

In actual practice, the antimony electrode is found not to furnish results of high accuracy. In fact, the reported slope values are smaller than the expected value (59 mV / pH) and varied in the range 53 ~ 59 mV / pH[1]. The condition of the metal, whether cast or electrodeposited, polished or etched, and that of the oxide, have influence on the behaviour of the electrode. The potential-pH plot has been reported to consist of several linear branches. In common with other oxidation-reduction electrodes, the antimony electrode is disturbed by oxidizing and reducing agents.

The rapid response and rugged structure of this electrode make it useful for continuous industrial recording when great accuracy is not required. It can be used at high temperatures and in basic solutions with cells of the simplest design. Antimony "micro" pH sensors will be discussed in 1-1-2-(2).

(b) Ion-selective field effect transistors (ISFET)[3]

Over the last twenty years, the currents flowing in tiny field effect transistors (FET) have been used to probe ion concentrations. The FET is made of n-p-n

semiconductors which form the source, channel and drain respectively. The current flowing between the source and the drain is influenced by a voltage applied to the gate. In an ISFET an ion-selective membrane acts as the gate and the electrical potential which the membrane exerts on the source-to-drain current depends on the extent to which substrate ions have entered the membrane. The current therefore reflects the ionic concentrations. To measure pH, the ion-selective membrane is typically a hydrated silica membrane. In this way pH can be measured on the surface of a tiny silicon chip. ISFETs are preferred in the food industry, since their non-glass measuring surface will not break and can be stored dry.

1-1-2. Measurement of local pH

Important electrochemical reactions are often associated with pH changes. The pH change at or near the interface affects the rate of the reaction and influences the mechanism of the processes. Hence, measurement of pH with high spatial resolution at or near the interface can further our understanding of the reaction mechanism.

The development of the scanning electrochemical microscope (SECM) has enabled the imaging of chemical species at or near a variety of substrates. In this technique, a microscopic electrode (the probe) is scanned across a substrate, and the electrochemical response is plotted as a function of position. In this manner, a chemical and/or topographical map of the surface can be obtained. For example, if the probe is a micro pH sensor, the pH of the solution close to the interface can be measured and plotted as a function of the tip position.

Among the pH-sensing electrodes discussed in the preceding section, the glass and antimony electrodes have been used for local pH measurements by a number of researchers. However, many attemps have also been made to develop other type of micro pH sensors, since the performance of the glass and antimony microelectrodes were not necessarily satisfactory. The increasing use of micro pH sensors as a research tool has led to various technical developments for fabrication of micro pH sensors. Previously reported micro pH sensors can be divided into two groups; i.e. amperometric sensors and potentiometric sensors.

1-1-2-(1). Amperometric microsensors

In the steady state, the microdisc electrode is surrounded by a hemispherical diffusion field. The steady-state diffusion controlled current, i_L, is given by

$$i_L = 4nFDca$$

where n is the number of electrons transferred in the reaction and F the Faraday constant, D and c the diffusion coefficient and the concentration of the species of interest, a the radius of the electrode. Maintaining all the other parameters unchanged, the steady-state current is directly proportional to the concentration of the species. Hence the concentration can be estimated by the measurement of the current at a potential where the reaction is diffusion controlled, on the condition that n, D and a are known or that a calibration has been performed. It is important to note that the steady-state current reflects the concentration of the species instead of the activity and thus a calibration (steady-state current vs. pH) is normally essential.
Two types of reliable amperometric micro pH sensors have been reported.

(a) H^+ reduction on Pt in acidic solutions
Three reactions on Pt microelectrodes were studied[4] for amperometric measurements of pH; i.e. hydrogen evolution, oxide formation and oxygen evolution. The quantitative pH estimation was found to be possible solely from the steady state limiting current for hydrogen evolution:

$$H^+ + e \rightarrow 1/2\ H_2$$

A linear relationship was found between the logarithm of the limiting current and pH[4] under their experimental conditions. The study on the effect of supporting electrolytes[5-7] showed that in the absence of supporting electrolytes the limiting current was considerably larger than the predicted diffusion-limiting current. However, at high electrolyte concentrations, the limiting current was found to agree with predicted values.

This method has been used for probing protons in the vicinity of polyaniline film[6, 7] and for measuring acidity in wines[8], oils[9] and polyprotic acids[10]. The application of this method is limited to situations where a steady-state current for proton reduction is obtained; ie. solutions with pH < 6.

(b) OH^- oxidation on Au in basic solutions

A well-defined wave for the oxidation of hydroxide ions was recorded by Abdelsalam et al[11, 12] in basic solutions on Au microelectrodes;

$$OH^- \rightarrow 1/4\ O_2 + 1/2\ H_2O + e$$

The logarithm of the limiting current for this reaction was found to depend linearly on pH over the pH range 9.0 ~ 12.5. Below pH 9 the wave could not be distinguished from the baseline, while above pH 12.5 the wave became erratic because of the convection created by the release of O_2 bubbles.

Daniele et al[13] studied this system theoretically in detail. They reported that solutions with low concentrations of supporting electrolyte yielded currents enhanced by migration contributions, and that even in solutions with excess electrolyte the limiting current depended on the concentration because D varies with the ionic strength and viscosity of the medium. They derived theoretical equations for the dependence of steady-state limiting currents on ionic strength and showed that the theoretical and experimental data compared satisfactorily. Furthermore, the determination of pH was shown to be possible by considering:

$$pH = \log \gamma_{OH^-} + \log [OH^-] - \log K_W$$

The advantages and disadvantages of amperometric micro pH sensors (H_3O^+ reduction on Pt and OH^- oxidation on Au) can be summarized as follows.

They both showed linear relationship between the logarithm of the limiting current and pH. It was possible to theoretically explain the experimentally observed limiting current, although the limiting current depended strongly on the concentration of supporting electrolytes. Hence, in general, pH measurement is expected to be possible with quite high accuracy and reproducibility using these methods, on the condition that a calibration has been made in the same solution. Another important advantage of amperometric

sensors is ease of handling; ie. (a) special pre-treatment of the electrode is unnecessary and (b) the influence of liquid junction potential (between the test solution and the solution of reference electrode solution) and *iR* drop is negligible, since great accuracy in the potential is not needed. In addition, when an amperometric sensor is applied as an SECM probe, the absolute tip-substrate distance can be determined using experimental approach curves.
However, the major drawback is their narrow pH range. It is impossible to cover acidic and basic solutions with a single sensor. Furthermore, suitable method has not been found for the pH range 6 ~ 9.5. It also has to be mentioned that redox species may affect their response (limiting current), and that when used as SECM sensors amperometric sensors can affect the concentration profile of the species generated or consumed at the substrate.

1-1-2-(2). Potentiometric micro pH sensors

A majority of the works, in which local pH measurements were attempted, employed potentiometric micro pH sensors, rather than amperometric sensors. Potentiometric sensors are passive sensors, so they do not affect the concentration profile of the species generated or consumed at the substrate. In addition, the superiority to amperometric sensors can be found in the wider pH range and less sensitivity to the concentration of supporting electrolytes.
However, the response of conventional potentiometric microsensors is unstable and far from theoretical. Potential / pH slope values often vary from one electrode to another even when a proven fabrication procedure is followed. Hence calibration for individual electrodes before and after pH measurements is normally essential. Furthermore, the stability, precision and reproducibility of the potentiometric response tend to worsen as the size of the sensor decreases. Another disadvantage of potentiometric sensors is the difficulty in determining the distance between the tip and the substrate in SECM experiments, since they cannot rely on positive or negative feedback diffusion. Several approaches are available, but most are cumbersome.
The potentiometric micro pH sensors can be divided into three categories; glass membrane electrodes, liquid membrane electrodes, and metal / metal oxide electrodes.

(a) Glass membrane microelecrodes

Glass membrane microelectrodes have been applied to measurement of intracellular pH[14]. Their clear advantage is the selectivity of the response; they are almost completely unaffected by oxidizing and reducing agents and not poisoned by heavy metals. In addition, with regard to lifetime and dynamic range, glass electrodes are superior to any other tools used for pH measurement. However, reducing the size of the glass electrodes proved a formidable problem. One difficulty is their fragility, which restricts their use in many situations. Another serious difficulty arises from their high electrical resistance. It is difficult to keep the resistance within practical limits, since the smaller the area of pH-sensitive glass (which is in contact with the test solution), the higher its resistance. To overcome this problem, recessed-tip microelectrodes[14] have been developed. In this configuration the pH-sensitive glass is confined inside the insulating tip. This allows a very small tip (the outside diameter of the tip can be less than 1.0 μm) with a comparatively large area of pH-sensitive glass in contact with the solution. Although high reliability and long lifetime have been reported, electrodes of this design are very difficult to fabricate and the response is inevitably slow.

(b) Liquid membrane microelectrodes[15-18]

For this type of micro pH sensors, a hydrogen sensitive liquid neutral charge carrier is used to plug the tip of a micropipette. An example of the electrochemical notation of a complete potentiometric cell assembly, is given as:

Ag | AgCl, KCl | | salt bridge | | sample | membrane | internal solution, AgCl | Ag

The cell potential reflects the dependence of the membrane potential on the primary ion activity. The membrane potential consists of the phase boundary potentials generated by ion-exchange processes at both interfaces and the intermembrane diffusion potential. For an ideally selective electrode, the measured cell potential is described by the Nernst equation:

$$E_{Cell} = \text{constant} - \frac{RT}{F} \ln a_{H^+}$$

In practice, however, deviation from the ideal electrode behaviour is common. This type of electrode has been applied to the studies of oxygen reduction on Pt microelectrodes[16], cut edge corrosion of galvanized steel sheets[17] and phosphating processes[15].

The pH range and selectivity of the liquid membrane microelectrodes can be optimised depending on the environment of interest by choosing a suitable charge carrier. The tip size can be as small as 20-50 nm, although the preparation of such a delicate device is not routine.

The drawbacks of the liquid membrane microelectrodes are: fabrication (the failure rate is often as high as 50% and reproducibility among electrodes is poor), variable response (not Nernstian), and poor stability (short lifespan; ~ 1 day). Because of these drawbacks, it is important to calibrate micropipette electrodes before and after the experiment. If the two calibrations show significant differences, the experiment has to be discarded and repeated.

(c) Metal/metal oxide electrodes

Metal / metal oxide electrodes, of which Sb / SbOx is the best known example, show potentials dependent on pH. According to Ives and Janz[1], a variety of metal / metal oxide electrodes have been considered. Among them, Sb / SbOx, Ir / IrOx, W / WOx and Pd / PdOx microelectrodes have been used for local pH measurements including a number of SECM studies.

Their popularity can presumably be attributed to their ease of fabrication and their relatively robust structure. The accuracy and reproducibility of the potentiometric response are not very high. The behaviour often varies from one electrode to another and hence calibration for individual electrodes before and after pH measurements is normally essential.

The properties of several metal / metal oxide electrodes are described below.

(c-1) Antimony electrodes

The antimony microelectrode has been the most employed M / MOx pH sensor. Electrodes with quite small sizes (d ~ 0.5 μm) have been reported. Electrodes are commonly fabricated by melting pure Sb shot and in some cases powdery Sb_2O_3 is added[19, 20], while Tsuru electrodeposited Sb on Au substrates[21]. The

antimony electrodes are normally used as pH sensors without pre-oxidization of the surface. When the antimony electrode is applied to SECM[22, 23], the tip-substrate distance can be determined by obtaining an experimental approach curve with the amperometric mode, since special pre-oxidation is not necessary before pH measurement.

The pH range is generally wide; e.g. Remis et al[24] reported a pH range of 2 ~ 10 for d = 0.5 ~ 1.0 μm electrodes, although the range varies among studies. The reported slope values vary in the range 35 ~55 mV / pH, and are significantly lower than the values observed for conventional size electrodes (53 ~ 59 mV / pH) or the expected value (59 mV / pH at 25 °C) from the potential determining process presented in 1-1-1-(3). It is also common to find different slopes; one for pH < 7 and the other for 7 < pH.

Antimony microelectrodes have been used to measure pH in the vicinity of Pt[22, 25] and Cu[20] electrodes, during various electrode reactions. pH profile near the cathode during metal deposition has also been demonstrated[19, 21, 26-29]. Some of the other applications were; monitoring local pH changes near bilayer lipid membrane[30] and an ion-exchange membrane[31].

(c-2) Iridium oxide electrodes[32-35]

Iridium oxide electrodes are also extensively used as micro pH sensors. Reasons for this include a wide range of pH response and a relatively low sensitivity to redox interferences[34].

Iridium oxide electrodes are normally prepared by electrochemical or thermal oxidation of Ir microelectrodes. More recently, direct electrochemical deposition of iridium oxide layer has also been reported[34, 35]. The potentiometric pH response of iridium oxide microelectrodes depends strongly on the preparation method. Anodically electrodeposited iridium oxide films coated with Nafion resin (AEIROF[35]) showed the widest effective pH range of 0 ~ 12.

Iridium oxide electrodes tend to show two different linear regions of pH response with the transition point around pH 6. It is also known that they tend to exhibit super-Nernstian pH response (typically, 60 ~ 90 mV / pH), which indicates less than one electron is transferred per H^+. Researchers have proposed several possible potential determining processes[32, 34], such as :

$$2[IrO_2(OH)_2 \cdot 2H_2O]^{2-} + 3H^+ + 2e \rightleftarrows [Ir_2O_3(OH)_3\ 3H_2O]^{3-} + 3H_2O$$

Bezbaruah et al[35] obtained slope values of 50 ~ 65 mV / pH for AEIROF and assumed one or both of the following as the potential determining reactions:

$$IrO_2 + H^+ + e \rightleftarrows IrO{\cdot}OH$$
$$2IrO_2 + 2H^+ + 2e \rightleftarrows Ir_2O_3 + H_2O$$

Iridium oxide microelectrodes have been used to study a pH profile across a biofilm[32], the localised pH changes during initiation, growth and repassivation processes of pitting corrosion of stainless steels[33] using SECM, and the pH profiles near the substrate during electrochemical reactions (oxidation and reduction of H_2O_2 and H_2 evolution on Pt electrodes) and enzymatic reactions[34].

(c-3) Tungsten / tungsten oxide electrodes

Tungsten / tungsten oxide microectrodes have been used to study localized corrosion[36] and endothelial cells[37]. Luo et al immersed a tungsten electrode in the test solution (0.05M NaCl) overnight to establish a stable oxide film. Yamamoto et al[37] formed an oxide layer on a tungsten wire by cycling the potential between +1.0 and +2.0 V vs. Ag/AgCl in 2.0 M H_2SO_4, and they coated the electrode with Nafion to protect it from protein and enzyme adsorption. The prepared electrodes were reported to show a linear pH response over a pH range of 2~ 12 with a slope of 53.5 mV/pH.

(c-4) Palladium / palladium oxide

The palladium / palladium oxide microelectrode has also been studied. Several oxidation processes have been proposed; ie. anodization in molten $NaNO_3$-LiCl[38, 39], high temperature oxidation of Pd wires coated with NaOH[40-42], and electrolysis in sulphuric acid using a combination of ac and dc potentials[43]. The suggested potential determining reaction is:

$$PdO + 2\,H^+ + 2\,e \rightleftarrows Pd + H_2O$$

The reported slope values are nearly Nernstian; ie. 55 ~70 mV / pH. The effective pH range was typically 3 ~ 9. Palladium / palladim oxide electrodes have been applied to the studies of immobilized cell layers[39].

1-1-2-(3). Summary

In general, local pH measurements are possible with quite high accuracy and reproducibility using amperometric pH microsensors. In addition, when an amperometric sensor is applied as an SECM probe, the absolute tip-substrate distance can be determined using experimental approach curves. It is impossible, however, to cover acidic and basic solutions with a single sensor, because of their limited pH range.

Although most potentiometric micro pH sensors possess wider pH range than amperometric sensors, they have been found not to yield results of high accuracy. They often do not show Nernstian response, and the behaviour often varies from one electrode to another, even when a proven fabrication procedure is followed. In general, the potentiometric response is worse for microelectrodes than for conventional size electrodes. This is thought to be caused by the difference in the surface area. Referring to reference electrodes, Ives and Janz[1] recommended making the electrodes as large as circumstances allow, since the larger the electrode-solution interface, the better the chance that it will be "representative", with local abnormalities "integrated out."

1-2. Palladium / hydrogen system

1-2-1. Palladium-hydride phases

Graham[44] first observed in 1866 that large volumes of hydrogen were absorbed by a palladium tube. Since then the unique ability of palladium to absorb large quantities of hydrogen has been the subject of numerous studies and reviews. The palladium-hydrogen system has widely been used as a model for the physical and chemical properties of hydrides. In addition to academic purposes, this system has been researched into for application to the purification and storage of hydrogen to be used as a general chemical reagent or as a fuel. From a practical point of view, however, a large specific gravity and a high cost have been the two main reasons for searching for other hydrogen-absorbing substances.

1-2-1-(1). Palladium-hydrogen (solid-gas) system

Many attempts have been made[45, 46] to account for the isothermal pressure-composition relationships derived in palladium-hydrogen (solid/gas) equilibration studies. Figure 1.1 shows the plots of P_{H2}– H/Pd relationships for the solid/gas system.

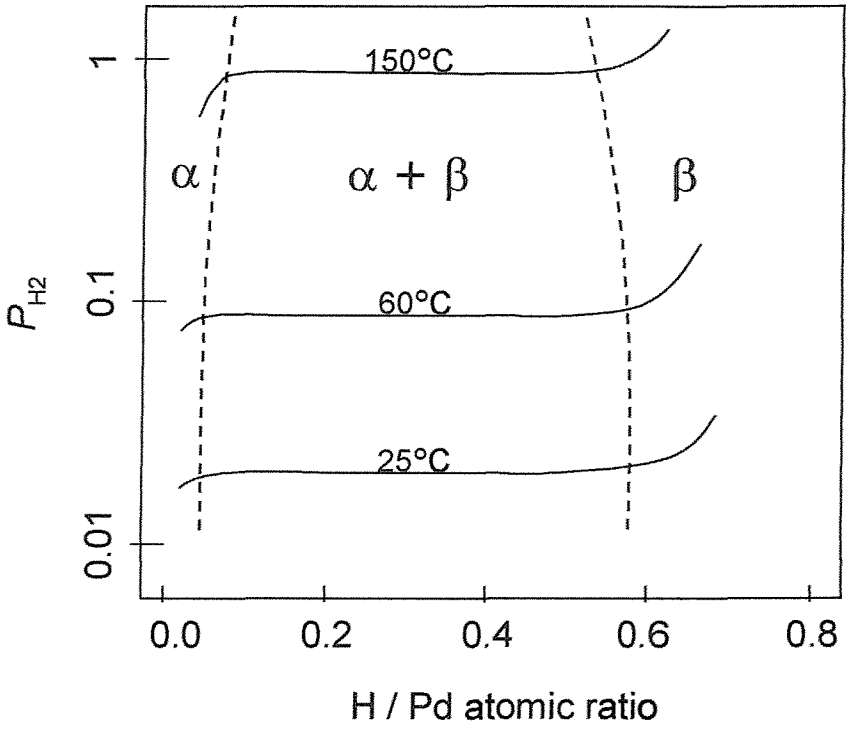

Figure 1.1. Schematic plots of P_{H2} – H/Pd relationships for the palladium – hydrogen system. Phase boundaries are shown by dotted lines.

When the hydrogen content is low, the equilibrium pressure shows a continuous increase. In this region the solid can be regarded as a solid solution of hydrogen in the original palladium lattice (α phase hydride).

The hydrogen content at which the pressure reaches a constant value corresponds to the maximum solubility of hydrogen in the α phase structure (α_{max}). It also represents the concentration at which a new hydride phase (β phase) begins to nucleate. The subsequent region where the equilibrium pressure remains constant corresponds to the hydrogen content range where α and β phase hydrides coexist. There is a continuous transformation from α to β

phase as the hydrogen content increases. The constant equilibrium pressure can be explained by the Gibbs phase rule. For a system at equilibrium, the number of degrees of freedom, F, which is the number of intensive variables that can be changed independently without disturbing the number of phases in equilibrium, can be expressed as :

$$F = C + 2 - P \qquad \textit{Equation 1.1}$$

where C is the number of components, and P is the number of independent phases present in the system. Only one degree of freedom is permitted in conditions of two components (H and Pd) and three phases (α, β and H_2).
Finally, when the phase transformation is completed, the hydrogen equilibrium pressure begins to increase again with a further increase in hydrogen content. In this region, a further solution of hydrogen in the β phase takes place. The composition at the end of the plateau corresponds to the initially formed β-phase (β_{min}).

1-2-1-(2). Properties of palladium-hydride phases

The absorption of hydrogen into palladium leads to physical changes. Key physical properties of palladium and Pd-hydride phases are summarized in Table 1.1.

Table 1.1. Physical properties of Pd and Pd-hydride .

Properties	Palladium	α phase	β phase
Lattice structure[a]	f.c.c.	f.c.c.	f.c.c.
Lattice constant[b] / kx	3.882	3.882-3.886	4.017-4.031
Diffusion coefficient of hydrogen[a]	-	$\approx 2 \times 10^{-7}$ cm^2 s^{-1}	$\approx 2 \times 10^{-6}$ cm^2 s^{-1}

[a] Lewis[45], [b] Aben and Burgers[47].

1-2-2. Potential of palladium hydride

1-2-2-(1). Experimental studies on the potential

A number of experimental works on the potential of palladium hydride electrodes as a function of hydrogen content have been published[47-50]. Several review articles on this issue were also published[1, 45].

Hoare and Schuldiner[49] studied the potential of palladium-hydrogen system in 2 M H_2SO_4 solution through which hydrogen gas was bubbled. They found that the spontaneous absorption of hydrogen led to a steady state with a constant H/Pd ratio of 0.025, approximately at the limit of the α-phase. At the same time, a steady electrode potential of +0.050 V vs RHE (a platinum-hydrogen electrode in the same solution) was recorded. Hydrogen was loaded further into Pd by cathodization, and the potential could be brought to zero. On open circuit, however, a potential of about +0.050 V was recovered. By correlating to the H/Pd ratio, the potential was found to be constant at about 0.050 V until a H/Pd ratio of 0.36. To explain the continuity of the 0.050 V potential to the H/Pd range at which α and β phases coexist, they suggested a mixed potential of α and β phases with the α phase being the potential determining.

Other workers[47, 50] later found that the absorption of hydrogen from acid solutions saturated by hydrogen gas does not stop at the limit of the α phase, but proceeds finally to the H/Pd ratio of 0.69, which is equal to the equilibrium concentration (H/Pd = 0.69) reported for direct absorption from the gas phase. This further absorption of hydrogen appeared to be more easily accomplished for palladium activated by anodization or palladization. The final potential of the electrode was 0 V vs. RHE.

Figure 1.2 gives the approximate representation of the potential and relative resistance, R/R_0, during hydrogen absorption from a hydrogen-saturated 2 N HCl solution, reported by Flanagan and Lewis[50]. Here, R is the electrical resistance of the specimen and R_0 is the initial "hydrogen-free" value of R.

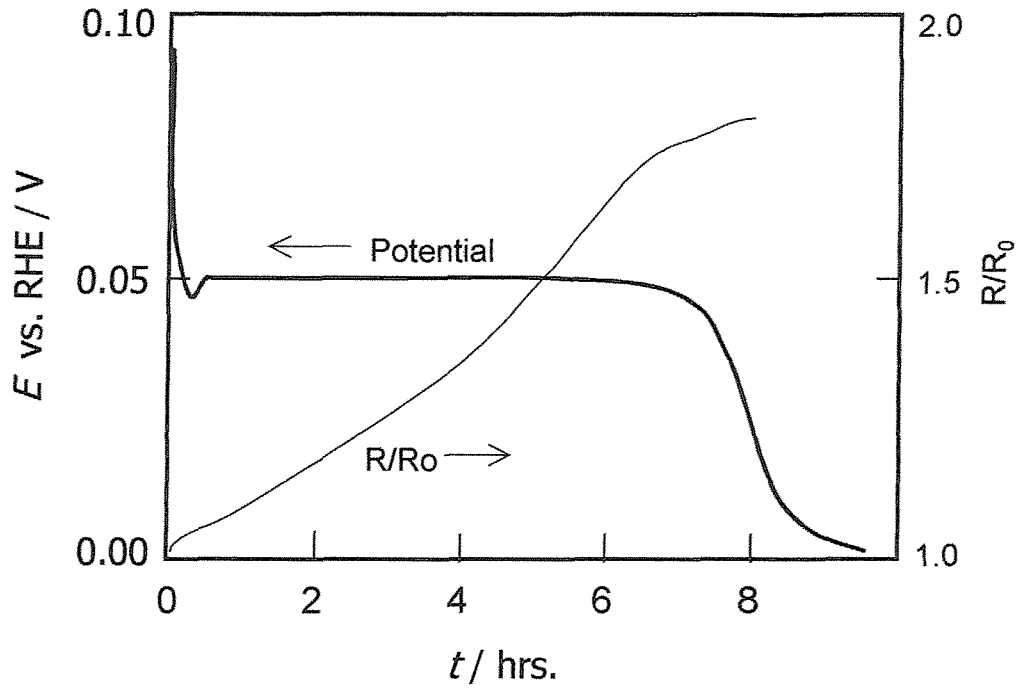

Figure 1.2. Schematic plots of the potential and the relative resistance (R/R_0) of a palladium wire (d=0.027 cm) during hydrogen absorption in a hydrogen saturated 2 N HCl solution (25 °C). Redrawn from reference[50].

The relative resistance was measured to monitor the hydrogen contents (H/Pd) using almost linear relationship between H/Pd ratio and R/R_0[51]. There is a very well marked plateau potential of about +0.050 V, constant over a wide range of H/Pd ratios. They attributed this plateau to the coexistance of α and β palladium hydride phases. The drop in potential at the beginning to the +0.050 V plateau was attributed to the pure α phase, and the subsequent drop to 0 V to the pure β phase. Aben and Burgers[47] supported the work of Flanagan and Lewis by correlating the potentials with the surface structure (phases) of the electrode during hydrogen absorption, using X-ray diffraction.

Vasile and Enke[52] used cathodically charged palladium hydride electrodes to study the relationship between the potential and the hydrogen content. Cathodically charged electrodes showed almost identical potential-H/Pd relationship to that obtained for palladium electrodes directly absorbing hydrogen in hydrogen-saturated solutions. As shown in Figure 1.3, the potential is a function of the composition at H/Pd < 0.05 and H/Pd > 0.5 but

independent of the composition at H/Pd ratio between 0.05 and 0.5. Considering that the reported H/Pd ratios of α_{max} and β_{min} were about 0.03 ~ 0.05 and about 0.6, H/Pd ratio appeared to be constant in most of the α+β region.

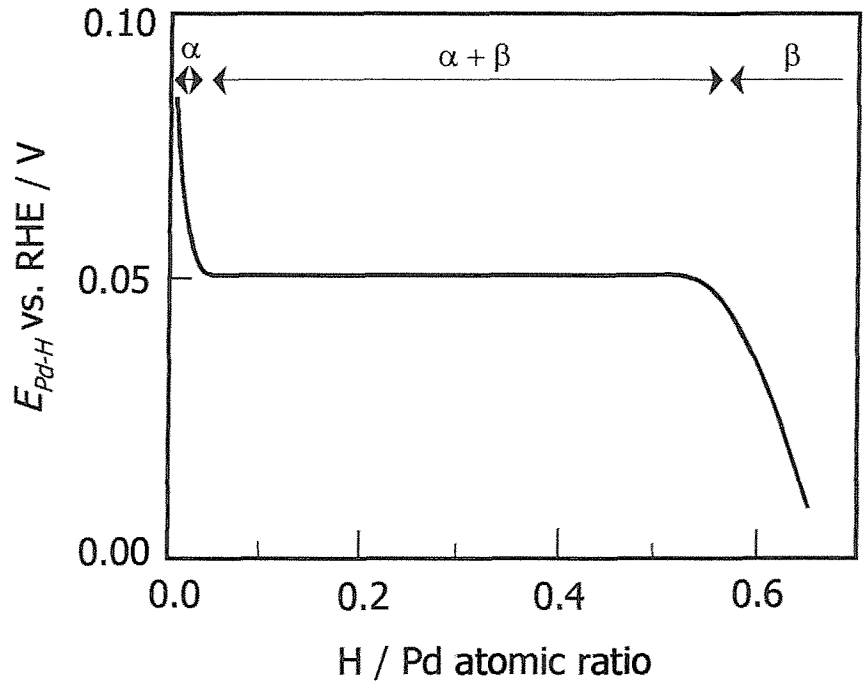

Figure 1.3. Potential vs. composition curve for a palladium-hydride electrode (redrawn from reference[52]). Test solution : 1 N perchloric acid, Temperature : 25 °C. A palladium wire (d=0.0125 in.) was loaded with hydrogen cathodically. The potential was measured after a short time of anodization for minimizing the hydrogen content gradient. The amount of hydrogen loaded into Pd was estimated with a gas chromatograph.

In the wide H/Pd range corresponding to the α+β phase, a steady potential of about +0.050 vs. RHE has been reported. In this region, any absorption or desorption of hydrogen simply changes the ratio of α to β phases, but does not affect the potential. Although slightly different values have been reported as the steady potential for α+β phase region, the potential may be taken as +0.050 ±0.001 V vs. RHE at 25 °C in acid solutions. Taking advantage of this stable and reproducible potential, α+β phase palladium-hydride electrodes have long been used as reference electrodes.

The potential determining reaction of the α+β palladium hydride has been suggested to be the following reaction :

$$H^+ + e \rightleftarrows H\ (Pd\text{-}H) \qquad \textit{Equation 1.2}$$

As can be expected from this reaction, the potential is dependent on the proton activity and hence α+β palladium hydride electrodes can also be used as pH sensors.

1-2-2-(2). Thermodynamic considerations on the potential

The potential of the palladium hydride electrode can be described by Nernst equation (see Equation 1.2) :

$$E_{Pd-H} = E^{o}_{Pd-H} + \frac{RT}{F}\ln\frac{a_{H^+}}{a_{H(Pd-H)}} \qquad \textit{Equation 1.3}$$

$$E^{o}_{Pd-H} = -\frac{1}{F}(\mu^{o}_{H(Pd-H)} - \mu^{o}_{H+} - \mu^{o}_{e}) \qquad \textit{Equation 1.4}$$

where μ_i^o is the standard chemical potential of the species *i*. Equation 1.3 shows that the potential of the palladium hydride electrode is a function of the activity of hydrogen in palladium hydride lattice ($a_{H(Pd\text{-}H)}$), as well as the activity of protons in the solution (a_{H+}).

The activity of hydrogen in the lattice ($a_{H(Pd\text{-}H)}$) at a certain temperature and H/Pd raito can be discussed by considering the palladium–hydrogen gas system (P_{H2} – H/Pd relationship was shown in Figure 1.1). When the palladium hydride phase is in equilibrium with the gas phase, the chemical potential of hydrogen in the lattice is equal to that of hydrogen gas.

$$2\ H\ (Pd\text{–}H) \rightleftarrows H_2 \qquad \textit{Equation 1.5}$$

$$2\mu_{H(Pd-H)} = \mu_{H_2} \qquad \textit{Equation 1.6}$$

where μ_i is the chemical potential of the species *i*. The chemical potentials in Equation 1.6 are described by :

$$\mu_{H(Pd-H)} = \mu^{o}_{H(Pd-H)} + RT \ln a_{H(Pd-H)} \qquad \textit{Equation 1.7}$$

$$\mu_{H_2} = \mu^{\circ}_{H_2} + RT \ln P_{H_2} \qquad \textit{Equation 1.8}$$

It is important to note that P_{H2} is the pressure of hydrogen when the reaction described by Equation 1.5 is in equilibrium in the solid-gas system. Substituting Equation 1.7 and Equation 1.8 into Equation 1.6 gives the expression for $a_{H(Pd-H)}$.

$$RT \ln a_{H(Pd-H)} = \frac{1}{2}\mu^{o}_{H_2} - \mu^{o}_{H(Pd-H)} + \frac{RT}{2} \ln P_{H_2} \qquad \textit{Equation 1.9}$$

This equation shows the relationship between the activity of hydrogen in the lattice ($a_{H(Pd-H)}$) and the pressure of hydrogen (P_{H2}) when the reaction described by Equation 1.5 is in equilibrium. In this derivation, the gas-solid equilibrium data were used only as a means to calculate $a_{H(Pd-H)}$. The establishment of the potential relies on the reaction described by Equation 1.2.
Substituting Equation 1.9 and Equation 1.4 into Equation 1.3 yields:

$$E_{Pd-H} = -\frac{1}{F}\left(\frac{1}{2}\mu^{\circ}_{H_2} - \mu^{\circ}_{H^+} - \mu^{\circ}_{e}\right) - \frac{RT}{2F} \ln P_{H_2} - \frac{2.303RT}{F} pH \qquad \textit{Equation 1.10}$$

The first term of the equation is equal to zero when we consider the potential with respect to SHE (by definition). Hence,

$$E_{Pd-H}\,(\text{vs. SHE}) = -\frac{RT}{2F} \ln P_{H_2} - \frac{2.303RT}{F} pH \qquad \textit{Equation 1.11}$$

This is the general expression of the potential of the palladium hydride electrode.

It is important to note here that P_{H2} in Equation 1.11 is the pressure of hydrogen in equilibrium with hydrogen in the palladium lattice. It is now generally accepted[52, 53] that there is an interdependence between $E_{Pd\text{-}H}$ vs H/Pd in acid solutions (Figure 1.3) and the P_{H2} vs H/Pd in solid-gas system (Figure 1.1) through Equation 1.11. This is discussed below, for each Pd-hydride phase.

(a) α phase region

As shown in Figure 1.1, the equilibrium pressure of hydrogen increases with H/Pd. This corresponds to the fact that $E_{Pd\text{-}H}$ is a function of the hydrogen content and becomes negative with H/Pd ratio (see Figure 1.3).

(b) α+β phase region

In the two phase region, the equilibrium pressure of hydrogen has been reported to be independent of the hydrogen contents, as can be seen in Figure 1.1. This corresponds to the constant potential reported for α+β palladium hydride electrodes. The values of the equilibrium pressure reported by various workers appeared to be somewhat different, depending on the procedure employed for their determination. Furthermore, hysteresis is often observed between the absorption and desorption isotherms. Using the average of their data calculated by Tsuruta and Macdonald, P_{H2} = 0.02 atm at 25 °C, Equation 1.11 can be rewritten as follows.

$$E_{Pd\text{-}H}\ (\text{V vs. SHE}) = -0.050 - 0.0592\,pH \quad (25\,^{\circ}\text{C}) \qquad \textit{Equation 1.12}$$

This is equivalent to –0.050 V vs. RHE, which is in good agreement with the reported plateau potentials for α+β palladium hydride electrodes.

(c) β phase region

As shown in Figure 1.1, the equilibrium pressure of hydrogen starts to increase in this region. This agrees with the gradual drop in the potential above the H/Pd ratio of about 0.5.

1-2-3. Palladium hydride electrodes

Taking advantage of the constant potential for α+β phase, Pd-hydride electrodes have been widely used as reference electrodes[52, 54-60]. Pd-hydride electrodes have a distinct advantage over platinum-hydrogen electrodes, since they carry their own hydrogen supply and the saturation of the electrolyte with hydrogen is not necessary.
The potential is dependent on the activity of protons in the solution (e.g. at 25 °C, Equation 1.12) and hence α+β palladium hydride electrodes have also been used as pH sensors[53, 61-68]. The α+β palladium hydride pH sensors have been reported to show almost theoretical potentiometric pH response, where the slope of the potential-pH calibration curve is about –0.059 V/pH (25 °C). They have been applied to experiments where the conventional glass electrode is not applicable; ie. under a high temperature and pressure condition, in fluoride solutions, etc.

Pd-hydride electrodes are normally prepared by loading hydrogen into Pd electrodes by bubbling hydrogen through the solution or by electrolysis. Before the loading procedure, palladium electrodes are subjected to an activation step (e.g. electroplating a Pd black layer, oxidation of the surface followed by electrolytic reduction of the surface) to attain a surface with high activity.
Various shapes of electrodes were examined, such as foils, plates, wires and rods. However, there have been no reports on Pd- hydride microelectrodes. The smallest of the reported Pd-hydride electrodes were prepared by Fleischmann et al[55], who loaded bare Pd wires (d ≈ 100 μm) with hydrogen cathodically and afterwards coated the curved part of the cylindrical surface with Lacomit varnish, care being taken that the tip remained exposed. They reported that it was possible to place the Pd-hydride electrode within 20 μm of the working electrode without undue screening. The electrode was reported to give the stable potential for periods up to 24 hours. However, the preparation method they used is clearly not applicable to conventional microdisc electrodes.

There are several possible reasons for the fact that there have not been successful Pd-hydride microelectrodes reported so far.
(1) The quality (stability, reproducibility, etc.) of the potentiometric response

cannot be expected to be comparable to that of conventional size Pd-hydride electrodes, considering that the potentiometric response of microelectrodes are generally worse than that of normal size electrodes.
(2) Charging a Pd microwire sealed in glass via its tip is expected to be difficult, considering the diffusion of hydrogen to the bulk. Using a limited volume electrode (e.g. a thin Pd film on a Au microelectrode) should make hydrogen loading easier. However, this is in turn expected to result in a short lifetime, because of the small amount of hydrogen loaded.

1-2-4. Hydrogen reactions on palladium electrodes

The absorption of hydrogen by cathodes of palladium during electrolysis was also first reported by Graham[69]. The hydrogen evolution reaction on palladium can take place by the multistep sequence (Volmer-Heyrovski-Tafel route)[70-72]. The first step in this process is the formation of adsorbed hydrogen atoms on the surface; ie. the Volmer reaction

$$H_3O^+ + e \rightarrow H_{ads} + H_2O \qquad \textit{Equation 1.13}$$

This is followed by either a further electrochemical reaction (the Heyrovski reaction)

$$H_{ads} + H_3O^+ + e \rightarrow H_2 + H_2O \qquad \textit{Equation 1.14}$$

or by combination of two adsorbed hydrogen atoms to give molecular hydrogen (the Tafel reaction)

$$H_{ads} + H_{ads} \rightarrow H_2 \qquad \textit{Equation 1.15}$$

The hydrogen reaction at a Pd electrode is further complicated by extensive permeation of atomic hydrogen into the metal lattice to form a bulk hydride. One of the important problems in the study of the hydrogen reactions of

palladium is the hydrogen absorption / desorption currents which are a few orders of magnitude higher than those of the surface processes. Several studies have shown that when thin films[73] or small particles[74-76] of palladium (of the order of a few nanometres) are used as electrodes, the adsorption and absorption processes can be distinguished.

At present, it is still unclear whether the adsorbed hydrogen atoms formed by the Volmer reaction are intermediates in the hydrogen absorption process. It is also not known how hydrogen atoms enter the metal. The formation of a subsurface layer[77-87] of sorbed hydrogen has been suggested as the first step of hydrogen incorporation during the absorption process. These uncertainties are discussed below.

(1) role of adsorbed hydrogen

Two pathways[72] have been suggested for hydrogen absorption into palladium. One involves hydrogen entering the metal through an adsorbed state. Adsorbed hydrogen atoms resulting from the Volmer reaction diffuse into the metal

$$H_{ads} \rightarrow H_{abs}$$

in competition with the Heyrovski and Tafel reactions.

The other establishes that hydrogen directly enters the metal without passing through the adsorbed state.

$$H_3O^+ + e \rightarrow H_{abs} + H_2O$$

(2) subsurface layer

It has been suggested that a subsurface layer of sorbed hydrogen may be involved in the hydrogen absorption process. According to the literature, the thickness of the subsurface layer varies from one layer to a value of 20-50 nm[79, 87, 88]. Conway et al[78], in their model of cathodic hydrogen sorption, postulated that before the formation of absorbed phases some kind of equilibrium between the adsorbed and subsurface states of hydrogen exists:

$$H^+ + e \underset{\text{electrosorption}}{\rightleftharpoons} H_{ads} \underset{\text{phase transfer}}{\rightleftharpoons} H_{diss} \xrightarrow[\text{diffusion and sorption}]{} H_{abs}$$

Where H_{diss} is a hydrogen atom dissolved directly below the surface. They divided the electrochemical hydrogen sorption into the following processes:

(a) proton discharge and coupled chemisorption of hydrogen

(b) phase transfer of hydrogen from the surface to interstitial sites in the host lattice, just below the surface

(c) transfer of hydrogen from state (b) into the bulk by diffusion along the chemical potential gradient of hydrogen

(d) parallel processes of desorption of the adsorbed hydrogen from the surface as H_2 by the Heyrovski or Tafel reactions.

Czerwinski et al[85-87] demonstrated that the H/Pd ratio in the Pd limited volume electrode (a thin layer of Pd deposited on Au), calculated from the charge of the hydrogen oxidation peak, depends significantly on the rate of the potential sweep and the thickness of the deposited layer of Pd. They have suggested that the subsurface layer of hydrogen exists not only during hydrogen sorption, but also during the opposite process, i.e. hydrogen desorption from the metal. They described the general scheme of hydrogen absorption / desorption in an acidic solution as follows:

$$H_\beta \longleftrightarrow H_\alpha \longleftrightarrow H_{sub} \longleftrightarrow H_{ad} \begin{array}{l} \longrightarrow 1/2\ H_2 \\ \longrightarrow H^+ + e \end{array}$$

They suggested that during the desorption process, hydrogen present in the subsurface layer (supposed to be more hydrogen rich than the α and β phases) is responsible for the generation of hydrogen adsorbed on the Pd surface, which can be directly oxidized electrochemically. The equillibria of other forms of hydrogen, i.e. the α and β phases contribute indirectly (supplying subsurface layers) to the total rate of desorption. The process of hydrogen desorption can be controlled either by the rate of the surface reaction or by bulk diffusion. The thickness and/or the hydrogen concentration of the subsurface layer in a basic solution appeared to be smaller than in an acidic solution, owing to the presence of alkali metal in palladium which enters there during hydrogen electrolysis[86].

(3) α ↔ β phase transition

Several theories have been proposed concerning the α ↔ β phase transition[89]. One theory describes the α+β mixed phases as a single phase which has a hydrogen diffusion coefficient different from those of either the α or β phase. On the other hand, hydrogen permeation through Pd-hydrogen diffusion electrodes associated with β→α transition have been carried out experimentally and explained theoretically[45]. The main point of the theory is that there exists a concentration discontinuity between the α and β phase regions and the phase transition is accompanied by the phase boundary moving. This was:

$$J = \frac{D_\beta (C_0 - C_1) + D_\alpha C_2}{L}$$

where C_0 is the β-phase concentration (H/Pd) at the entry surface, C_1 the β phase concentration at the phase boundary, C_2 the α phase concentration at the phase boundary and L the thickness of the membrane. The concentration at the exit surface is assumed to be zero. Good overall agreement was found between permeation rates obtained experimentally and those calculated from this theoretical relationship.

1-3. Nanostructured films deposited from liquid crystalline phases

1-3-1. Principle of fabrication

In 1995 Attard et al.[90] developed a method for the preparation of ordered mesoporous materials, which they called the true liquid crystal templating (TLCT) mechanism. This new method used a high concentration of surfactant (> 30 %) to generate a homogeneous liquid crystalline template. The characteristics of this approach are;

(1) The nanostructure of the final material is determined by the structure of the lyotropic liquid crystalline phase. Hence the nanostructure can be varied in a predictable fashion by the choice of surfactant and by the addition of co-solvents, based upon the knowledge of the phase behaviour of the system.

(2) The method can be used to produce nanostructured materials not only by chemical but also electrochemical means. Electrochemical deposition makes it possible to form nanostructured thin films on electrodes, where the thickness of the films can be directly controlled by the amount of charge passed for the deposition.

Attard et al. have used the method to produce nanostructured Pt thin films[91, 92] by electroreduction of hexachloroplatnic acid within the aqueous domains surrounding the surfactant template. TEM micrograph of the Pt film indicated that the nanostructure consisted of cylindrical holes (approximately 2.5 nm in diameter) arranged in a hexagonal lattice and separated by walls of Pt (approximately 2.5 nm thick). It was found possible to control the pore diameter over a range of 1.7 ~ 10 nm by using either surfactants with different alkyl chain lengths or by adding hydrophobic swelling agents (e.g. n-heptane) to the deposition mixture. They refer to these as H_1-e films to denote the fact that they have a regular nanostructure and are formed by electrochemical deposition from the H_1 lyotropic liquid crystalline phase. Similarly, Co[93], Sn[94, 95], metal alloys[96, 97], Ni[98, 99], Pd[100-102], semiconductors[103] and polymers[104] have been electrodeposited from liquid crystalline phases.

Figure 1.4 shows the principle of the deposition of a metal (Me) using the true liquid crystalline technique. Initially, the surfactant molecules aggregate into rods which orientate to form a three-dimensional template. Upon application of the potential, electrochemical deposition of the metal takes place in the aqueous region surrounding the liquid crystalline templates. After the deposition the liquid crystalline templates are simply removed by water, to leave a metal film with nanostructured pores. The resulting nanostructured metal film is a direct cast of the lyotropic crystalline phase from which it is deposited.

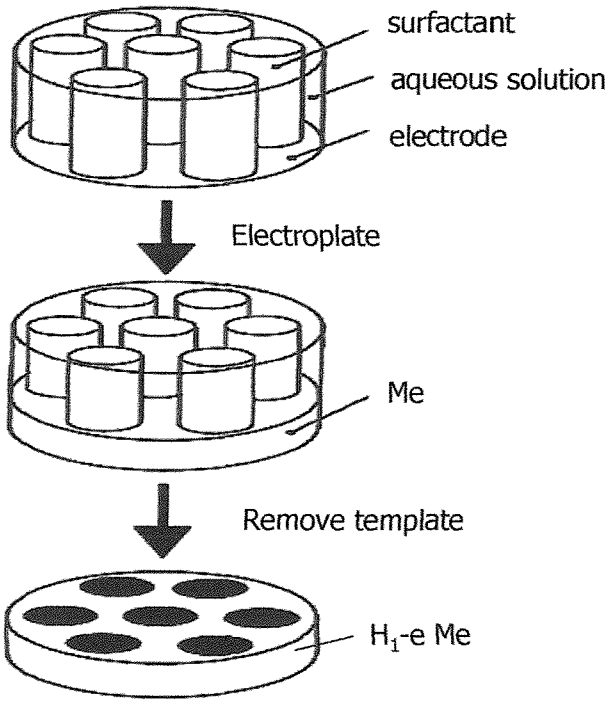

Figure 1.4. Schematic representation of the true liquid crystalline technique. The cylinders represent the micellar rods in the lyotropic liquid crystalline phase.

1-3-2. Application

Elliot et al[105] deposited H_1-e Pt films onto Au microdisc electrodes and found that the films had high electroactive areas (with roughness factors of ca. 210) as a direct consequence of their electrochemically accessible nanostructure. The electrodes were shown to combine a high electroactive area with efficient mass transport characteristics unique to microelectrodes. They suggested the significance of the nanostructured films to the fields of electroanalysis. Indeed, it was later shown that H_1-e Pt microelectrodes could be used as electrode materials for the measurement of oxygen[106] and hydrogen peroxide[107, 108].

Nanostructuring of metal films can also be used to control their physical properties. Bartlett et al[93] have shown by magnetic measurements on nanostructured Co films that the coercivity of these cobalt films is three to five times greater than that for polycrystalline Co and that it varies systematically with the size of pores.

1-3-3. H_1-e Pd films

Bartlett et al[100-102] used the hexagonal (H_1) lyotropic liquid crystalline phases of nonionic surfactants to template the electrochemical deposition of nanostructured palladium films on 1 mm diameter Au electrodes. They used two non-ionic surfactants namely octaethyleneglycol monohexadecyl ether ($C_{16}EO_8$) and Brij®56. Brij®56 is a polydisperse surfactant mixture with a distribution of headgroup sizes, the major components being from $C_{16}EO_4$ to $C_{16}EO_{12}$ with $C_{16}EO_8$ as the most abundant. In their work, the phase behaviour of the mixtures of non-ionic surfactant and $(NH_4)_2PdCl_4$ solution was investigated in detail. The phase diagram of mixtures of $C_{16}EO_8$ and $(NH_4)_2PdCl_4$ solution, reported by Bartlett et al[101], is shown in Figure 1.5

The hexagonal, H_1, phase exists between 30-40 wt.% $C_{16}EO_8$ and 80-90 wt.% at room temperature. The bicontinuous cubic, V_1, phase has a smaller region between 55-60 wt.% and 80-90 wt.% at higher temperature than H_1 phase. There is no evidence for the existence of the bicontinuous cubic phase at room temperature. At high concentrations of $C_{16}EO_8$ the lamellar, L_α, phase predominates.

In the case of mixtures of Brij®56 and $(NH_4)_2PdCl_4$ solution, a phase behaviour similar to that of $C_{16}EO_8$ and $(NH_4)_2PdCl_4$ solution, was reported. Both phase diagrams, using different non-ionic surfactants ($C_{16}EO_8$ or Brij®56) showed large composition and temperature ranges over which the H_1 phase is stable and the compositions of the palladium deposition mixtures were chosen to correspond to the H_1 phase.

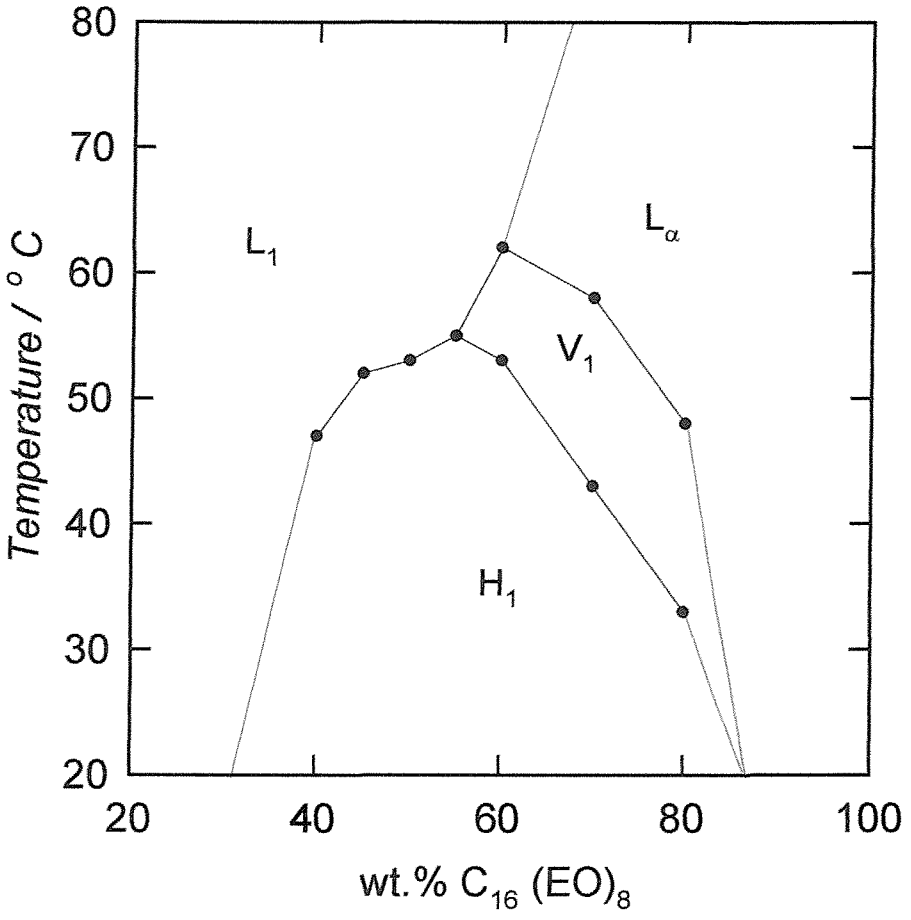

Figure 1.5. Phase diagram of $C_{16}EO_8$ and water in which the concentration of $(NH_4)_2PdCl_4$ was kept fixed at 1.40 mol dm^{-3}. H_1 is the hexagonal phase, V_1 the cubic phase, L_α the lamellar phase and L_1 the micellar solution. Redrawn from reference[101].

Thus deposited H_1-e Pd films were reported to possess regular hexagonal arrays of cylindrical pores separated by palladium walls (pore diameter : 2.0 ~ 2.5 nm, wall thickness : 2.0 ~ 2.5 nm) and very high surface areas (typical roughness factor : 250).

They studied the hydrogen reactions on the H_1-e Pd films deposited on 1 mm diameter Au disc electrodes in 1 M H_2SO_4 solutions. The formation of adsorbed hydrogen could be readily distinguished because of the high electroactive area to volume ratio of the films. Hydrogen absorption / desorption reactions were

found to be very fast. The electrodes were reported to be stable towards repeated cycling to form the β phase showing that the hydrogen insertion and concomitant lattice expansion (about 3 %) does not destroy the nanostructure. The $\alpha \rightarrow \beta$ transition was observed at the potential similar to those reported for bulk palladium, which was consistent with the results from X-ray studies showing that the film had the same structure and lattice parameters as bulk Pd.

No attempt has been made to study the potentiometric response of H_1-e Pd films. Very fast hydrogen absorption / desorption reactions (corresponding to a high exchange current) are expected to be clear advantages of H_1-e Pd films, in cases where the films are applied as potentiometric sensors. To reach the α+β phase equilibrium potential of a Pd-hydride electrode, its exchange current must be large. If the exchange current is too low, not only may the electrode become polarizable, but it may no longer be able to attain its proper equilibrium potential at all. Some other process dependent upon impurities but capable of sustaining a higher exchange current may take over.

1-4. Summary

Measurement of local pH

The glass electrode is widely used to measure pH because it is much more convenient and versatile than any other pH sensing electrodes. It shows almost theoretical response over wide range of pH, and its response is almost completely unaffected by oxidizing and reducing agents. However, it is difficult to make reliable microelectrodes using ion selective glass, because of its fragility and high electrical resistance.

Amperometric micro pH sensors showed linear relationship between the logarithm of the limiting current and pH. The experimentally observed limiting currents corresponded to the theoretical values, and hence pH measurement is expected to be possible with quite high accuracy and reproducibility using these methods. It is impossible, however, to cover acidic and basic solutions with a single sensor, because of their limited pH range.

Although most potentiometric micro pH sensors possess wider pH range than amperometric sensors, they have been found not to yield results of high accuracy.

They normally do not show Nernstian response, and the behaviour often varies from one electrode to another, even when a proven fabrication procedure is followed. Hence careful calibration before and after the pH measurement is normally essential. Their response generally worsens as the size of the sensor decreases.

Pd-hydride electrodes

The potential of a Pd-hydride electrode has been shown to be independent of the composition in the wide α+β phase region. In this region, a steady potential of about +0.050 vs. RHE has been reported. Taking advantage of this stable and reproducible potential, α+β phase palladium-hydride electrodes have long been used as reference and pH electrodes. The α+β palladium hydride pH sensors have been reported to show almost theoretical potentiometric pH response, where the slope of the potential-pH calibration curve is about –0.059 V/pH (25 °C). However, there have not been any report on Pd-hydride microelectrodes. There are several difficulties expected when Pd-hydride "micro" pH sensors are considered; (1) the quality of the potentiometric response cannot be expected to be comparable to conventional size Pd-hydride electrodes, considering that the potentiometric response of microelectrodes is generally worse than that of normal size electrodes, (2) charging a Pd microwire sealed in glass from the tip is expected to be difficult, but using a limited volume electrode (e.g. a thin Pd film on a Au microelectrode) is in turn expected to result in a significant shorter lifetime.

Nanostructured Pd films

Bartlett et al used the hexagonal (H_1) lyotropic liquid crystalline phases of nonionic surfactants to template the electrochemical deposition of nanostructured Pd films on 1 mm diameter Au electrodes. Thus deposited films appeared to possess regular hexagonal arrays of cylindrical pores separated by palladium walls (pore diameter: 2.0 ~ 2.5 nm, wall thickness : 2.0 ~ 2.5 nm) and very high surface areas (typical roughness factor : 250). Hydrogen absorption / desorption were found to be very fast. The electrodes were reported to be stable towards repeated cycling to form the β phase showing that the hydrogen insertion and concomitant lattice expansion (about 3 %) does not destroy the nanostructure. The α → β transition was observed at the potential similar to

those reported for bulk palladium, which was consistent with the results from X-ray studies showing that the film had the same structure and lattice parameters as bulk Pd.

Objectives of the present study

In the present study, taking advantage of the stable and reproducible potential of α+β phase, an attempt was made to fabricate Pd-hydride micro pH sensors for the first time. Aiming for truly reliable micro pH sensors with a wide effective pH range, nanostructured films (H_I-e Pd films) were thought to be advantageous for the following reasons:

(a) On H_I-e Pd films deposited on 1 mm diameter Au electrodes, hydrogen absorption / desorption reactions were reported to be very fast. The rapid potential determining process, which corresponds to a high exchange current, is believed to contribute to the quality of the potentiometric response.

(b) H_I-e Pd films possess huge electroactive areas, which might allow microelectrodes to show behaviour similar to normal size electrodes.

(c) Hydrogen loading into the film is rapid. Hence, the loading can be completed in relatively short time and repeated frequently if needed.

(d) The H_I-e Pd films were reported to be stable towards repeated cycling to form the β phase (the nanostructure was not destroyed). This means that H_I-e Pd films can be loaded with hydrogen and used as pH sensors repeatedly.

The majority of the results presented in this thesis was obtained with H_I-e Pd films deposited on Pt (not Pd) microdisc electrodes to avoid the diffusion of hydrogen deep into the bulk of the microwire.

The objectives of the present study were set as follows:

(1) Establish the preparation method of H_I-e Pd-hydride (α+β) microelectrodes. This includes the deposition of H_I-e Pd films on Pt microdisc electrodes and the loading procedure of hydrogen into the H_I-e Pd films.

(2) Study the potentiometric response of H_I-e Pd-hydride microelectrodes and verify the applicability to potentiometric pH sensors (e.g. in SECM

experiments).

(3) Assess the role of H_I nanostructure in potentiometric response of H_I-e Pd-hydride microelectrodes.

Structure of the thesis

The next chapter will present the reagents, experimental conditions, equipment and techniques used throughout this thesis.

In Chapter 3, the deposition behaviour of H_I-e Pd and plain Pd films will be described first. The results for characterization of deposited films will then be presented. Optimum deposition conditions will be discussed.

Chapter 4 will describe the hydrogen absorption behaviour of H_I-e Pd films. The behaviour during the potentiostatic loading procedure will be discussed by focusing on the effect of loading potential. The method to control the H/Pd ratio via the loading potential and the loading time will be established and presented.

In Chapter 5, the potentiometric response of H_I-e Pd-hydride films loaded with hydrogen cathodically under the condition discussed in the preceding chapter will be presented. Results will be shown which illustrate that the potentiometric response of H_I-e Pd films is stable, reproducible, rapid and almost theoretical in deaerated solutions over the pH range investigated in the present study (2 ~ 12). The effect of oxidizing species will also be discussed.

In Chapter 6, the outstanding properties of H_I-e Pd films (shown in Chapter 4, 5) will be compared with polished Pd microdisc electrodes and plain Pd films, in order to clarify the role of the nanostructure. The advantages of H_I-e Pd films over Pd microelectrodes without the nanostructure will be discussed.

Overall conclusions will be presented in Chapter 7. In this chapter, future work will also be described.

Chapter 2. Experimental

2-1. Generalities

2-1-1. Reagents

All reagents were used as received without further purification. The details of each reagent are listed in Table 2.1.

2-1-2. Purified water

All aqueous solutions were prepared using purified water (< 0.1 μS cm^{-1}). Purification of water was accomplished in two steps. Water was first passed through a Whatman RO50 water filtering system. This filtered water was then deionised by passing it through a Whatman STILLplus carbon filter.

2-1-3. Glassware

All glassware was soaked overnight in 5 % Decon 90 (BDH) solutions and rinsed thoroughly with purified water before use.

Table 2.1. Reagents used in the present study

H_1-e Pd film plating mixture

Chemical formula	Name	Grade	Manufacturer
$(NH_4)_2PdCl_4$	ammonium tetrachloropalladate	99.998 %	Alfa Aesar
$C_{16}H_{33}(OCH_2CH_2)_8OH$	octaethylene glycol monohexadecyl ether ($C_{16}EO_8$)	> 98 %	Fluka
$C_{16}H_{33}(OCH_2CH_2)_nOH$	Brij® 56 ($C_{16}EO_n$; n = 4 - 12)	-	Aldrich
$CH_3(CH_2)_5CH_3$	n-heptane	99 %	Lancaster

Test solutions for electrochemical measurements

Chemical formula	Name	Grade	Manufacturer
H_2SO_4	sulphuric acid	ARISTAR	BDH
Na_2SO_4	sodium sulphate	ARISTAR	BDH
HCl	hydrochloric acid	ARISTAR	BDH
KCl	potassium chloride	ARISTAR	BDH
$HClO_4$	perchloric acid	ARISTAR	BDH
$NaClO_4\ nH_2O$	sodium perchlorate hydrate	99.99 %	Aldrich
NaOH	sodium hydroxide pellets	AnalaR	BDH
$Ru(NH_3)_6Cl_3$	hexaamine ruthenium (III) chloride	98 %	Aldrich
$Na_2HPO_4\ 12H_2O$	di- sodium hydrogen orthophosphate 12-hydrate	AnalaR	BDH
$NaH_2PO_4\ H_2O$	sodium di-hydrogen orthophosphate 1- hydrate	AnalaR	BDH
Na_2CO_3	sodium carbonate anhydrous	AnalaR	BDH
$NaHCO_3$	sodium hydrogen carbonate	AnalaR	BDH
$C_8H_5O_4K$	potassium hydrogen phthalate	99.7 %	SIGMA

Fabrication of reference electrodes

Chemical formula	Name	Grade	Manufacturer
KCl	potassium chloride	AnalaR	BDH
K_2SO_4	potassium sulphate	AnalaR	BDH
Hg	mercury	99.999 %	Alfa Aesar
Hg_2Cl_2	mercurous chloride	AnalaR	Hopkin and Williams
Hg_2SO_4	mercurous sulphate	> 97 %	Fluka

Buffer solutions for combination pH electrode calibration

Chemical formula	Name	Grade	Manufacturer
-	pH 1.679 ± 0.030 (25 °C)	-	Fluka
-	pH 4.00 ± 0.01 (25 °C)	-	Aldrich
-	pH 7.00 ± 0.01 (25 °C)	-	Aldrich
-	pH 10.00 ± 0.01 (25 °C)	-	Aldrich

2-2. Electrochemical measurements

2-2-1. Electrochemical cells

Glass cells for electrochemical measurements were constructed by the glass blower. They were water-jacketed cells and connected to a water bath (W14, Grant) to maintain the temperature at 25 ± 1 °C. The volume of the test solutions was about 5 ml. When necessary, de-oxygenation was accomplished by passing Ar gas (BOC) through the solution for at least 15 minutes. The Ar bubbling was terminated before starting each measurement. A small flow of Ar gas was then introduced to the gas layer of the cell to keep the solution de-oxygenated throughout the measurement.

2-2-2. Reference electrodes

2-2-2-(1). Saturated mercury / mercurous sulphate electrode (SMSE)

Homemade Hg / Hg_2SO_4, K_2SO_4 (saturated) reference electrodes (SMSE) were used in most experiments instead of saturated calomel elecrodes (SCE) to prevent Cl^- ion contamination into the test solutions. The electrodes were prepared according to the procedure described by Bartlett[109]. The electrodes were combinations of two glass bodies; a glass tube with one closed end through which a platinum wire was sealed, and a pipette with a sinter at the tip. Drops of mercury were placed into the glass tube until the platinum wire was covered. A paste comprising of K_2SO_4 / Hg_2SO_4 (1/1) mixture and a saturated K_2SO_4 solution was then placed onto the mercury layer. Glass wool was then inserted into the tube to hold the mercury and the paste in place. The glass tube was then inserted in the glass pipette filled with a saturated K_2SO_4 solution.
Freshly prepared electrodes were left to stand for at least 24 hours in saturated K_2SO_4 solutions to reach equilibrium. SMSEs were stored in saturated K_2SO_4 solution and rinsed with purified water before use. The electrodes were tested regularly against a commercial SMSE (CRL/HG2SO4, Russell), which was always soaked in a saturated K_2SO_4 solution and solely used for testing

homemade SMSEs. Homemade SMSEs were deemed suitable for use only if the potential against the commercial SMSE was less than 1 mV.

2-2-2-(2). Saturated calomel electrode (SCE)

Homemade Hg / Hg_2Cl_2, KCl (saturated) electrodes (SCE) were used as reference electrodes in some experiments (e.g. in solutions containing Cl^- ions). The preparation procedure was the same as for the SMSEs, except that Hg_2SO_4 was replaced by Hg_2Cl_2, and K_2SO_4 by KCl. Homemade SCEs were stored in saturated KCl solutions and rinsed with purified water before use. The electrodes were tested regularly against a commercial SCE (COLE PARMER), which was always soaked in a saturated KCl solution and solely used for testing homemade SCEs. Homemade SCEs were deemed suitable for use only if the potential against the commercial SCE was less than 1 mV

2-2-3. Experimental set-up

In electrochemical measurements, care was taken to prevent electrical noise. All experiments were carried out in an aluminium Faraday cage connected to the earth. Electric connections were made using shielded cables, and the cables were made as short as possible.

2-2-3-(1). Voltammetric and chronoamperometric measurements

Voltammetry and chronoamperometry were undertaken using a two-electrode system, where the reference electrode (either SMSE or SCE) served also as a counter electrode. Small potential shift of the reference / counter electrode due to the small current on microelectrodes makes it possible to use a two-electrode configuration. The potential of the working electrode was controlled using a waveform generator (HiTek PPR1), while the current was recorded using a homemade current follower. Figure 2.1 is the schematic diagram of the experimental arrangement used in voltammetric and chronoamperometric measurements.

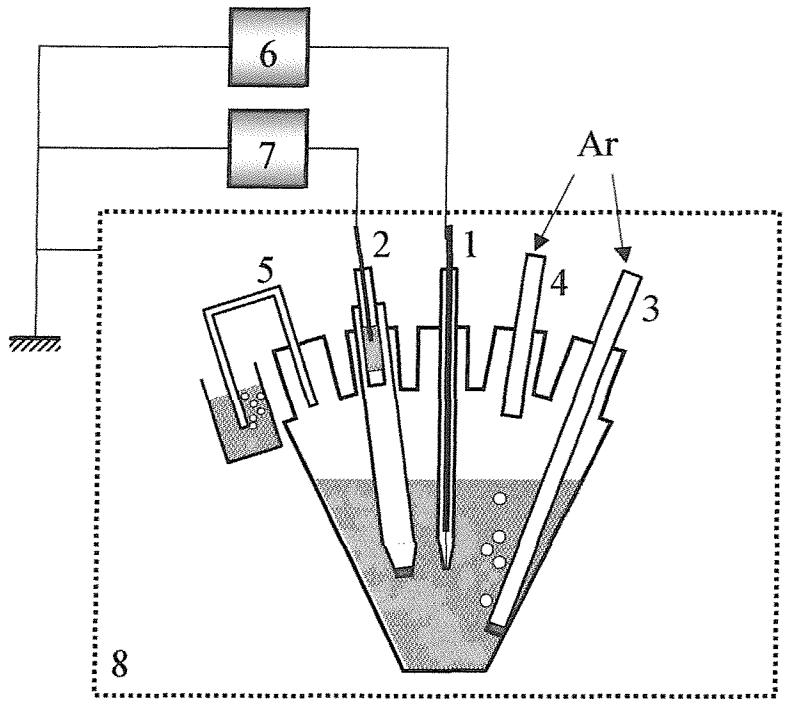

Figure 2.1. Schematic diagram of the experimental arrangement for voltammetric and chronoamperometric measurements. (1) Working electrode (microelectrode); (2) Reference / counter electrode (SMSE or SCE); (3) Ar gas inlet used before measurements; (4) Ar gas inlet used during measurements; (5) Ar gas outlet; (6) Waveform generator; (7) Current follower; (8) Faraday cage

To check the potential shift of the reference / counter electrode in this system, a preliminary experiment was performed. Cyclic voltammetry in 1 M H_2SO_4 was conducted using a nanostructured Pt electrode as the working electrode and an SMSE as the reference / counter electrode. During the cyclic voltammetry, the potential of the reference / counter electrode was recorded against another SMSE placed in the same solution. The experimental conditions were chosen so that a current up to ± 5 μA was passed between the working and the reference / counter electrodes. This is a much greater current than that passed in other experiments of the present study. The potential shift of the reference / counter electrode was proportional to the current (3 mV / μA). In most experiments reported here, the current is typically less than 0.3 μA and the potential shift is therefore expected to be smaller than 1 mV. It is also important to note that the

potential of the reference / counter electrode was reversible in the current range tested, which ensures that the potential returns to the initial value instantaneously by termination of the current.

2-2-3-(2). Potentiometric measurements

In potentiometric measurements, the input impedance of the measuring apparatus has to be high enough to ensure that the input bias current is negligibly small. This is particularly important when microelectrodes are used, since the current may either produce a significant voltage error or cause a chemical change to the sensor surface. In the present study, a homemade battery operated high-input impedance differential amplifier was used. In this instrument, the potential difference between the microelectrode and a large inert Pt wire electrode is compared to the potential difference between a reference electrode and the Pt wire. The Pt wire is connected to the electrical ground of the electronic circuit. High-input-impedance operational amplifiers are used as voltage followers to buffer the input of both the microelectrode and the reference electrode. The potential differences are compared with a precision unit-gain differential amplifier (AMP03GP form Analog Devices).
The differential amplifier was located inside the Faraday cage to prevent noise. Figure 2.2 is the schematic diagram of the system used in potentiometric measurements.

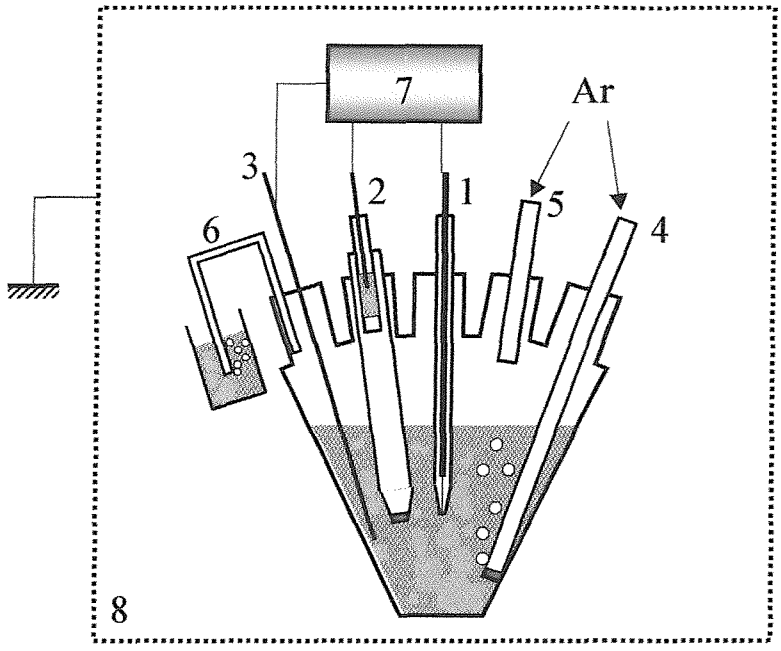

Figure 2.2. Schematic diagram of the experimental arrangement for potentiometric measurements. (1) Indicator electrode (microelectrode); (2) Reference (SMSE or SCE); (3) Pt wire; (4) Ar gas inlet used before measurements; (5) Ar gas inlet used during measurements; (6) Ar gas outlet; (7) Differential amplifier; (8) Faraday cage

2-3. Preparation of microelectrodes

2-3-1. Pt and Pd microdisc electrodes

2-3-1-(1). Fabrication of microdisc electrodes

Microdisc electrodes were prepared in a similar way to the procedure described by Denuault[110]. A Pt (d = 10 or 25 μm; 99.99%, Goodfellow) or Pd (d = 25 μm; 99.9%, Goodfellow) microwire was inserted into a soda glass pipette (constructed by the glass blower) and the narrow end of the pipette was sealed using a Bunsen burner. The pipette was then evacuated from the open end and the sealed end of the pipette was inserted into a heating coil. This caused the glass to melt and collapse around the microwire. The coil was moved slowly until about 5 mm of the microwire was left exposed in the pipette. After the vacuum

line was opened, the pipette was left to cool for about 5 minutes. To make an electrical contact between the microwire and a copper wire, finely cut indium was inserted into the pipette and heated with an electric heat gun until the indium melted and covered the exposed part of the microwire. A copper wire was then inserted into the molten indium and twisted to ensure a good contact. The copper wire was fixed at the open end of the pipette using epoxy resin to prevent the copper/indium/microwire connection from being damaged.

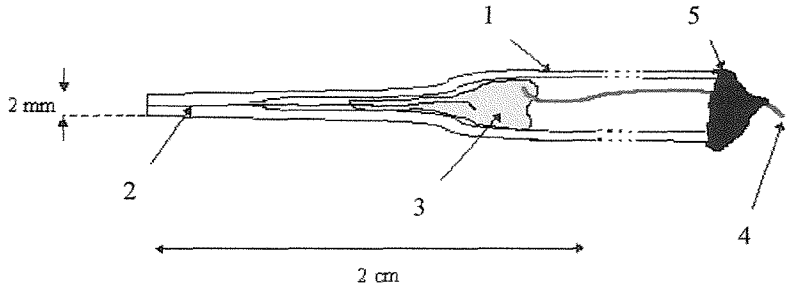

Figure 2.3. Schematic of a microdisc electrode. (1) Soda glass pipette; (2)Pt or Pd microwire; (3)Indium; (4) Copper wire; (5) Epoxy resin.

2-3-1-(2). Polishing and cleaning

The microdisc electrodes were polished using SiC paper (#320 → #600 → #1200) and polishing pads (MICROCLOTH®, BUEHLER) with alumina/water slurries (alumina : 1.0 μm → 0.3 μm; MICROPOLISH®, BUEHLER). The electrodes were washed with purified water and wiped gently with velvet microcloth to remove the remaining alumina powder and water. The microdisc electrodes were then transferred into 1 M H_2SO_4 solutions and cycled until the voltammogram stabilized.

2-3-2. Deposition of H_1-e Pd films

2-3-2-(1). Preparation of the plating mixture

The preparation of H_1-e Pd film deposition mixture followed the composition and procedure described by Bartlett et al[101]. The plating mixture consisted of 12 wt% $(NH_4)_2PdCl_4$, 47 wt% surfactant (either $C_{16}EO_8$ or Brij® 56), 2 wt% heptane and 39 wt% purified water. Water (1.17 g) and $(NH_4)_2PdCl_4$ (0.36 g) was first put in a glass container. The surfactant (1.41 g) and heptane (0.06 g) were then added and the mixture was stirred thoroughly for 15 minutes using a glass rod. The mixture appeared to be very viscous at the room temperature. To ensure its homogeneity, the mixture was gently warmed to about 35 °C (the mixture became less viscous) and stirred for another 15 minutes. The paste was then allowed to equilibrate at 25 °C for 2 hours before the deposition was carried out. The presence of the homogeneous hexagonal (H_1) phase in the mixture was confirmed by polarising light microscopy. A small amount of the paste was placed onto a glass slide and was observed with a polarizing optical microscope. The sample appeared to have the charcoal-like texture, which is characteristic[111] of the H_1 liquid crystalline phase.

2-3-2-(2). Electrodeposition of H_1-e Pd films

The H_1-e Pd films were deposited using a two-electrode configuration with a Pt microdisc electrode as the working electrode and an SCE as the reference / counter electrode. The plating mixture was placed at the bottom of the glass cell thermostated at 25 °C.

For each microdisc electrode, the alumina polishing (1.0 μm → 0.3 μm) and the cleaning (cycling in 1 M H_2SO_4) were done just before the deposition, to ensure uniformity and reproducibility of the film morphology. Cycling in 1 M H_2SO_4 was repeated until the voltammogram stabilized. A typical voltammogram for a Pt microdisc electrode is shown in Figure 2.4. The electrode was polished again if it showed unusual behaviour (distorted peaks, large current etc.).

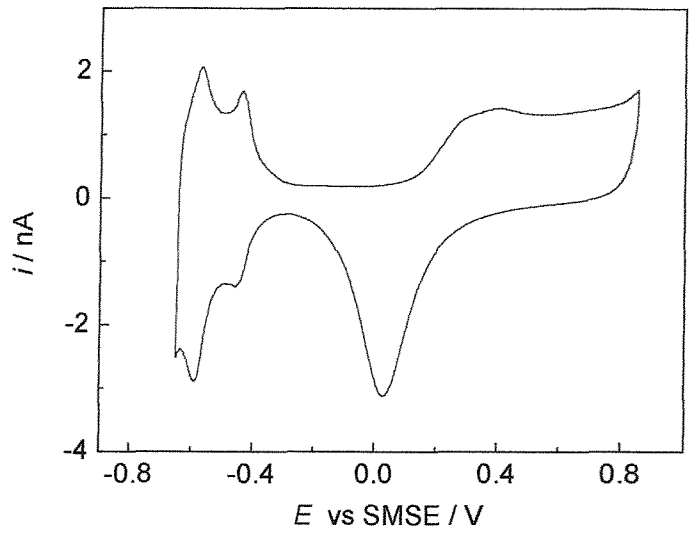

Figure 2.4. A typical cyclic voltammogram for Pt microdisc (d=25 μm) electrodes used as substrates for Pd film deposition. Test solution : 1 M H_2SO_4. Scan rate : 100 mV s^{-1}.

The Pt microdisc electrode was then removed from the 1 M H_2SO_4 solution, rinsed with purified water, and placed in the plating mixture. The deposition of the H_1-e Pd films was initiated by stepping the potential from +0.3 V to + 0.1 V versus SCE. The potential was kept constant until the desired charge was passed. The total amount of Pd was controlled by the deposition charge, which was varied between 5.5 and 44 μC. The electrode was then removed from the plating mixture, rinsed with purified water, and soaked in purified water for at least 24 hours, to remove the remaining surfactant from the surface.

2-3-3. Deposition of plain Pd films

Plain Pd films (without nanostructure) were deposited using a two-electrode system, where a 25 μm diameter Pt microdisc electrode was the working electrode and an SCE was the reference / counter electrode. The plating bath composition (40 mM $(NH_4)_2PdCl_4$) reported by Guerin[100] was employed. The same pre-treatment as described in the preceding section was applied to a 25 μm diameter Pt microdisc electrode. The electrode was then placed in the plating

bath, and the potential was stepped from +0.4 V to various deposition potentials (+ 0.1, + 0.2, + 0.3 V). After 11 μC was passed, the electrode was removed from the plating bath and rinsed with copious amount of purified water.

2-4. pH measurements with a combination pH electrode

The pH of test solutions was measured using a combination pH electrode (InLab®409, METTLER TOLEDO). In the present study, the pH values obtained with the combination pH electrode were used as standards when testing the potentiometric pH response of H_I-e Pd-hydride microelectrodes. Hence, it was crucial to have high accuracy over a wide pH range and great care was taken on pH measurements with the pH electrode.

The output of the pH electrode (potential difference between a pH sensing electrode and an internal reference electrode) was monitored with a pH meter (#320, METTLER TOLEDO). All the pH measurements were conducted at 25 °C. The output (in mV) was recorded after it reached a stable value (typically, 20 ~60 s.). The output was then converted to pH using a calibration curve, which had been obtained according to the procedure described below.

The electrode was calibrated before starting pH measurements. The combination pH electrode was placed in commercial buffer solutions (pH 1.68, 4.00, 7.00 and 10.00) thermostated at 25 °C. The output (in V) was then recorded and plotted against the buffer pH. An example of calibration curves is shown in Figure 2.5 The slope and the intercept of the calibration curve were determined from the linear regression. Linearity of the pH electrode response was excellent, where the typical r^2 value was –0.99998. From the calibration curves, pH measured with the combination pH electrode was estimated to have an error of ± 0.01 pH unit within the tested pH range (1.68 ~ 10.00).

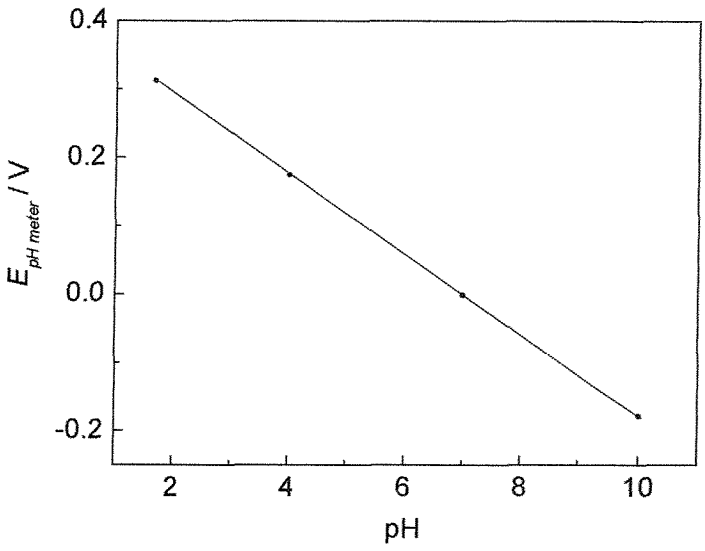

Figure 2.5. An example of calibration curve for the combination pH electrode. The potential difference between a pH sensing electrode and an internal reference electrode was measured in buffer solutions at 25 °C.

2-5. Scanning electron microscopy

A scanning electron microscope (XL30 ESEM, Philips) was used to study the surface morphology of microelectrodes. This microscope has a "wet mode" (environmental mode), which allows a gaseous atmosphere (0.1~20 Torr) in the microscope chamber, in contrast to the conventional SEMs which require high vacuum.

In "wet mode", a specially designed electron detector (GSED; gaseous secondary electron detector) provides high resolution comparable to conventional SEMs, in spite of the presence of a gas in the chamber. The detector carries a positive bias with respect to the sample, which accelerates secondary electrons from the sample surface towards the detector. The accelerated electrons ionise the gas molecules, creating additional electrons and positive ions. The electrons from this cascade are collected by the detector as an amplified secondary electron sample signal.

In this mode, the sample surface charge is neutralized by ionized gas created by

the electron beam and the detector ionization process. Since there is no charging of non-conductive specimens, sample preparation such as Au or C coatings is not necessary in this mode. This feature makes it possible to observe microelectrodes before and after electrochemical experiments.

In the present study, "wet mode" was used to observe the microelectrode surface before and after Pd film deposition. Furthermore, changes in Pd film morphology caused by lattice expansion due to hydrogen absorption in the film were studied. Scanning electron micrographs were taken under the following conditions. Accelerating voltage : 25 kV, electron detector : GSED, pressure : 0.5~0.6 Torr. The water vapour was provided from a built–in water reservoir.

Chapter 3. Deposition and characterization of Pd films

3-1. Deposition of Pd films

3-1-1. Plating mixtures

H_I-e Pd and plain Pd films were deposited on Pt microdisc electrodes, which had been polished and cleaned prior to the deposition. The detailed procedures of polishing, cleaning and deposition were described in Chapter 2. The compositions of the plating mixtures are summarized in Table 3.1.

Table 3.1. Plating mixtures for H_I-e Pd (A), H_I-e Pd (B), and Plain Pd films.

Pd films	$(NH_4)_2PdCl_4$	$C_{16}EO_8$	Brij® 56	n-heptane	Water
H_I-e Pd (A)[a]	12 wt%	47 wt%	-	2 wt%	39 wt%
H_I-e Pd (B)[a]	12 wt%	-	47 wt%	2 wt%	39 wt%
Plain Pd[b]	40 mM (11.4 g/l)	-	-	-	aqueous solution

[a] Bartlett et al[101] [b] Guerin[100]

For H_I-e Pd films, plating mixtures reported by Bartlett et al[101] were employed. As non-ionic surfactants, $C_{16}EO_8$ and Brij® 56 were used. $C_{16}EO_8$ is a highly purified and monodisperse material, while Brij® 56 is a polydisperse surfactant mixture with a distribution of headgroup sizes. Marwan[102] investigated Brij® 56 by mass spectroscopy, and reported that the major components of Brij® 56 were from $C_{16}EO_4$ to $C_{16}EO_{12}$ with $C_{16}EO_8$ as the most abundant. He also found that there was quantitative variation from batch to batch. Hence, only one batch of Brij® 56 was used in the present study.

The nanostructure of H_I-e Pd films deposited from plating mixtures, containing $C_{16}EO_8$ and having the same compositions as shown in Table 3.1, was studied by Marwan[102]. Films scraped from evaporated gold electrodes (area 1 cm^2) were

used as TEM and XRD samples. The films were reported to contain regular arrays of cylindrical pores 2.0~2.5 nm in diameter arranged in a hexagonal array with a wall thickness of about 2.0~2.5 nm. The palladium in the walls of the nanostructure was found to be polycrystalline with the expected face centred cubic structure. The grain size was estimated to be around 20 nm.
In all the plating mixtures, $(NH_4)_2PdCl_4$ was used as a palladium salt. The deposition of Pd is expected to follow the reaction :

$$[PdCl_4]^{2-} + 2e \rightarrow Pd + 4Cl^- \qquad \textit{Equation 3.1}$$

The Faradaic efficiency for H_1-e Pd film deposition from the plating mixtures shown in Table 3.1 was reported to be as high as 95~98 %[101]. In the present study, the total amount of deposited palladium was estimated assuming 98 % faradaic efficiency of the process.

3-1-2. H_1-e Pd (A) film deposition

H_1-e Pd (A) films were deposited using plating mixtures containing $C_{16}EO_8$. Figure 3.1 shows a cyclic voltammogram for a Pt microdisc electrode (d = 25 μm) in the plating mixture. On the forward sweep of the first cycle, the reduction current for Pd deposition was observed from about +0.2 V. On the reverse sweep, however, the deposition current continued to flow until about +0.25 V. In the second and the third cycles, the current was observed from about +0.25 V. In the first forward sweep, the nucleation is thought to require a high overpotential, compared to the following sweeps where relatively low overpotential was needed for the growth. This shift in deposition potential has also been observed for Pd film deposition on conventional size Au electrodes[100].
In Figure 3.1, the current was greater for the reverse (anodic) sweep than for the forward (cathodic) sweep in each cycle, and the current increased with the number of cycles. These phenomena have not been observed for Pd film deposition on conventional size Au electrodes[100]. This difference cannot be attributed to the substrate materials, since an almost identical cyclic voltammogram to Figure 3.1 was obtained for a Au microdisc electrode in the

present study. The difference was thought to be related to the small size of the electrodes.

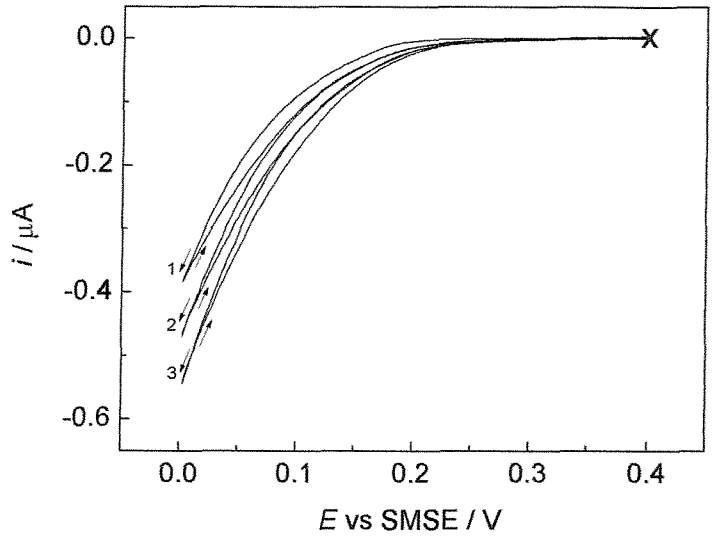

Figure 3.1. Cyclic voltammograms for a Pt microdisc (d=25 μm) electrode recorded in the H_I-e Pd (A) plating mixture (containing $C_{16}EO_8$ as a surfactant) between +0.4 V and 0.0 V at 10 mV s^{-1}. Numbers in the graph show the order of cycles.

To study whether the mass transport limiting current also increases with the number of cycles, the potential was scanned further cathodic (Figure 3.2). The limiting current appeared to be greater for the second cycle than the first cycle, suggesting that the geometric area of the microelectrode was enlarged by the Pd deposition.

Bartlett et al used the deposition potential of +0.1 V in the same plating mixuture for H_I-e Pd film deposition on conventional size Au electrodes. Figure 3.1 shows that, at this potential, the depositon current is controlled by the kinetics of the process, not by mass transport. The deposition potential of +0.1 V was, therefore, thought to be suitable also for the deposition on Pt microdisc electrodes.

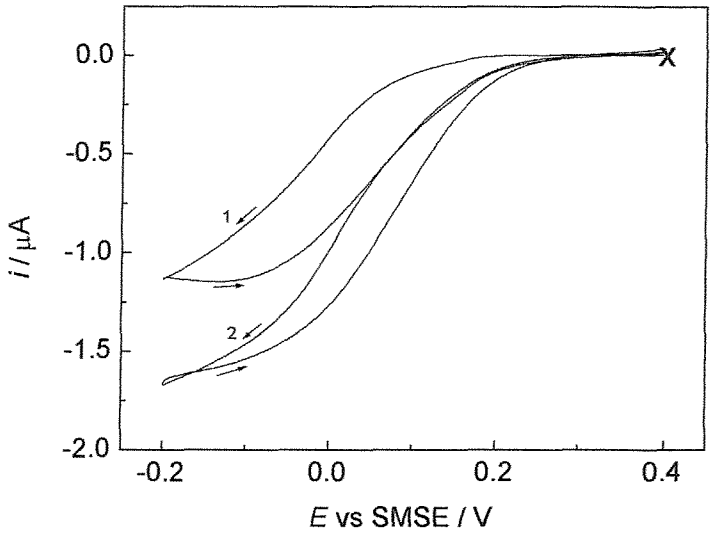

Figure 3.2. Cyclic voltammograms for a Pt microdisc (d=25 μm) electrode recorded in the H_1-e Pd (A) plating mixture (containing $C_{16}EO_8$ as a surfactant) between +0.4 V and –0.2 V at 10 mV s^{-1}. Numbers in the graph show the order of cycles.

Figure 3.3 shows a current transient recorded during H_1-e Pd (A) film deposition on a Pt microdisc (d = 25 μm) electrode. As the potential was stepped from 0.4 V, where the current was virtually zero, to the deposition potential (+ 0.1 V), the current increased rapidly and after showing a sharp peak, the current decayed to about –0.085 μA and started to increase steadily. This steady increase in current again suggests that the geometric area of the microelectrode was enlarged by the Pd deposition.

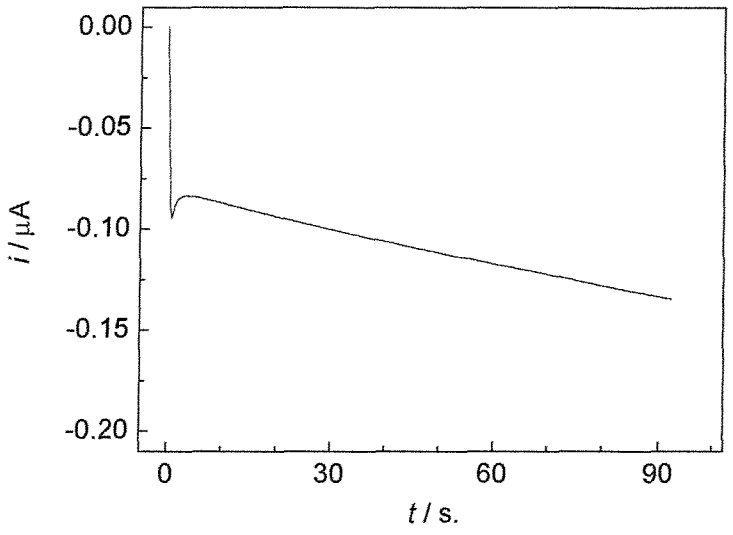

Figure 3.3. Current transient recorded during the deposition of a H1-e Pd (A) film on a Pt microdisc (d=25 μm) electrode. Potential was stepped from +0.4 V to +0.1 V at t=0. Deposition charge : 11 μC.

The change in the geometric area was confirmed by scanning electron microscopy. Figure 3.4 shows scanning electron micrographs of a Pt microdisc electrode before and after H_1-e Pd (A) film deposition. The micrographs show that the deposit was largely smooth. The edge effect characteristic of mass transport to microdiscs can be seen, where the film has a thickness larger at the edge than at the centre. The deposit has spread over the surface of the glass insulator effectively increasing the geometric surface area. The measured diameters from Figure 3.4 were 25.5 μm (before deposition) and 30.7 mm (after deposition; Q_{Dep} = 11 μC); this is equivalent to 45% geometric area increase. This reasonably agrees with the increase in the current observed in Figure 3.3; from –0.085 to –0.132 μA (55 % increase).

The edge effect is attributed to the nonuniform current density at the microdisc electrode during the deposition. The current density at the edge of the electrode is expected to be higher than at the centre and this results in a higher rate of deposition which is thought to have caused the deposit to spread over the surface of the surrounding glass. Similarly, an increase in geometric area due to the edge effect has been reported for H_1-e Pt film deposition on Pt microdisc electrodes[106, 108].

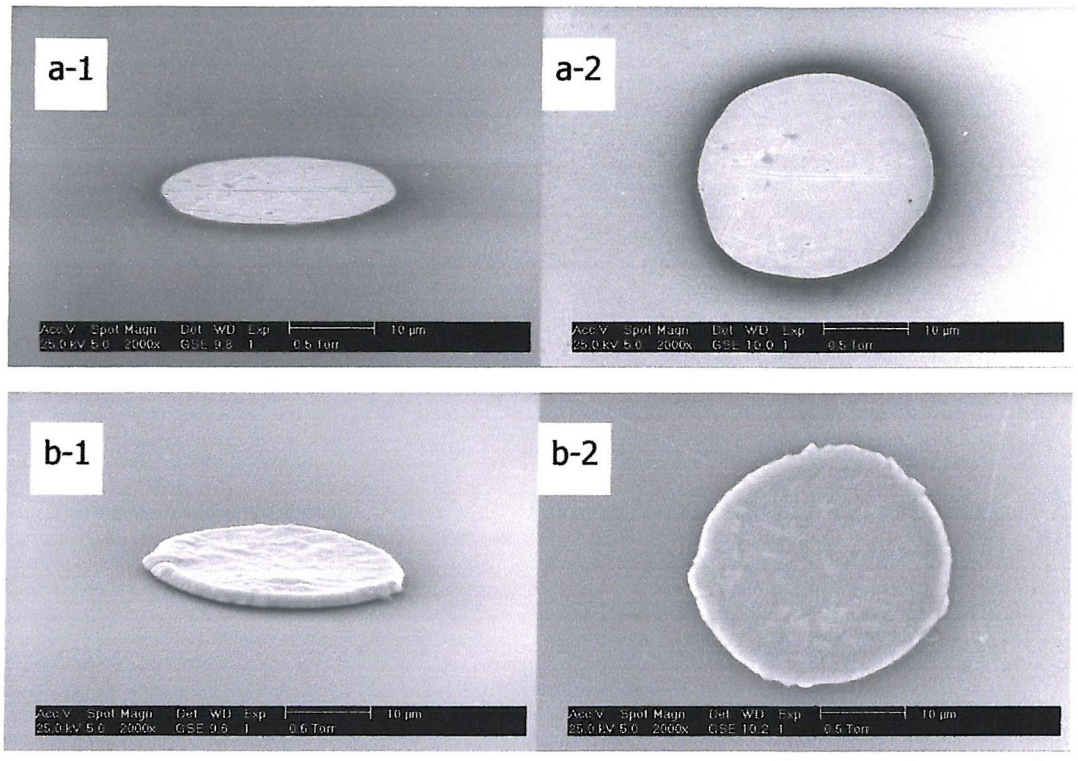

Figure 3.4. Scanning electron micrographs of a Pt microdisc (d=25 μm) electrode before and after deposition of an H_1-e Pd (A) film. (a) : Polished Pt microdisc (d=25 μm) electrode. Tilt angle (1) 70 °, (2) 0 °. (b) After depositing an H_1-e Pd (A) film (Q_{Dep} = 11 μC). Tilt angle (1) 70 °, (2) 0 °.

Marwan[102] has studied the current transient under the same conditions, using conventional size (d = 1 mm) Au electrodes as substrates. In his result, after showing a sharp peak, the current decreased slowly and tended to stabilize. The steady increase in the current found in Figure 3.3 was not observed in his study. For 1 mm diameter electrodes, the increase in geometric diameter due to the edge effect (of the order of a few micrometers) was so small compared to the original diameter, that the resulting increase in current was thought to be negligibly small.

3-1-3. H_1-e Pd (B) film deposition

Figure 3.5 shows a cyclic voltammogram for a Pt microdisc (d=25 μm) electrode recorded in the H_1-e Pd (B) plating mixture. This cyclic voltammogram showed a very similar shape to that recorded in the H_1-e Pd (A) plating mixture (Figure 3.1), although the magnitude of the current was smaller. Hence, the same deposition potential (+ 0.1 V) as that for H_1-e Pd (A) film was used for H_1-e Pd (B) film deposition.

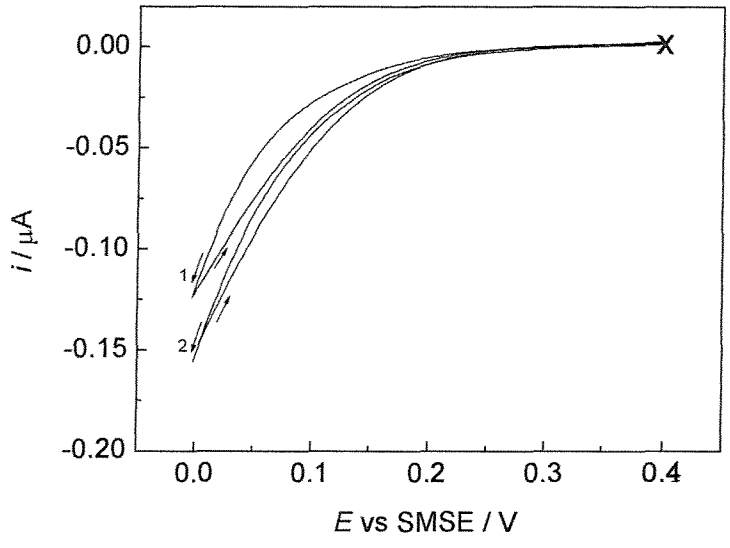

Figure 3.5. Cyclic voltammograms for a Pt microdisc (d=25 μm) electrode recorded in the H_1-e Pd (B) plating mixture (containing Brij® 56 as a surfactant) between +0.4 V and 0.0 V at 10 mV s^{-1}. Numbers in the graph show the order of cycles.

Figure 3.6 shows the current transient during the H_1-e Pd (B) film deposition on a Pt microdisc (d=25 μm) electrode. The magnitude of the deposition current was smaller than that for H_1-e Pd (A) film deposition. The difference in the magnitude of current can probably be attributed to the physical nature of the plating mixtures. At the room temperature, the plating mixture containing Brij (for H_1-e Pd (B) film) was considerably thicker than that containing $C_{16}EO_8$ (for H_1-e Pd (A) film). It was therefore difficult to avoid introducing bubbles when preparing the H_1-e Pd plating mixture containing. More inclusion of

bubbles may cause less uniform contact between the microelectrode and the plating mixture. Considering the distribution of bubbles in such a viscous paste, the contact area between the mixture and the electrode was expected to be less reproducible for H_1-e Pd (B) film deposition. In fact, the current transient recorded during H_1-e Pd (B) film deposition on different electrodes was less reproducible than that recorded during H_1-e Pd (A) film deposition.

In addition, in H_1-e Pd (B) mixture, the diffusion coefficient of $[PdCl_4]^-$ is expected to be lower than in H_1-e Pd (A) mixture because of the higher viscosity. This is another possible cause for the lower current observed during H_1-e Pd (B) deposition.

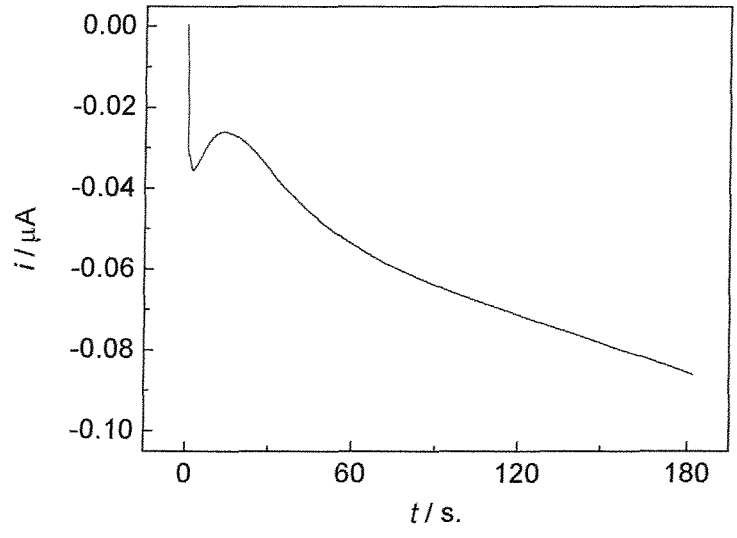

Figure 3.6. Current transient recorded during the deposition of a H1-e Pd (B) film on a Pt microdisc (d=25 μm) electrode. Potential was stepped from +0.4 V to +0.1 V at t=0. Deposition charge : 11 μC.

SEM images of a H_1-e Pd (B) film on a Pt microdisc (d=25 μm) electrode are shown in Figure 3.7. The diameter of the film (30.0 μm) was approximately the same as that for the H_1-e Pd (A) film. However, the film appeared to be rather rough, with an almost granular morphology. This can be attributed to nonuniform contact between the electrode and the plating mixture due to the

presence of bubbles. Round shaped depressions in the film are assumed to be the result of the presence of tiny bubbles in the mixture.

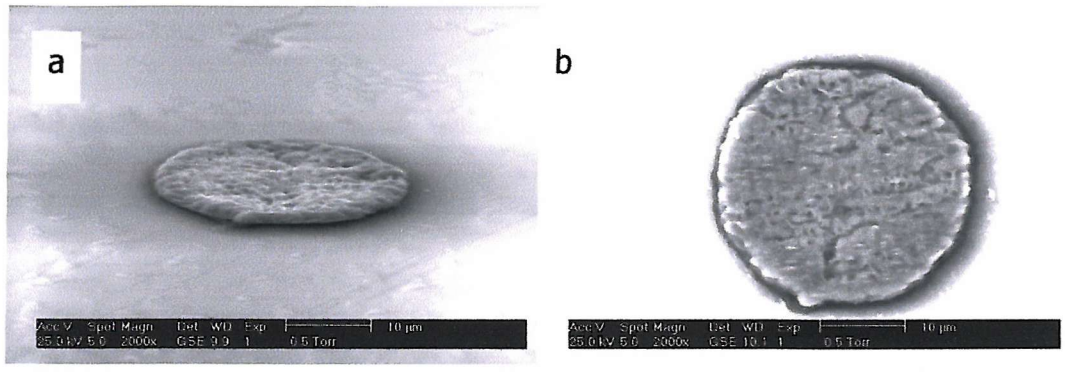

Figure 3.7 Scanning electron micrographs of an H_1-e Pd (B) film deposited on Pt microdisc (d=25 μm) electrode. Q_{Dep} = 11 μC. Tilt angle : (a) 70 °, (b) 0 °.

It should be noted that the increase in current after t = 15 s. in Figure 3.6 is larger than in Figure 3.3 (H_1-e Pd (A) film). This cannot be explained solely by the increase in the geometric area during the deposition. The increase in the contact area between the electrode and the plating mixture by surface roughening as well as geometric diameter enlargement is assumed to lead to the increase in the deposition current.

3-1-4. 'Plain' Pd film deposition

For 'plain' Pd film deposition, a simple plating bath consisting of 40 mM $(NH_4)_2PdCl_4$, reported by Guerin[100], was used. A cyclic voltammogram for a Pt microdisc (d=25 μm) electrode recorded in the plating bath is shown in Figure 3.8. The similar behaviour to H_1-e Pd film deposition was observed; namely, (a) the current was larger for the second cycle than for the first cycle, and (b) larger overpotential was required for deposition in the first scan. These can be explained again by (a) the geometric area enlargement, and (b) the difference in overpotential required for nucleation and for growth of Pd, respectively.

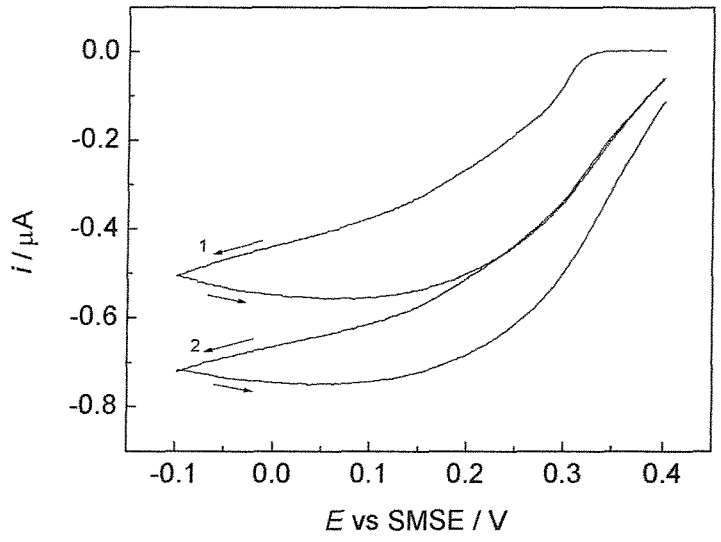

Figure 3.8 Cyclic voltammograms for a Pt microdisc (d=25 μm) electrode recorded in the plain Pd film plating bath between +0.4 V and –0.1 V at 10 mV s^{-1}. Numbers in the graph show the order of cycles.

Guerin used the deposition potential of + 0.1 V. As can be seen from Figure 3.8, however, the deposition current appeared to be mass transport limited at this potential, where non-uniform deposits were expected. Hence, in order to find a suitable potential for depositing smooth films at which the deposition is kinetically controlled, plain Pd films were deposited at several potentials (+ 0.1, + 0.2 and + 0.3 V) and the morphology of the films was studied with SEM.

The current transients during the deposition of plain Pd films on Pt microdisc (d = 25 μm) electrodes are shown in Figure 3.9. The shapes of the curves were similar to that of H_{UPD}-e Pd (A) film deposition except the transient for E_{Dep} = 0.3 V, where the current peak just after starting the deposition was not observed.

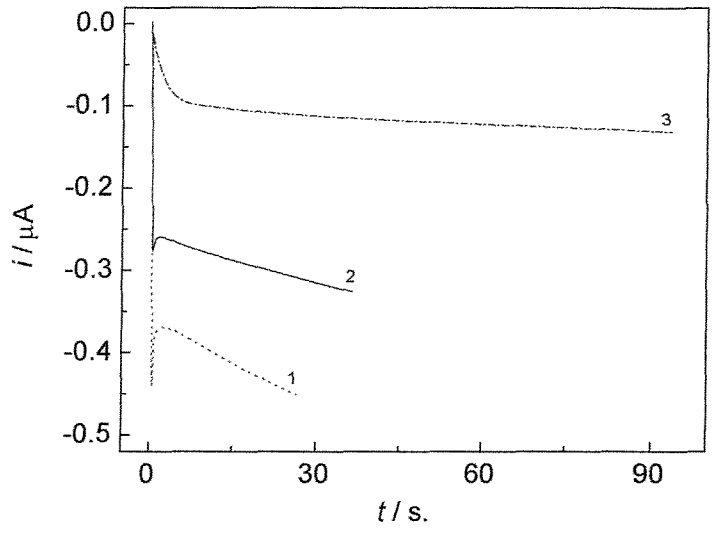

Figure 3.9 Current transients recorded during the deposition of plain Pd films on Pt microdisc (d=25 μm) electrodes. At t = 0, the potential was stepped from +0.4 V to : (1) +0.1 V (2) +0.2 V (3) +0.3 V. Deposition charge : 11 μC.

In Figure 3.10, the scanning electron micrographs of plain Pd films (E_{Dep} = + 0.1 V and + 0.3 V) are shown. An extreme edge effect was found for the deposit with E_{Dep} = + 0.1 V. Palladium appeared to be deposited mostly at the edge. This edge effect tends to be weakened at more positive potentials (less overpotentials). The plain Pd film deposited at 0.3 V was rather uniform and smooth. Hence, +0.3 V was chosen as the deposition potential for plain Pd films in the present study. The diameter of the film deposited at 0.3 V was about 29.5 μm, which was roughly the same as that of H_1-e Pd films.

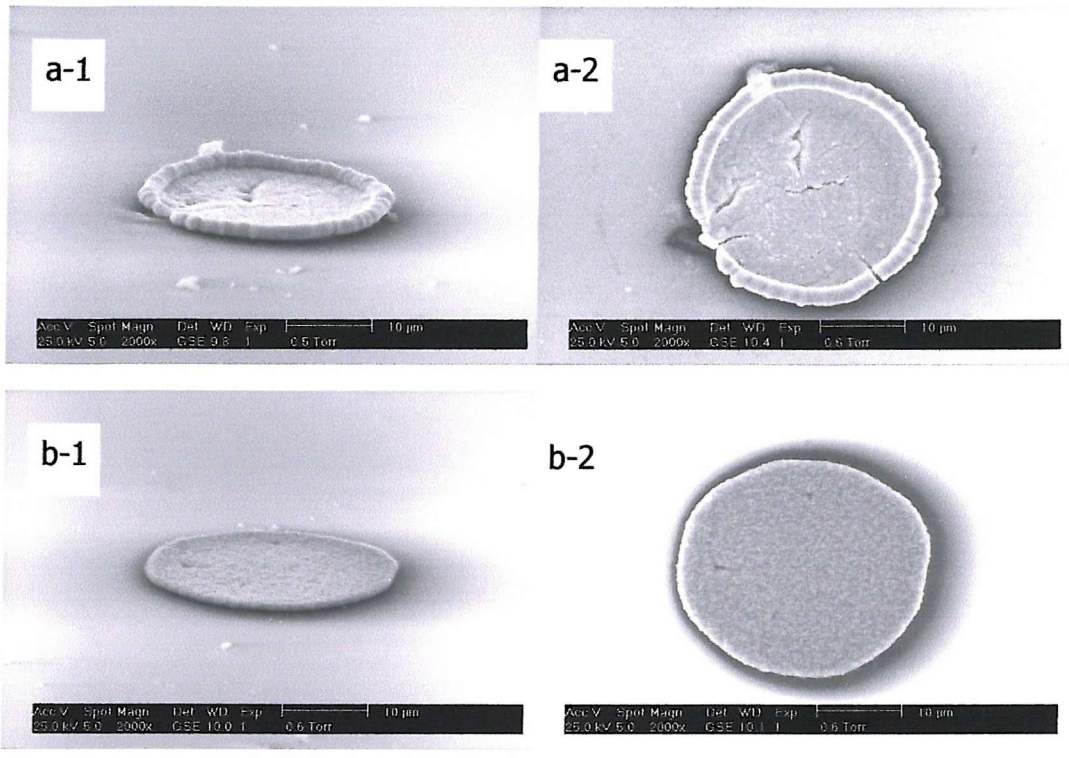

Figure 3.10 Scanning electron micrographs of plain Pd films deposited (using a plating bath without a surfactant) on Pt microdisc (d=25 μm) electrodes. (a) : Deposition potential +0.1 V. Tilt angle (1) 70 °, (2) 0 °. (b) Deposition potential +0.3 V. Tilt angle (1) 70 °, (2) 0 °.

3-2. Characterization of Pd films

3-2-1. Electroactive surface area

Cyclic voltammetry in 1 M H_2SO_4 solutions was used to study the electrochemical behaviour of Pd microelectrodes. In this section, the electroactive areas for various Pd microelectrodes were estimated from the surface oxide stripping charges observed on the voltammogram. The hydrogen reaction peaks on the voltammograms will be analysed and discussed in section 3-3.

Figure 3.11 shows the first 5 cyclic voltammograms at 20 mV s^{-1} for a freshly prepared H_1-e Pd (B) film on a 25 μm diameter Pt microdisc. The electrode was soaked in water for 48 hours to dissolve the remaining plating mixture after the

deposition, rinsed with purified water, then transferred to a 1 M H_2SO_4 solution where the voltammetry was performed. The features of the voltammograms were very similar to those seen for conventional size H_1-e Pd films[101].

The surface oxide formation began in the anodic sweep from about +0.1 V. On the return, this surface oxide was removed in the cathodic sweep, giving rise to the sharp stripping peak at about +0.01 V. The peaks in the voltammetry at the potentials below –0.4 V. are associated with hydrogen reactions and will be discussed in section 3-3.

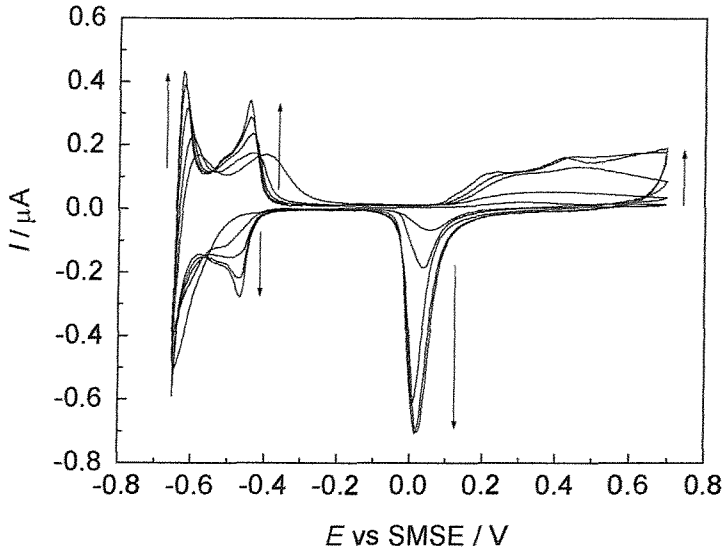

Figure 3.11. First 5 cycles of cyclic voltammograms for an H_1-e Pd (B) film on Pt microdisc (d=25 μm) electrodes at 20 mV s^{-1} in 1 M H_2SO_4. The film was soaked in water for 48 hours then transferred to 1 M H_2SO_4. Q_{dep} : 44 μC.

The currents for formation and stripping of the surface oxide increased with each successive cycle, in the first five cycles. This indicates that the electroactive area increased by cycling. According to Bartlett et al[101], this occurs as the surfactant, originally in the pores within the H_1-e Pd film, is replaced by the 1 M H_2SO_4 solution. As a result the total surface area of palladium in contact with the solution increased. After five cycles, the

voltammogram stabilized and further cycling did not produce an increase in the currents, indicating that the removal of the surfactant was completed.

Very small currents for surface oxide formation / stripping in the first cycle suggest that most of the surfactant in the pores was not removed by the 48-hour soaking in purified water prior to the cyclic voltammogram. For the films with the same thickness (Q_{Dep} = 44 μC), longer soaking up to 168 hours did not cause appreciable change in the number of cycles needed for the current to stabilize, while more cycles were needed for thicker films.

Palladium is known to dissolve[101, 112, 113] in the potential range where the surface oxide formation takes place, in acidic solutions. This is one reason the oxide stripping charge is often used as a measure of the real surface area of palladium electrodes, as opposed to the oxide formation charge. In order to avoid significant degradation of the nanostructure of the H_1-e Pd films caused by this dissolution, freshly prepared films were used in every experiment in the present study. Before each experiment, a freshly prepared H_1-e Pd microelectrode was cycled between –0.65 V and + 0.70 V in 1M H_2SO_4 solutions until the cyclic voltammogram stabilised. Care was taken to avoid unnecessary cycling in the oxide formation potential range.

Figure 3.12 shows the cyclic voltammograms for a 25 μm diameter polished Pt microdisc electrode and H_1-e Pd (B) films with different deposition charges. It can be seen that the current was more than two orders of magnitude greater for H_1-e Pd films than for the polished Pt microdisc electrode in the whole potential range. This demonstrates that the current from the substrate (Pt microdisc) is negligible when electrochemical properties of H_1-e Pd films are studied, even if the substrate is not completely covered with the film. In fact, an H_1-e Pd (B) film deposited on a 25 μm diameter Au microdisc electrode showed an identical voltammogram to Figure 3.12 (line 2), confirming that the current from the substrate does not affect the overall response.

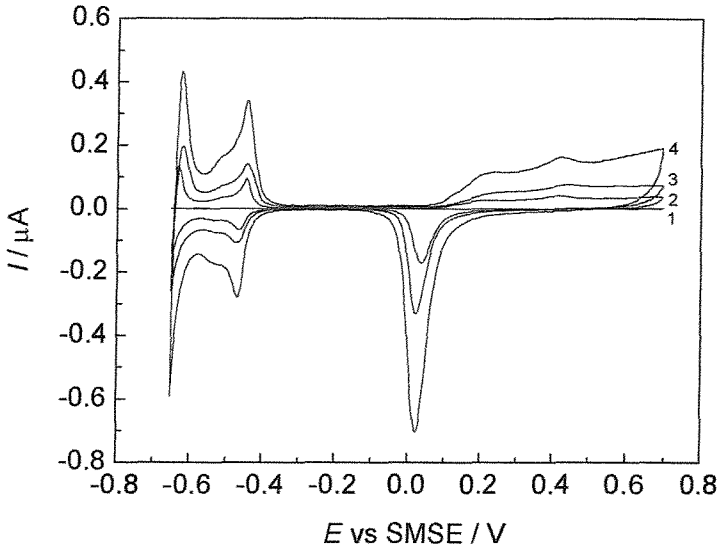

Figure 3.12. Cyclic voltammograms in 1 M H_2SO_4 at 20 mV s^{-1}. (1) a polished Pt microdisc (d=25 μm) electrode; (2)~(4) H_1-e Pd (B) films on Pt microdisc (d=25 μm) electrodes, deposition charge : 11, 22, 44 μC.

For H_1-e Pd films, the height of each peak in Figure 3.12 increased with the deposition charge. By increasing the deposition charge of H_1-e Pd films, both the amount of Pd deposited and the electroactive area of the film were expected to increase. The electroactive area was estimated from the charge under the surface oxide stripping peak on the voltammogram. The surface oxide formation and stripping behaviour of polycrystalline palladium in 1 M sulphuric acid has been studied by Rand and Woods[112, 114]. The electroactive area was calculated using their conversion factor of 424 μC cm^{-2} for the surface oxide stripping peak. In this calculation, it is assumed that one oxygen atom per surface palladium atom is adsorbed on a (100) plane. The results for various palladium microelectrodes are summarized in Table 3.2.

Table 3.2. Estimated electroactive areas for various microelectrodes

Electrode type	Substrate		Deposition of films			Results from CVs in 1 M H_2SO_4		
	Material	Nominal diameter / μm	Surfactant	Charge Q_{Dep} / μC	Charge density / C cm^{-2}	Oxide stripping charge[a] $Q_{Str}(Ox)$ / μC	Electroactive area[b] / 10^{-3} cm^2	Specific surface area / m^2 g^{-1}
Polished Pt	Pt	25	-	-	-	-	0.013[c]	-
H1-e Pd(A) film	Pt	25	$C_{16}EO_8$	11	2.2	1.51	3.6	58.8
	Pt	25	$C_{16}EO_8$	22	4.5	2.84	6.7	55.2
	Pt	25	$C_{16}EO_8$	44	9.0	5.20	12.3	50.6
H1-e Pd(B) film	Pt	25	Brij® 56	5.5	1.1	0.37	0.87	28.5
	Pt	25	Brij® 56	11	2.2	0.76	1.8	29.5
	Pt	25	Brij® 56	22	4.5	1.27	3.0	24.7
	Pt	25	Brij® 56	44	9.0	2.76	6.5	26.8
	Pd	25	Brij® 56	11	2.2	0.73	1.7	28.4
	Pt	10	Brij® 56	1.8	2.2	0.105	0.25	25.5
Plain Pd film	Pt	25	-	11	2.2	0.015	0.035	-
Polished Pd	Pd	25	-	-	-	0.0043	0.010	-

[a] Q_{Str} values are averages of two different electrodes

[b] Electroactive areas were calculated using the conversion factor of 424 μC cm^{-2}.

[c] Electroactive area of the polished Pt microdisc electrode was calculated from hydrogen adsorption/desorption charges, using the conversion factor of 210 μC cm^{-2} [115].

H_1-e Pd films were confirmed to possess very large electroactive areas compared to plain Pd films and polished palladium microdisc electrodes. The calculated electroactive surface areas for H_1-e Pd (A) and H_1-e Pd (B) films are plotted against the Q_{Dep} in Figure 3.13. The electroactive area for both H_1-e Pd (A) and H_1-e Pd (B) films appears to be approximately proportional to the Q_{Dep}. This indicates that H_1-e Pd films have a uniform nanostructure regardless of the thickness, and that the pores are accessible to the solutions throughout the film.

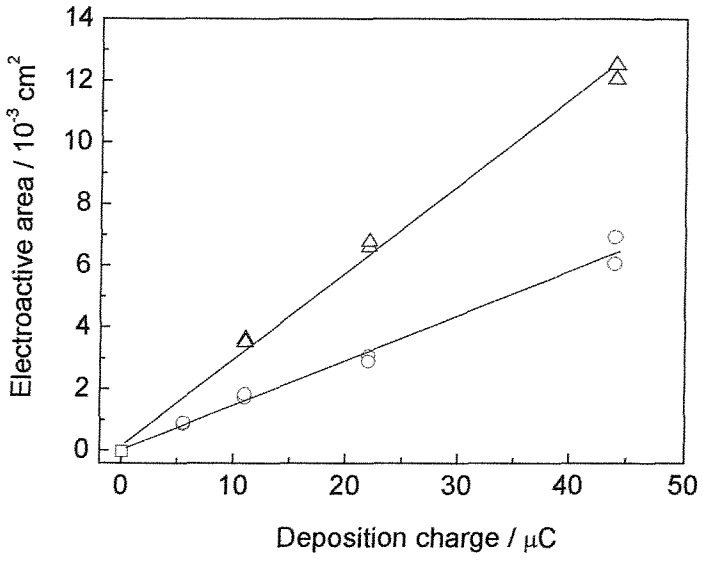

Figure 3.13. Effect of deposition charge on the electroactive area. Values were estimated using surface oxide stripping charges from cyclic voltammograms in 1 M H_2SO_4 at 20 mV s^{-1}. □, polished Pt microdisc (d=25 μm) electrodes; △, H_1-e Pd films deposited using $C_{16}EO_8$; ○, H_1-e Pd films deposited using Brij® 56

It should also be noted that for the same Q_{Dep}, H_1-e Pd (A) films have almost twice the electroactive area of H_1-e Pd (B) films. This difference is not attributed to a difference in the amount of deposited Pd (corresponding to the Faradaic efficiency of the deposition), since there was no appreciable difference found in the amount of hydrogen absorbed into H_1-e Pd (A) and H_1-e Pd (B) films. This will be discussed in Chapter 4. The difference in the electroactive area between H_1-e Pd (A) and H_1-e Pd (B) films is, therefore, attributed to the nanostructure of the films, which is determined by the liquid crystalline phases formed by surfactants in the plating mixtures.

Marwan[102] studied the nanostructure of H_1-e Pd films deposited on evaporated gold electrodes (area 1 cm^2) by TEM and XRD, and compared the films deposited using two different surfactants, $C_{16}EO_8$ and Brij® 56. He reported that the nanostructure was more uniform and the continuity of the pores were better for H_1-e Pd films deposited from the plating mixture containing $C_{16}EO_8$. This result was reasonable since $C_{16}EO_8$ is a highly purified and monodisperse material, while Brij® 56 is a polydisperse surfactant mixture[102]. In the present

study, the electroactive area of H_1-e Pd (B) films was smaller than that of H_1-e Pd (A) film, presumably because of the irregular nanostructure of H_1-e Pd (B) films.

Also shown in Table 3.2 are specific surface areas in $m^2\ g^{-1}$. These values were calculated on the assumption that faradaic efficiency for deposition of the H_1-e Pd films was 98 %. The estimated specific surface areas of around 50~60 $m^2\ g^{-1}$ for H_1-e Pd (A) films reasonably agree with the calculated value (36~60 $m^2\ g^{-1}$) for the nanostructure (pore diameter : 2.0~2.5 nm, wall thickness : 2.0~2.5 nm) found by TEM and XRD, for H_1-e Pd films deposited from plating mixture containing $C_{16}EO_8$.

Table 3.2 also show that the specific surface area ($m^2\ g^{-1}$) depends on the surfactant ($C_{16}EO_8$ or Brij) contained in the plating mixture, but not on the material (Pt or Pd), size (d = 10 or 25 μm) of the substrate electrode or the Q_{Dep} of the film. This confirms that H_1-e Pd films possess a nanostructure unique to the surfactants and that the entire film is nanostructured with the pores throughout the film accessible to the electrolyte solution.

3-2-2. Geometric diameter

In section 3-1, the geometric area of microelectrodes appeared to be enlarged by the Pd film deposition procedure, owing to the edge effect. In order to study the change in the geometric characteristic caused by the H_1-e Pd film deposition, steady state voltammetry was performed in a deaerated 10 mM $Ru(NH_3)_6Cl_3$, 0.2 M KCl solution for the reduction of $[Ru(NH_3)_6]^{3+}$:

$$[Ru(NH_3)_6]^{3+} + e \rightarrow [Ru(NH_3)_6]^{2+} \qquad \textit{Equation 3.2}$$

This reaction was chosen because it is a fast one-electron redox process and $[Ru(NH_3)_6]^{3+}$ does not adsorb readily on the electrode surface.

The limiting current for a microdisc electrode is given by :

$$i_L = 4nFDca \qquad \textit{Equation 3.3}$$

where n is the number of electrons transferred, F is the Faraday constant, D is the diffusion coefficient, c is the concentration of the redox species, and a is the radius of the microdisc. To estimate D for $[Ru(NH_3)_6]^{3+}$, preliminary experiments were performed using polished Pt microdisc electrodes of 10, 25 and 50 μm diameters in the same solution. The limiting current, i_L, for each electrode, obtained from steady state voltammograms, was plotted against the radius, a, and D was determined from the slope of the plot. D was found to be ~8.8 × 10^{-6} cm^2 s^{-1}, which is close to the value (8.0 × 10^{-6} cm^2 s^{-1})[116] reported previously for $[Ru(NH_3)_6]^{3+}$ in 0.1 M NaCl.

Figure 3.14 shows the voltammograms of H_1-e Pd films with different Q_{Dep} on 25 μm diameter Pt microdisc electrodes, in a deaerated 10 mM $Ru(NH_3)_6Cl_3$, 0.2 M KCl solution. An extremely slow scan rate of 2 mV s^{-1} had to be used in this experiment because of the large double-layer charging current due to the massive electroactive area of H_1-e Pd films. The charging current increased with the deposition charge (Q_{Dep}) because of the increase in the electroactive area.

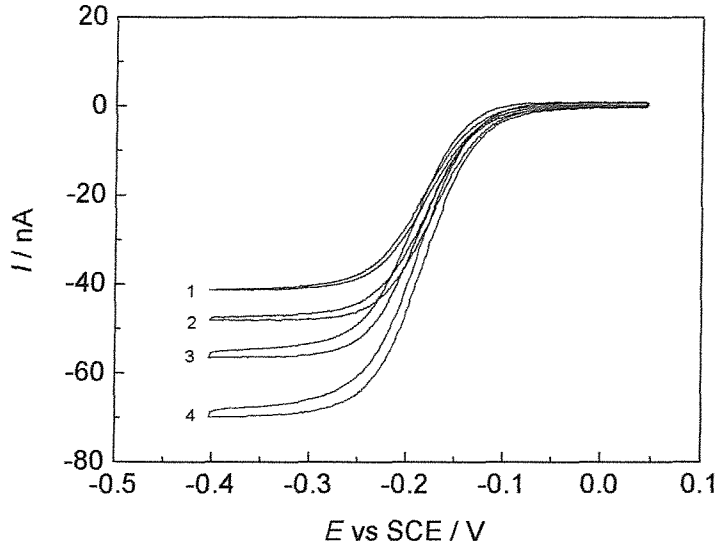

Figure 3.14. Steady state voltammograms for (1) a polished Pt microdisc electrode and (2)~(4) H_1-e Pd (B) films deposited on Pt microdisc (d=25 μm) electrodes, recorded at 2 mV s^{-1} in a deaerated 10 mM $Ru(NH_3)_6Cl_3$, 0.2 M KCl solution at 25 °C. Deposition charges of H_1-e Pd (B) films : (2) 11μC; (3) 22 μC; (4) 44 μC

The reduction current for the redox species clearly increases with the Q_{Dep}. Since the limiting current of microdisc electrodes is proportional to the radius of the microdisc via Equation 3.3, the increase in the current indicates that the geometric diameter increased with Q_{Dep}.

The effective geometric diameter ($d = 2a$) was calculated for various Pd microelectrodes by substituting the limiting currents (i_L) to Equation 3.3, and the results are shown in Table 3.3.

Table 3.3. Effective diameters estimated from limiting currents for $[Ru(NH_3)_6]^{3+}$ reduction

Electrode type	Substrate		Deposition of films			Results from voltammograms	
	Material	Nominal diameter / μm	Surfactant	Charge Q_{Dep} / μC	Charge density / C cm^{-2}	Limiting current[a] i_L / nA	Effective diameter / μm
Polished Pt	Pt	25	-	-	-	43.0	25.3
H1-e Pd(A) film	Pt	25	$C_{16}EO_8$	11	2.2	50.8	29.9
	Pt	25	$C_{16}EO_8$	22	4.5	59.8	35.2
	Pt	25	$C_{16}EO_8$	44	9.0	71.6	42.2
H1-e Pd(B) film	Pt	25	Brij® 56	5.5	1.1	45.0	26.5
	Pt	25	Brij® 56	11	2.2	51.4	30.3
	Pt	25	Brij® 56	22	4.5	58.3	34.3
	Pt	25	Brij® 56	44	9.0	71.8	42.3
	Pd	25	Brij® 56	11	2.2	50.7	29.9
	Pt	10	Brij® 56	1.8	2.2	23.6	13.9
Plain Pd film	Pt	25	-	11	2.2	50.0	29.4
Polished Pd	Pd	25	-	-	-	42.5	25.0

[a] i_L *values are averages of two different electrodes.*

The effective geometric diameters estimated from the steady state voltammograms were around 30 μm for H1-e Pd (A), H1-e Pd (B), and plain Pd films with Q_{Dep} of 11 μC. This result agrees well with the SEM studies, presented in section 3-1. This agreement confirms the appropriateness of using the steady state voltammogram to estimate the geometric diameter.

The increase in the effective geometric diameter was found to occur with all the Pd films deposited on microdisc electrodes in this study, including plain Pd films, regardless of the substrate diameter and the substrate material. Shown in Figure 3.15 is the geometric diameter as a function of Q_{Dep}, for H_1-e Pd films deposited from plating baths containing different surfactants; (A) $C_{16}EO_8$ and (B) Brij. The geometric diameter increases linearly with Q_{Dep}, and no appreciable difference is found between H_1-e (A) and H_1-e (B) Pd films.

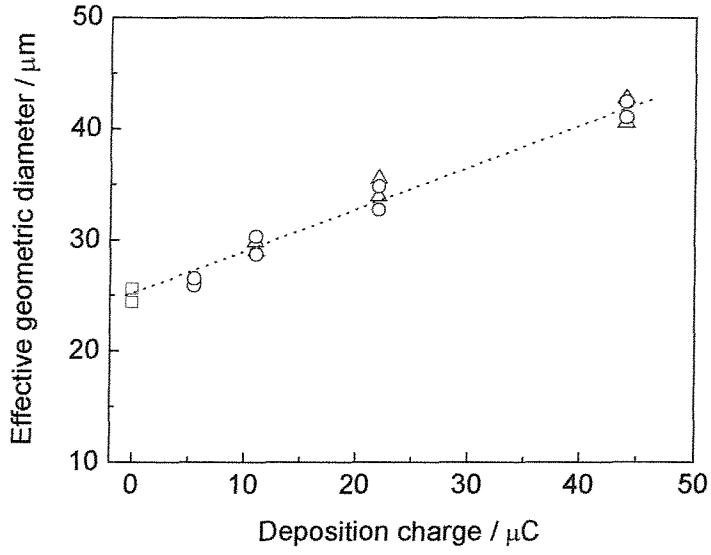

Figure 3.15. Effect of deposition charge on the effective diameter. Values were estimated using limiting currents for $[Ru(NH_3)^6]^{3+}$ reduction. □, polished Pt microdisc (d=25 μm) electrodes; △, H_1-e Pd films deposited using $C_{16}EO_8$; ○, H_1-e Pd films deposited using Brij® 56.

3-2-3. Roughness factor and thickness

The roughness factor (R_F) is a ratio of the electroactive area to the geometric area of the electrode and is widely employed to compare electrodes with different dimensions. For the microelectrodes used in the present study, R_F values were calculated using the electroactive area (Table 3.2) and the geometric diameter

(Table 3.3) obtained in the previous sections, and are shown in Table 3.4. The R_F values for H_1-e Pd films ranged from 157 to 877 depending on the thickness (Q_{Dep}) and the surfactants. These values are far greater than polished Pd microdisc (R_F = 2.1) and normal Pd film (R_F = 5.2) electrodes. Comparing the films with the same Q_{Dep} (= 11 μC), R_F values of H_1-e Pd (A) and H_1-e Pd(B) films were greater than those of plain Pd films by 100 times and 50 times respectively. The average thickness was calculated using the geometric surface area estimated in the preceding section, assuming the Faradaic efficiency of the deposition was 98 %. The average thickness of the microelectrodes used in the present study, which is also shown in Table 3.4, ranged from 0.6 to 1.9 μm.

The films mainly used in the experiments shown in the later chapters are the H_1-e Pd films with Q_{Dep} of 11 μC. They were about 30 μm in diameter and about 1 μm in thickness, with roughness factors of about 508 (H_1-e Pd (A) film) or 248 (H_1-e Pd (B) film).

Table 3.4. Estimated values of the roughness factor and the average film thickness

Electrode type	Substrate		Deposition of films			Experimental results		Calculated parameters	
	Material	Nominal diameter / μm	Surfactant	Charge Q_{Dep} / μC	Charge density / C cm^{-2}	Electroactive area / 10^{-3} cm^2	Geometric surface area / 10^{-3} cm^2	Roughness factor R_F	Average thickness / μm
Polished Pt	Pt	25	-	-	-	0.013	0.0050	2.6	-
H1-e Pd(A) film	Pt	25	$C_{16}EO_8$	11	2.2	3.6	0.0070	508	0.9
	Pt	25	$C_{16}EO_8$	22	4.5	6.7	0.0097	688	1.4
	Pt	25	$C_{16}EO_8$	44	9.0	12.3	0.0140	877	1.9
H1-e Pd(B) film	Pt	25	Brij® 56	5.5	1.1	0.87	0.0055	157	0.6
	Pt	25	Brij® 56	11	2.2	1.8	0.0072	248	0.9
	Pt	25	Brij® 56	22	4.5	3.0	0.0092	324	1.4
	Pt	25	Brij® 56	44	9.0	6.5	0.0141	463	1.9
	Pd	25	Brij® 56	11	2.2	1.7	0.0070	242	0.9
	Pt	10	Brij® 56	1.8	2.2	0.25	0.0015	163	0.7
Plain Pd film	Pt	25	-	11	2.2	0.035	0.0068	5.2	0.7
Polished Pd	Pd	25	-	-	-	0.010	0.0049	2.1	-

3-3. Hydrogen reactions in 1 M H_2SO_4 solution

3-3-1. H_1-e Pd film on Pt microdisc

In this section, hydrogen reactions on H_1-e Pd films in 1 M H_2SO_4 solutions are studied by analysing cyclic voltammograms.

In Figure 3.16, a cyclic voltammogram in 1 M H_2SO_4 for an H_1-e Pd (B) film is compared with that for a plain Pd film with the same Q_{Dep}. The overall shapes of the cyclic voltammograms are almost identical to the results obtained with Pd films on conventional size Au electrodes, reported by Bartlett et al[101]. Several striking differences can be seen between the H_1-e Pd and the plain Pd films.

First, surface oxide formation / stripping currents are much larger for the H_1-e Pd film than for the plain Pd, while the formation and stripping processes occur at the same potentials for the two films. This difference arises because the H_1-e Pd film has a significantly larger electroactive area owing to the presence of the nanostructure.

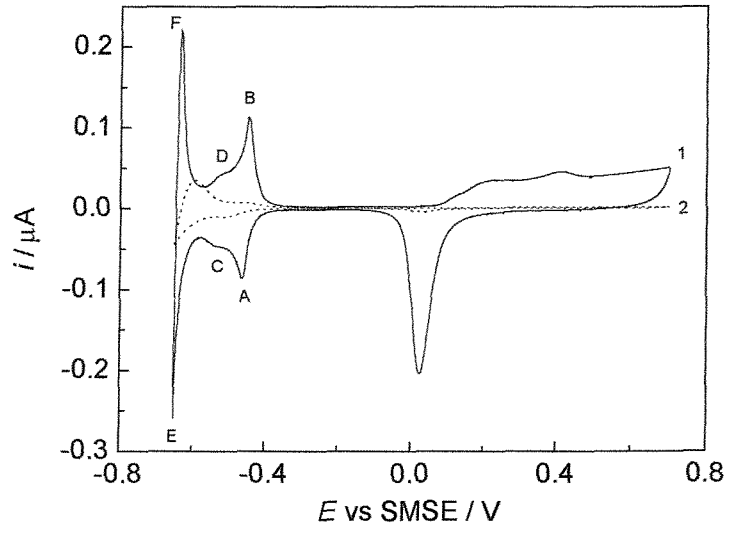

Figure 3.16. Cyclic voltammograms for Pd films (Q_{Dep} = 11 μC) on 25 μm diameter Pt microdisc electrodes, in 1 M H_2SO_4 at 20 mV s^{-1}; (1) an H_1-e Pd (B) film (2) a plain Pd film.

At potentials below –0.4 V, the H_I-e Pd film exhibited three pairs of reduction / oxidation waves (A/B, C/D and E/F). In contrast, voltammetry of the plain Pd film in this potential range is broad and unresolved. Figure 3.17 shows a cyclic voltammogram for a polished Pd microdisc electrode in 1 M H_2SO_4, together with the cyclic voltammogram for the plain Pd film (the same voltammogram as shown in Figure 3.16). The cyclic voltammogram of the polished Pd microdisc was even less resolved than that for the plain Pd film in the cathodic potential range, where only one wave of cathodic current and one peak for anodic current were seen. The observation of well resolved peaks in the cyclic voltammogram for the H_I-e Pd film is believed to arise because of the presence of the nanostructure.

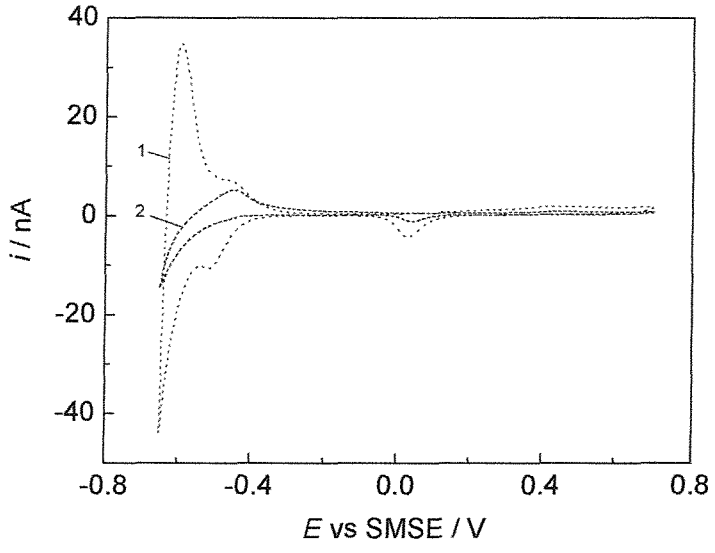

Figure 3.17. Cyclic voltammograms in 1 M H_2SO_4 at 20 mV s^{-1}. (1) a Plain Pd film (Q_{Dep} = 11 μC) on 25 μm diameter Pt microdisc electrode (2) a Pd microdisc electrode.

The peaks in the cathodic potential range in a voltammogram for an H_I-e Pd film on a conventional size Au electrode were analysed in detail by Bartlett et al[101]. The well resolved sharp pair of peaks (A/B) for the H_I-e Pd film in Figure 3.16 was reported to correspond to the formation and removal of adsorbed hydrogen.

The remaining two pairs of peaks (C/D and E/F) are associated with absorption/stripping of hydrogen. They are reported to correspond to the α-phase formation and the start of the β-phase formation, respectively. In contrast to plain Pd films and polished Pd microdiscs, the peaks for adsorption and absorption of hydrogen were readily distinguished in the case of H_1-e Pd films, owing to the very high surface to volume ratio.

To study the β-phase formation in more detail, the potential was scanned to more negative values and the resulting voltammogram is shown in Figure 3.18. The formation / oxidation of the β-phase (E/F in Figure 3.16) produced two large peaks.

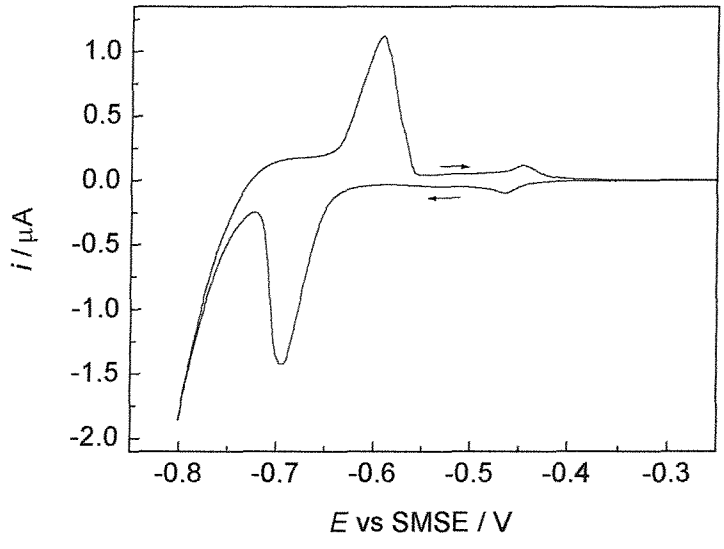

Figure 3.18 Cyclic voltammogram for an H_1-e Pd (B) film (Q_{Dep} = 11 μC) on a 25 μm diameter Pt microdisc electrode, in 1 M H_2SO_4 at 20 mV s^{-1}. Although the potential was scanned between –0.8 V and +0.7 V, only the results for the potential range between –0.8 V and –0.25 V is shown.

To estimate the amount of hydrogen absorbed in the Pd film, the anodic current was integrated in the potential range below –0.47 V (anodic current in the potential range of –0.47 ~ –0.40 V was assumed to be due to desorption of adsorbed hydrogen). The charge was found to be 3.49 μC. This charge can be converted to the H/Pd ratio using the Q_{Dep} together with the assumption that the

faradaic efficiency for the deposition was 98 %. The H/Pd ratio was estimated to be 0.65, which indicates that the film was loaded with hydrogen to form the β-palladium hydride phase.

On the other hand, the cathodic charge (total for cathodic and anodic scans) in the potential range below –0.49 V was found to be –8.87 μC, which is far greater than the anodic charge. This difference implies that the cathodic charge includes the charge for hydrogen gas evolution, as well as that for hydrogen absorption into the Pd film. Between –0.723 and –0.49 V, the cathodic charge was found to be 3.37 μC, which reasonably agrees with the oxidation charge of 3.49 μC. This indicates that the large cathodic current observed below –0.723 V corresponds mainly to hydrogen gas evolution.

3-3-2. H_1-e Pd film on Pd microdisc

The effect of the substrate material on the voltammetric response of H_1-e Pd films was studied. As stated earlier, H_1-e Pd films on Pt microdisc and Au microdisc electrodes showed identical voltammograms in 1 M H_2SO_4, which confirmed that the influence of the current from the substrate is negligible. It is expected, however, that Pd microdisc substrates will affect the voltammetric response of H_1-e Pd films by causing the diffusion of absorbed hydrogen from the film into the substrate. Figure 3.19 shows a cyclic voltammogram for an H_1-e Pd (B) film deposited on a 25 μm diameter Pd microdisc electrode in 1 M H_2SO_4.

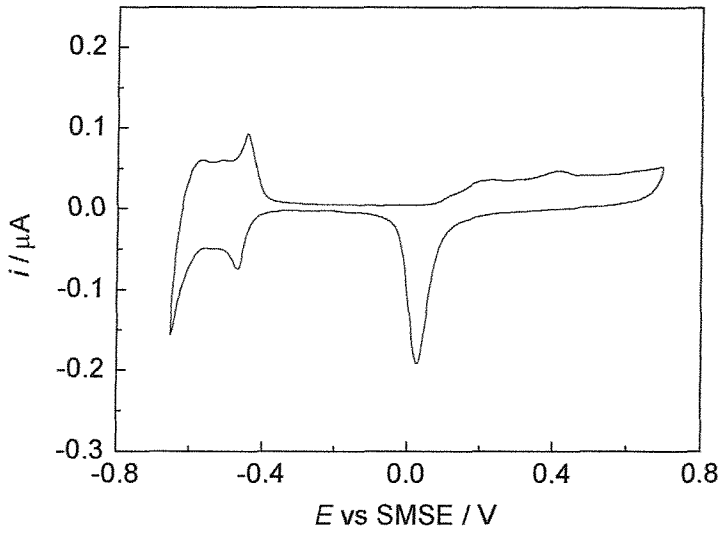

Figure 3.19. Cyclic voltammogram for an H_1-e Pd (B) film on a 25 μm diameter Pd microdisc electrode in 1 M H_2SO_4 at 20 mV s^{-1}.

Comparing this with the voltammogram for an H_1-e Pd (B) film on a Pt microdisc electrode (Figure 3.16), a marked difference is found for the anodic sweep in the potential range below –0.55 V. The anodic current corresponding to the oxidation of absorbed hydrogen (β-phase) in this potential range is substantially smaller for the H_1-e Pd film on the Pd microdisc than on the Pt microdisc. For the H_1-e Pd film on a Pd microdisc, the anodic charge for the oxidation of absorbed hydrogen is evidently smaller than the cathodic charge for absorption of hydrogen. This result indicates that not all the hydrogen atoms absorbed in the Pd film were oxidized in the reverse scan, presumably because of the diffusion of hydrogen into the substrate.

Although a notable difference in hydrogen absorption/stripping behaviour was found between H_1-e Pd films on Pd microdisc and Pt microdisc electrodes, no evident difference was found for hydrogen adsorption/desorption or surface oxide formation/stripping behaviour.

3-4. Summary

Overview

In this chapter, H_I-e Pd films were deposited using plating mixtures whose behaviour had been investigated for deposition on conventional size Au electrodes. The films deposited on microdisc electrodes were then characterized electrochemically. These films were confirmed to possess very large electroactive areas, indicating the presence of the desired nanostructure.

Deposition behaviour

The current for H_I-e Pd and plain Pd film deposition appeared to increase as the deposition proceeded. This is unique to the deposition on microelectrodes. Since the limiting current for the process was found to increase, it was assumed that the geometric diameter was enlarged during the deposition. As expected, SEM and steady state voltammetry revealed that the diameter was enlarged by the deposition. The edge effect was clearly seen, where the film thickness was larger at the edge than at the centre of the film. The increase in the diameter is believed to result from nonuniform current distribution. This edge effect worsened when the process was mass transport controlled.

H_I-e Pd (B) films were found by SEM to be rather rough, compared to H_I-e Pd (A) films. This is thought to result from the presence of more bubbles in the H_I-e Pd (B) plating mixture, due to the high viscosity of the mixture.

Characterization

The roughness factor, R_F, for H_I-e Pd films was 157~877 depending on the thickness (Q_{Dep}) and the surfactants; this is far greater than that for polished Pd microdiscs ($R_F \sim 2.1$). Comparing the films with the same Q_{Dep}, R_F values for H_I-e Pd (A) and H_I-e Pd(B) films were greater than those of plain Pd films by factors of circa 100 and 50 respectively.

It was shown that H_I-e Pd (A) films had almost twice the Electroactive areas of H_I-e Pd (B) films. This presumably reflects the difference in the nanostructure, which is determined by the liquid crystalline phases formed by surfactants in the plating mixture. Taking into account the nanostructure of H_I-e Pd films on conventional size Au electrodes previously studied by Marwan, H_I-e Pd (B) films were assumed to possess less uniform nanostructure.

The estimated specific surface areas of around 50~60 $m^2\ g^{-1}$ for H_I-e Pd (A) films reasonably agree with the calculated value (36~60 $m^2\ g^{-1}$) for the nanostructure (pore diameter : 2.0~2.5 nm, wall thickness : 2.0~2.5 nm) reported by Marwan. The specific surface area ($m^2\ g^{-1}$) was found to depend on the surfactant ($C_{16}EO_8$ or Brij), but not on the material, size of the substrate electrode or the Q_{Dep} of the film. This confirms that H_I-e Pd films possess a nanostructure unique to the surfactants and that the entire film is nanostructured with the pores throughout the film being accessible to the solution.

Hydrogen reactions in 1 M sulphuric acid

In contrast to plain Pd films and polished Pd microdiscs, the peaks for adsorption and absorption of hydrogen were readily distinguished in the case of H_I-e Pd film, owing to the very high surface to volume ratio. In the cyclic voltammetric studies, H_I-e Pd films on Pt microdiscs were readily loaded with hydrogen to β-phase and all the hydrogen was oxidized on the anodic sweep. Therefore, it is possible to estimate the absolute H content in the film. In contrast, in the case of H_I-e Pd films on Pd microdisc electrodes, only part of the absorbed hydrogen was removed by the anodic sweep. It is thought to arise because of the diffusion of hydrogen further into the substrate. In the case of H_I-e Pd films on Pd microdisc electrodes, it is therefore expected to be difficult to keep the H/Pd ratio near the surface in the α+β phase region, or to estimate the H/Pd ratio close to the surface. Hence, H_I-e Pd films on Pt microdisc electrodes were chiefly employed to fabricate and characterise H_I-e Pd-hydride micro pH sensors, which will be described in the later chapters.

H1-e Pd films on Pt microdisc electrodes

The hydrogen absorption behaviour will be discussed in the following chapter, using H1-e Pd films on Pt microdisc electrodes deposited through the method described in this section. The potentiometric response of the films loaded with hydrogen will then be reported in chapter 5.

The electrodes mainly investigated in the later chapters were H1-e Pd films with Q_{Dep} of 11 μC deposited on Pt microdisc (d = 25 μm) electrodes. The films were about 30 μm in diameter and about 1 μm in thickness, with roughness factors of about 508 (H1-e Pd (A) film) or 248 (H1-e Pd (B) film).

Chapter 4. Hydrogen absorption behaviour of H_1-e Pd films

In the present study, cathodic electrolysis is employed for loading H_1-e Pd films with hydrogen to prepare H_1-e Pd-hydride micro pH sensors. In this chapter, the basic electrochemistry of H_1-e Pd films in solutions chosen as test solutions (e.g. 0.5 M Na_2SO_4 + H_2SO_4 (pH ≈ 2)) will first be introduced. Hydrogen absorption behaviour will then be considered and the procedure and the conditions of cathodic hydrogen loading will be discussed. In addition, to verify the applicability of the cathodic loading to various solutions, hydrogen absorption behaviour in solutions containing different supporting electrolytes was studied and the results will be presented. At the end of this chapter, the effect of pH on hydrogen absorption behaviour will be discussed.

4-1. H absorption behaviour in 0.5 M Na_2SO_4 + H_2SO_4 (pH ≈ 2) solutions

4-1-1. Cyclic Voltammetry

4-1-1-(1). Fundamental electrochemical behaviour

Cyclic voltammetry was performed in a 0.5 M Na_2SO_4 + H_2SO_4 solution (pH =1.88), over a wide potential range including the surface oxide region. The resulting voltammogram for an H_1-e Pd (B) film deposited on a Pt microdisc (d= 25 μm) is shown in Figure 4.1. Each peak on this voltammogram is shifted negative compared to that on the voltammogram recorded in 1 M H_2SO_4 (e.g. Figure 3.16; line 1), because of the difference in pH of the two solutions. In the surface oxide region, the shapes of the voltammograms recorded in the two solutions are very similar. In the hydrogen region, the same peaks are observed in the 0.5 M Na_2SO_4 + H_2SO_4 solution as in the 1 M H_2SO_4 solution, although differences are found in their shape. Based on the discussion of the voltammogram in Figure 3.16, the current waves on the cathodic scan in Figure 4.1 are assumed to be : (A) hydrogen adsorption, (C) hydrogen absorption to form the α phase, (E) the beginning of hydrogen absorption to form the β phase.

The peaks on the anodic scan (B), (D) and (F) are stripping peaks corresponding to (A), (C) and (E) respectively.

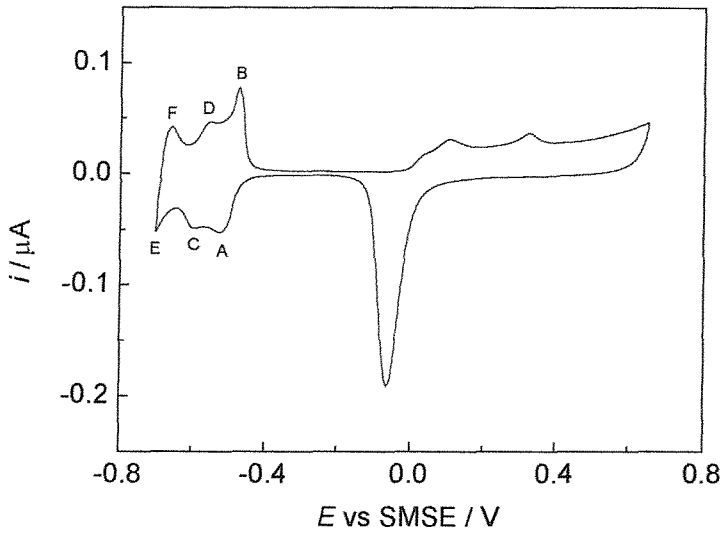

Figure 4.1 Cyclic voltammogram for an H_1-e Pd (B) film (Q_{Dep} = 11 μC) deposited on a Pt microdisc (d = 25 μm) electrode in a deaerated 0.5 M Na_2SO_4 + H_2SO_4 solution (pH =1.88) at 20 mV s^{-1}. (A) hydrogen adsorption, (C) hydrogen absorption to form the α phase, (E) the beginning of hydrogen absorption to form the β phase, (B), (D), (F) stripping peaks corresponding to (A), (C), (E).

Comparison of the shape of peaks corresponding to hydrogen reactions (peaks A ~ F) with those on the voltammogram recorded in 1 M H_2SO_4 reveals that the peak (A) is less sharp for the 0.5 M Na_2SO_4 + H_2SO_4 solution. In relation to this, shown in Figure 4.2 are voltammograms for an H_1-e Pd (A) film recorded in a 0.5 M Na_2SO_4 + H_2SO_4 solution, over two different potential ranges, ie. –0.70 ~ +0.65 V and –0.70 ~ –0.15 V. Peak (A) appears to be much sharper when the potential was cycled only in the hydrogen region and the double layer region. This suggests that the shape of peak (A) was affected by scanning the potential to the surface oxide formation / stripping region. The cause for this change in the shape of peak (A) is unclear from the experimental results, although the specific adsorption of anions might interfere with the hydrogen adsorption.

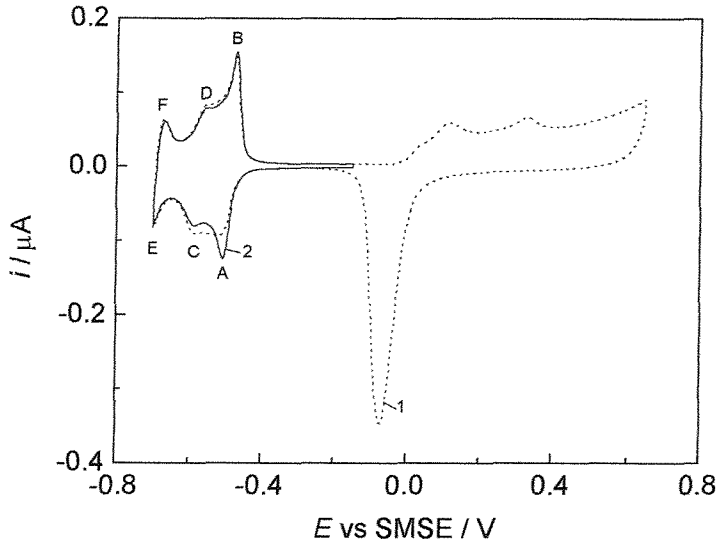

Figure 4.2. Cyclic voltammograms for an H_1-e Pd (A) film (Q_{Dep} = 11 μC) deposited on a Pt microdisc (d=25 μm) electrode in a 0.5 M Na_2SO_4 + H_2SO_4 (pH =1.88) solution at 20 mV s^{-1}. (1) between –0.70 and +0.65 V, (2) between –0.70 V and –0.15 V.

The effect of the scan rate was investigated next and the resulting voltammograms recorded at four different scan rates are shown in Figure 4.3. It is clear by comparing the voltammograms recorded at 100 mV s^{-1} (Figure 4.3; line 4) with that recorded at 20 mV s^{-1} (Figure 4.1) that increasing the scan rate broadens the peaks. Moreover, the height of peaks for surface reactions, ie. surface oxide formation / stripping and hydrogen adsorption / desorption, was not proportional to the scan rate.

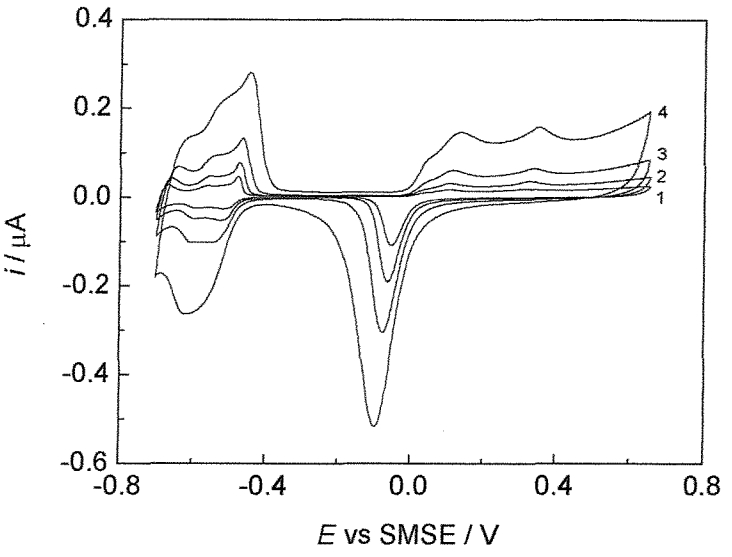

Figure 4.3. Cyclic voltammograms for an H_1-e Pd (B) film (Q_{Dep} = 11 μC) deposited on a Pt microdisc (d=25 μm) electrode in a deaerated 0.5 M Na_2SO_4 + H_2SO_4 (pH =1.88) solution. Scan rates : (1) 10 mV s^{-1}; (2) 20 mV s^{-1}; (3) 40 mV s^{-1}; (4) 100 mV s^{-1}

It is also important to mention that, with increasing scan rates, peaks on the cathodic scan shifted cathodic and those on the anodic scan shifted anodic. These features are thought to be caused by the change in proton concentration within the pores of the nanostructure. The pH within the pores is expected to rise when protons are consumed by cathodic reactions, eg.

$$PdO + 2\,H^+ + 2\,e \rightarrow Pd + H_2O$$
$$H^+ + e \rightarrow H\,(Pd)$$

The rise in the pH within the pores causes the negative shift in potential, since the equilibrium potentials for the reactions are dependent on the pH.

$$E_{PdO/Pd} = E_0 + \frac{RT}{F}\ln a_{H^+}$$
$$= E_0 - 0.059pH$$

$$E_{H+/H(Pd)} = E_0 + \frac{RT}{F}\ln\frac{a_{H+}}{a_{H(Pd)}}$$
$$= E_0 - 0.059\,pH - 0.059\log a_{H(Pd)}$$

As a result, the surface oxide reduction peak was broad and extended to the hydrogen region at 100 mV s^{-1}. In addition, the currents for hydrogen adsorption and the α phase formation are not resolved and observed as one peak at 100 mV s^{-1}.

On the other hand, the pH within the pores is expected to fall when protons are released by anodic reactions, e.g.

$$Pd + H_2O \rightarrow PdO + 2\,H^+ + e$$
$$H\,(Pd) \rightarrow H^+ + e$$

By the same discussion as cathodic reactions, the peaks for anodic reactions are extended and shifted positive. In view of the peak separation in the voltammogram, the scan rate of 20 mV s^{-1} was chiefly used in subsequent cyclic voltammetric studies.

4-1-1-(2). Hydrogen absorption / desorption behaviour

The potential was scanned to more negative values to study the hydrogen absorption behaviour. The cathodic part of a cyclic voltammogram for an H_1-e Pd (B) film (Q_{Dep} = 11 μC) on a 25 μm diameter Pt microdisc electrode in a deaerated 0.5 M Na_2SO_4 + H_2SO_4 solution (pH =1.88), recorded between −1.00 V and +0.65 V is shown in Figure 4.4 (line 1). Peaks (A) / (C) correspond to hydrogen adsorption / desorption and peak (B) corresponds to hydrogen absorption to form the α phase, as shown in Figure 4.1. On the cathodic scan, large reduction current is observed below −0.7 V, which shows a peak at about −0.89 V. This is thought to correspond to hydrogen absorption to form the β phase. Another wave of a large reduction current begins to flow at about −0.92 V, and is assumed to be the evolution of hydrogen gas. On the anodic scan, a large oxidation peak (−0.57 V) for the stripping of absorbed hydrogen is seen. Here, the currents for the oxidation of the β phase and the α phase are not separated, because of the massive current for the β phase oxidation.

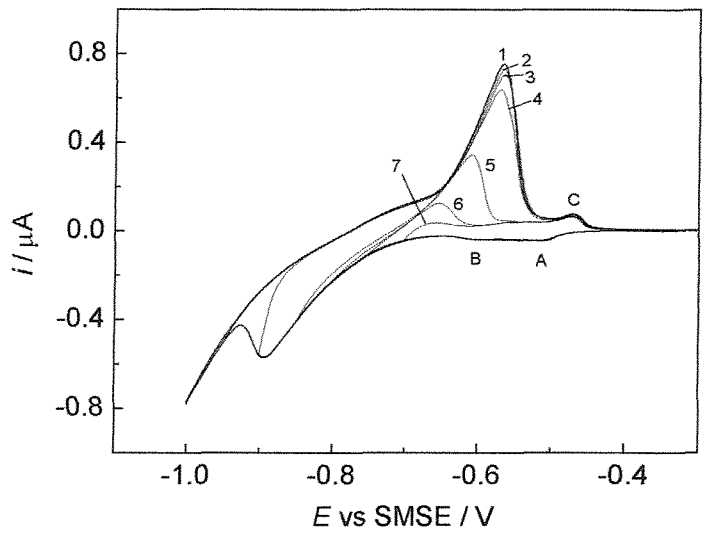

Figure 4.4. Cyclic voltammograms for an H_1-e Pd (B) film (Q_{Dep} = 11 μC) on a 25 μm diameter Pt microdisc electrode, in a deaerated 0.5 M Na_2SO_4 + H_2SO_4 (pH =1.88) solution at 20 mV s^{-1}. Results for the potential range between –1.0 V and –0.3 V are shown, while the potential was scanned between E_{C_Lim} and +0.7 V. E_{C_Lim} : (1) –1.0 V, (2) –0.95 V, (3) –0.90 V, (4) –0.85 V, (5) –0.80 V, (6) –0.75 V, (7) –0.70 V.

To study the two large current waves on the cathodic scan in more detail, cyclic voltammograms were recorded with different cathodic limits, E_{C_Lim}, and are shown in Figure 4.4 (line 2 ~ 7). Cathodic and anodic charges were calculated for each cycle and are shown in Table 4.1. By employing more negative E_{C_Lim}, the cathodic charge increased continuously. The anodic charge also increased until –0.85 V, but stayed almost constant with E_{C_Lim} of –0.90, –0.95 and –1.00 V. This indicates that the H_1-e Pd film was saturated with hydrogen on the cycles with E_{C_Lim} of –0.90, –0.95 and –1.00 V. The difference between cathodic and anodic charges for these voltammograms can be explained by hydrogen gas evolution. For the voltammograms with $E_{C\_Lim} \geq$ –0.85 V, the anodic charge was almost equal to the corresponding cathodic charge. This indicates that hydrogen gas was not evolved during these cycles.

Table 4.1. Analysis of cathodic and anodic charges on the voltammograms shown in Figure 4.4.

No. in Figure 4.4	Cathodic limit E_{C_Lim} / V	Charges	
		Cathodic / μC	Anodic / μC
1	−1.00	−9.25	3.54
2	−0.95	−6.08	3.51
3	−0.90	−4.10	3.46
4	−0.85	−2.89	2.87
5	−0.80	−1.44	1.44
6	−0.75	−0.67	0.65
7	−0.70	−0.40	0.39

* The charge for the double layer charging was subtracted.

From these results, the currents observed on the voltammogram with E_{C_Lim} = −1.00 V (Figure 4.4; line 1) can be summarized as follows. On the cathodic scan, after showing the peaks for hydrogen adsorption (−0.52 V) and hydrogen absorption to form the α phase (−0.60 V), the large current corresponding to the hydrogen absorption to form the β phase begins to flow. This large current shows a peak at −0.89 V. The current for hydrogen gas evolution is seen from about −0.92 V. At this point, the H_1-e Pd film is believed to be saturated with hydrogen. The hydrogen gas evolution continues to the anodic scan until the potential reaches −0.77 V. Anodic peaks at about −0.57 V and −0.47 V correspond to desorption of absorbed and adsorbed hydrogen, respectively.
The cathodic peak associated with the β phase formation was extended towards negative potentials. This again can be attributed to a pH rise within the pores, caused by the proton consumption during hydrogen absorption.

In Chapter 3, H_1-e Pd (A) films appeared to have almost twice the electroactive area of H_1-e Pd (B) films with the same deposition charge. This difference was thought to be attributed to the better uniformity and continuity of the pores of the nanostructure. To study the difference in hydrogen absorption behaviour between H_1-e Pd films with the different nanostructure, cyclic voltammetry was

carried out for an H_1-e Pd (A) film and the resulting voltammogram is compared with that for H_1-e Pd (B) film in Figure 4.5.

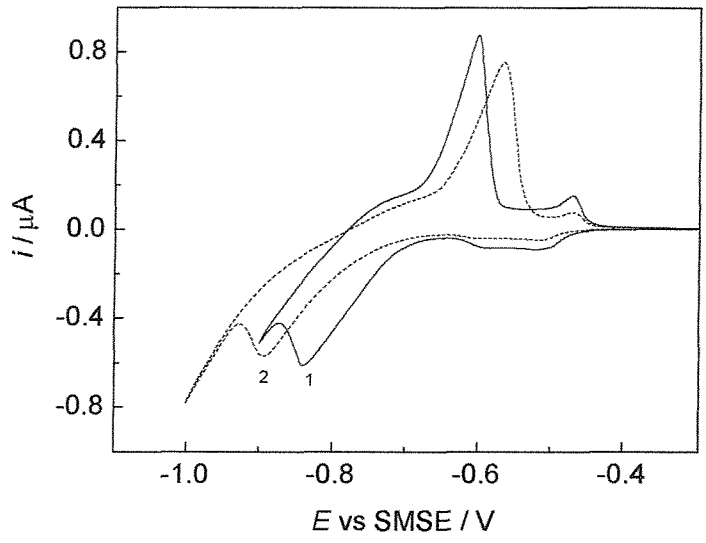

Figure 4.5. Cyclic voltammograms for H_1-e Pd films of two kinds (Q_{Dep} = 11 μC) on 25 μm diameter Pt microdisc electrodes, in a deaerated 0.5 M Na_2SO_4 + H_2SO_4 solution (pH =1.88) at 20 mV s^{-1}. Results for the potential range between –1.0 V and –0.3 V are shown, while the potential was scanned between –1.0 V and +0.7 V. (1) H_1-e Pd (A) film, (2) H_1-e Pd (B) film.

It is clear that hydrogen absorption to form the β phase and corresponding hydrogen desorption are both greatly enhanced on the H_1-e Pd (A) film, compared to the H_1-e Pd (B) film. As a result, absorption and desorption peaks are close to each other on the H_1-e Pd (A) film. Furthermore, the evolution of hydrogen gas appears to be enhanced on the H_1-e Pd (A) film. The comparison of the magnitude of the currents at the potential range of –0.70 → –0.80 V (cathodic scan; hydrogen absorption to form the β phase), –0.90 → –0.80 V (anodic scan; hydrogen gas evolution) and –0.65 → –0.61 V (anodic scan; desorption of absorbed hydrogen) reveals that the currents on the H_1-e Pd (A) film are about 1.6 ~ 2 times those of the H_1-e Pd (B) film.

The cathodic and anodic charges passed during the voltammetry on the H_1-e Pd (A) film were –5.98 and +3.71 μC respectively (the charge for the double layer

charging was subtracted). The larger cathodic charge indicates that the film was already saturated with hydrogen and that the difference in the charge (–2.27 μC) corresponds to the hydrogen gas evolution. Subtracting the charge for desorption of adsorbed hydrogen (ca. 0.28 μC) from the total anodic charge (3.71 μC), the charge associated with the stripping of absorbed hydrogen is estimated to be 3.43 μC. In the same way, the charge corresponding to the stripping of absorbed hydrogen for H_1-e Pd (B) film (Figure 4.5; line 2) was found to be 3.38 μC (total anodic charge: 3.54 μC, the charge for desorption of adsorbed hydrogen: ca. 0.16 μC). It was shown from this calculation that H_1-e Pd (A) and H_1-e Pd (B) films can absorb almost the same amount of hydrogen.

Lastly, the effect of thickness (Q_{Dep}) of H_1-e Pd films on the hydrogen absorption / desorption current was investigated. Figure 4.6 shows cyclic voltammograms for H_1-e Pd (B) films with Q_{Dep} of 5.5 μC and 11 μC.

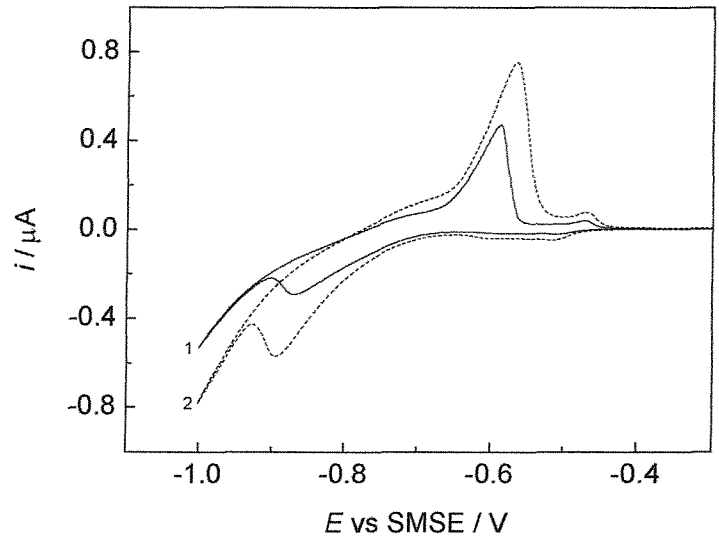

Figure 4.6. Cyclic voltammograms for H_1-e Pd films with different Q_{Dep} on 25 μm diameter Pt microdisc electrodes, in a deaerated 0.5 M Na_2SO_4 + H_2SO_4 solution (pH =1.88) at 20 mV s^{-1}. Results for the potential range between –1.0 V and –0.3 V are shown, while the potential was scanned between –1.0 V and +0.7 V. (1) Q_{Dep} = 5.5 μC, (2) Q_{Dep} = 11 μC.

As discussed in Chapter 3, the film with Q_{Dep} = 11 μC has the greater amount of deposited Pd and greater electroactive area by about two times, than that with Q_{Dep} = 5.5 μC. Currents for hydrogen absorption to form the β phase, hydrogen gas evolution and desorption of absorbed hydrogen are all greater for the thicker film (Q_{Dep} =11 μC). However, the enhancement of currents was limited, taking into account that the thicker film (Q_{Dep} = 11 μC) had about twice the electroactive area of the thinner film (Q_{Dep} = 5.5 μC). Close observation of the currents for the hydrogen absorption to form the β phase (cathodic scan; –0.70 → –0.84 V), the evolution of hydrogen gas (anodic scan; –1.00 → –0.90 V) and desorption of absorbed hydrogen (anodic scan; –0.64 → –0.60 V) reveals that the currents on the H_1-e Pd film with Q_{Dep} = 11 μC are only 1.3 ~ 1.5 times those on the film with Q_{Dep} = 5.5 μC. As a result, β phase formation peak shifted negative and the peak for desorption of absorbed hydrogen shifted positive. The limited enhancement is presumably due to the pore length of the nanostructure. The pH gradient along the pores caused by the proton consumption and generation is thought to be more pronounced for thicker films, because of the greater pore lengths.

4-1-2. Potentiostatic loading of H

4-1-2-(1). H/Pd ratio as a function of loading potentials

To study the hydrogen absorption behaviour of H_1-e Pd films in detail, the films were loaded with hydrogen potentiostatically, and the effect of the loading potential on the hydrogen absorption behaviour was investigated. The procedure of potentiostatic loading of hydrogen was as follows.

First, a fresh H_1-e Pd film deposited on a Pt microdisc electrode was cycled in a 1 M H_2SO_4 (–0.65 ↔ +0.70 V) solution then in a 0.5 M Na_2SO_4 + H_2SO_4 solution (–0.70 ↔ +0.65 V), until stable voltammograms (e.g. Figure 4.1) were obtained. The potential was then held at –0.20 V (double layer region) where the current was zero. The hydrogen loading was started by stepping the potential from –0.20 V to the loading potential, E_L. The potential was held at E_L for the loading time, t_L, until the current reached a stable value. The length of t_L was varied in each case, in order to ensure that sufficient time was allowed for the

system to reach the steady state at E_L. Examples of current transients monitored during loading hydrogen at E_L = –0.67 V and –0.75V are shown in Figure 4.7. In these examples, the current reached stable values within t = 10 s (E_L = –0.67 V) and at around t = 45 s (E_L = –0.75 V). The shape of the current transient will be analysed in 4-1-2-(2).

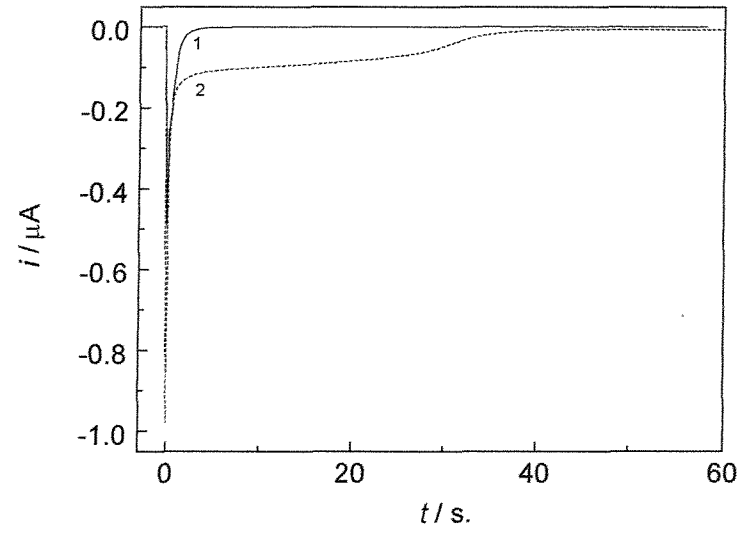

Figure 4.7. Current transients recorded while loading hydrogen into an H_1-e Pd (B) film (Q_{Dep} = 11 μC) on a 25 μm diameter Pt microdisc electrode in a 0.5 M Na_2SO_4 + H_2SO_4 solution (pH =1.88). The potential was stepped from –0.20 V to the loading potential, E_L at t = 0. (1) E_L = –0.67 V, (2) E_L = –0.75 V.

The amount of hydrogen loaded into the Pd film was estimated from the charge under the oxidation peak observed on anodic sweep voltammogram (10 mV s^{-1}). Figure 4.8 shows the anodic sweep voltammograms recorded after an H_1-e Pd film was loaded with hydrogen at E_L = –0.67 V and –0.75 V.

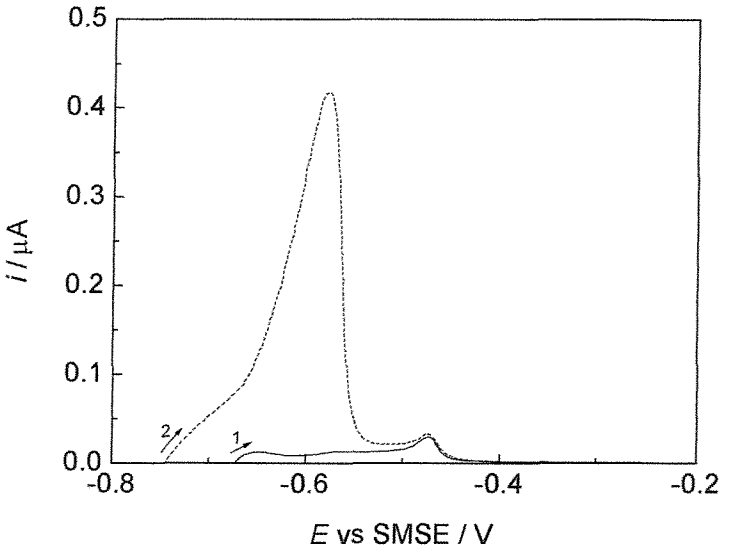

Figure 4.8. Linear sweep voltammograms for stripping adsorbed and absorbed hydrogen from an H_1-e Pd (B) film (Q_{Dep} = 11 μC) on a 25 μm diameter Pt microdisc electrode in a 0.5 M Na_2SO_4 + H_2SO_4 solution (pH =1.88), recorded at 10 mV s^{-1}. The anodic sweep was started immediately after the electrode was loaded with hydrogen. Loading conditions: (1) E_L = –0.67 V, t_L = 60 s. (2) E_L = –0.75 V, t_L = 60 s.

Anodic currents observed below –0.5 V correspond to the oxidation of absorbed hydrogen in the Pd film, while the peak at –0.48 V corresponds to the oxidation of adsorbed hydrogen on the surface of the film. The charge associated with the stripping of hydrogen, $Q_{Str(H)}$, was calculated by subtracting the charge for double layer charging from the whole anodic charge. The double layer charge was estimated using the current at –0.25 V as the double layer charging current. Thus calculated $Q_{Str(H)}$ for an H_1-e Pd (B) film (Q_{Dep} = 11 μC) as a function of E_L is shown in Figure 4.9. It is important to note here that $Q_{Str(H)}$ is the sum of the charges for stripping absorbed and adsorbed hydrogen.

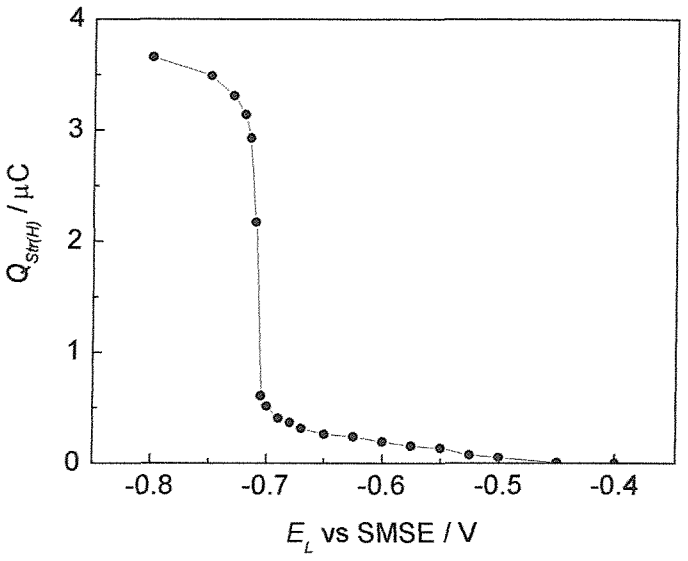

Figure 4.9. The charges for stripping adsorbed and absorbed hydrogen from an H1-e Pd (B) film (Q_{Dep} = 11 μC) on 25 μm diameter Pt microdisc electrode (the charge for the double layer charging was subtracted). First, the film was loaded with hydrogen at E_L in a 0.5 M Na_2SO_4 + H_2SO_4 (pH =1.88) solution (e.g. Figure 4.7). The anodic sweep for stripping hydrogen (e.g. Figure 4.8) was performed immediately after loading hydrogen. Sweep rate : 10 mV s^{-1}.

In cyclic voltammetry (e.g. Figure 4.1 and Figure 4.2), the current for hydrogen adsorption was observed from about –0.45 to –0.56 V. Similarly, in Figure 4.9, $Q_{Str(H)}$ was virtually zero until –0.45 V when $Q_{Str(H)}$ began to increase. $Q_{Str(H)}$ continued to increase until –0.55 V when the rising slope became less steep. Hence, it is assumed that the $Q_{Str(H)}$ value (at –0.55 V) of 0.14 μC corresponds to the desorption of adsorbed hydrogen on the film. Comparing this charge with the oxide stripping charge obtained in Chapter 3, the coverage is estimated to be 0.37 H atoms per surface Pd atom.

Assuming that hydrogen adsorption is completed at –0.55 V, the stripping charges for absorbed hydrogen can be calculated by subtracting 0.14 μC from $Q_{Str(H)}$. This charge can be converted into the ratio of hydrogen to palladium at each potential by using the Q_{Dep} (the Pd film deposition charge) together with the Faradaic efficiency of Pd deposition efficiency. The Faradaic efficiency of

98 % was used in this calculation (the efficiency was reported to be as high as 95-98 %[100-102]). The H/Pd ratios thus calculated are plotted against E_L and shown in Figure 4.10. The results obtained using H_1-e Pd (B) with two different Q_{Dep}, ie. 11 μC and 44 μC, are shown in the graph.

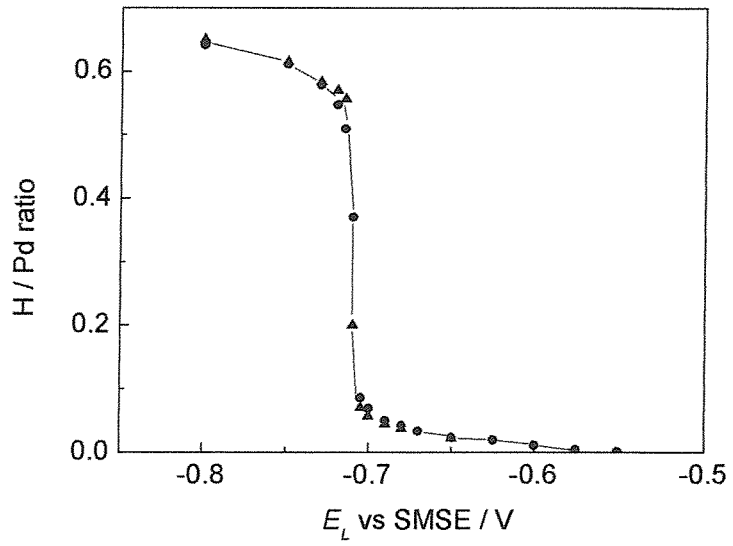

Figure 4.10. Plot of the H/Pd ratio as a function of the loading potential for H_1-e Pd (B) films on 25 μm diameter Pt microdisc electrodes. Hydrogen was loaded into the film at E_L in a 0.5 M Na_2SO_4 + H_2SO_4 solution (pH =1.88). The H/Pd ratios were estimated from stripping charges (charges for double layer charging and hydrogen adsorption were subtracted). Pd film deposition charges : ●, Q_{Dep} = 11 μC, ▲, Q_{Dep} = 44 μC.

Below –0.55 V, the H/Pd ratio increases gradually and reached a small plateau (–0.625 ~ –0.65 V) of about H/Pd =0.025. This H/Pd ratio is close to the reported maximum solubility of hydrogen (0.03) in the α phase. The H/Pd ratio began to increase again and rose sharply at around –0.71 V, which corresponds to the formation of the β phase. The sharp rise began from an H/Pd ratio of about 0.1 and ended at about 0.5. At more cathodic potentials the H/Pd ratio continued to increase gradually, in the β phase Pd-hydride region. The H_1-e Pd films with different thickness (Q_{Dep} = 11 and 44 μC) showed almost identical relations between H/Pd ratio and E_L. The results were similar to that obtained for H_1-e

Pd films deposited on 1 mm diameter gold disc electrodes in 1 M H_2SO_4 solutions, reported by Bartlett et al[101], except for the potential shift due to the pH difference.

The rise in H/Pd ratio at around –0.71 V, corresponding to the α→β phase transition, was very sharp. The H/Pd ratio rose from about 0.1 to 0.5 in a very narrow potential range. This result suggests that the potential of H_1-e Pd-hydride films will be almost constant regardless of the H/Pd ratio over a wide H/Pd range (0.1 ~ 0.5). It has to be noted that this constant potential will vary with pH at –0.0592 V / pH. This is the basis of the α+β phase Pd-hydride pH sensors aimed at in the present study.

4-1-2-(2). Analysis of current transients

As discussed above, the open circuit potential of hydrogen-loaded H_1-e Pd films is expected to be almost constant in the H/Pd ratio of about 0.1 ~ 0.5, in the α+β phase region. In the preparation of potentiometric micro pH sensors, H_1-e Pd films should be loaded with hydrogen to H/Pd ratio of 0.5 or higher in order to make the most of the wide H/Pd ratio, because Pd-hydride electrodes lose hydrogen slowly under an open circuit condition (continuous loss of hydrogen will be discussed in detail in Chapter 5). The H/Pd ratio of 0.5 or higher can be achieved by employing E_L below –0.71 V.

To investigate the hydrogen absorption behaviour at the potentials below –0.71 V in more detail, current transients recorded during the potentiostatic loading of hydrogen into H_1-e Pd films were analysed. The current transients recorded at E_L = –0.73 V, –0.75 V, and –0.80 V are shown in Figure 4.11. The current transient curves showed the same shapes regardless of the E_L; ie. the curves begin with a large current followed by a sharp decay, and after showing a first plateau, the current decreases again and reaches a second plateau. The current values for the first and second plateaus, and the length of the first plateau are dependent on the E_L.

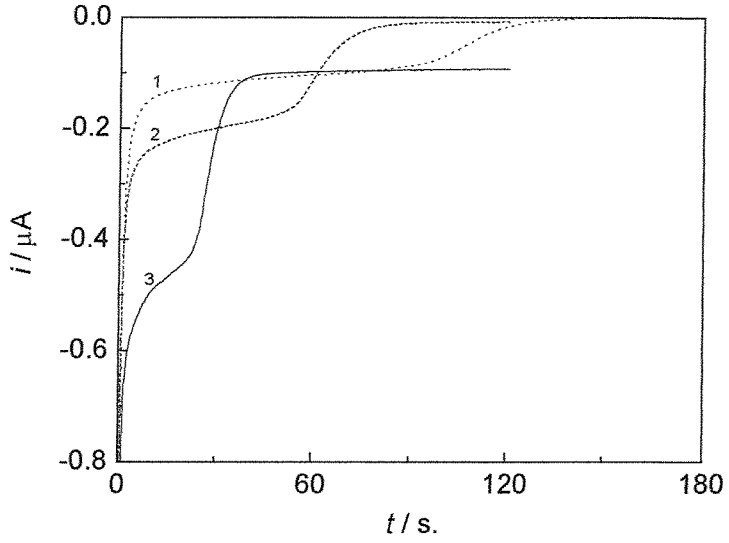

Figure 4.11. Current transients recorded during loading hydrogen into an H_1-e Pd (B) film (Q_{Dep} = 44 μC) on a 25 μm diameter Pt microdisc electrode in a 0.5 M Na_2SO_4 + H_2SO_4 solution (pH =1.88). The potential was stepped from –0.20 V to the loading potential, E_L at t = 0. (1) E_L = –0.73 V, (2) E_L = –0.75 V, (3) E_L = –0.80 V.

To study the reactions taking place in different regions of the current transients, the transient recorded at E_L = –0.80 V was investigated in more detail. First, the applied charge was calculated by integrating the current transient and is shown in Figure 4.12 (line 1). To estimate the charge used for loading hydrogen into the film as a function of the loading time, t_L, the potential was swept back after being held at E_L (–0.80 V) for 23, 35, 45 and 90 seconds. The stripping charges were calculated by integrating the current on the reverse sweep voltammograms and are shown in Figure 4.12 (open circles with the line 2).

Two features can be found from Figure 4.12. First, the stripping charge remained constant after t = 35 s, which shows that the total amount of hydrogen adsorbed and absorbed to the Pd film was constant although the applied charge increased continuously in this period. This indicates that the H absorption into the H_1-e Pd film was completed before reaching the second plateau, despite the substantial cathodic current still flowing in the second plateau region. The

current observed during the second plateau is thought to correspond to hydrogen gas evolution, since the stripping charge remained constant.

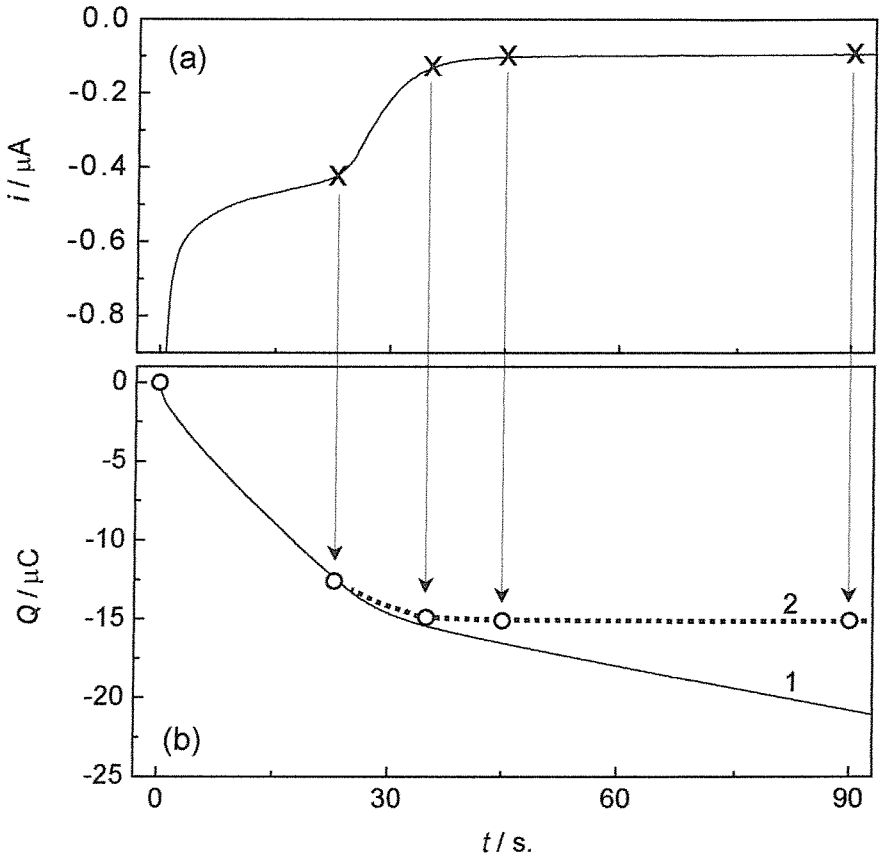

Figure 4.12. Hydrogen loading behaviour of an H_1-e Pd (B) film (Q_{Dep} = 44 μC) on a 25 μm diameter Pt microdisc electrode at E_L = –0.8 V in a 0.5 M Na_2SO_4 + H_2SO_4 solution (pH =1.88). (a) Current transient. (b)-(1) The applied charge calculated from the current transient. (b)-(2) The charges for stripping adsorbed and absorbed hydrogen from the H_1-e Pd (B) film, calculated from reverse sweep voltammograms.

Secondly, at t = 23 s, the stripping charge was approximately equal to the applied charge. It indicates that adsorption and absorption of hydrogen occurred at about 100 % Faradaic efficiency until the end of the first plateau.

In the same way, the current transient recorded at E_L = –0.73 V and –0.75 V were analysed. Their applied charges and stripping charges were calculated for several conditions (E_L and t_L), and results are shown in Table 4.2, together with the results for E_L = –0.80 V. The results for E_L = –0.73 and –0.75 V were consistent with those for E_L = –0.80 V. For E_L = –0.75 V, the Faradaic efficiency was *ca* 100 % at the end of the first plateau (t = 50 s), but fell to 96 % at t = 120 s because of the current in the second plateau region (assumed to be H_2 evolution current). For E_L = –0.73 V, although the current reached the second plateau at around t = 150 s, the Faradaic efficiency was still about 100 % at t = 180 s, since the current in the second plateau region was negligibly small.

Table 4.2. Analysis of hydrogen loading behaviour of an H_1-e Pd (B) film (Q_{Dep} = 44 μC) on a 25 μm diameter Pt microdisc electrode in a 0.5 M Na_2SO_4 + 0.05 M H_2SO_4 solution.

No. in Figure 4.12	E_L / V	t_L / s.	Applied charge / μC (A)	Stripping charge* / μC (B)	Faradaic efficiency / % –(B)/(A) x 100
1	–0.73	180	–13.8	13.6	99
2	–0.75	120	–14.8	14.2	96
		50	–12.4	12.5	101
3	–0.80	90	–20.8	14.9	72
		45	–16.8	14.9	89
		35	–15.3	14.7	96
		23	–12.3	12.4	101

* The charges for the double layer charging (≈ 0.1 μC) were not subtracted from the data.

To summarize the results mentioned above, the reactions during hydrogen loading can be described as shown in Figure 4.13. The current transient curve begins with a large current, which is thought to correspond chiefly to hydrogen adsorption and α phase formation (the charge for double layer charging is smaller by an order), followed by a sharp decay. Hydrogen absorption to form α+β phase is completed by the end of the first plateau, at the Faradaic efficiency of about 100%. After completion of hydrogen adsorption and absorption, hydrogen gas starts to evolve (second plateau). Currents for the first plateau and for the second plateau are both dependent on the E_L. The more negative E_L, the

higher the driving force, the higher the rate of absorption and the shorter the length of the first plateau.

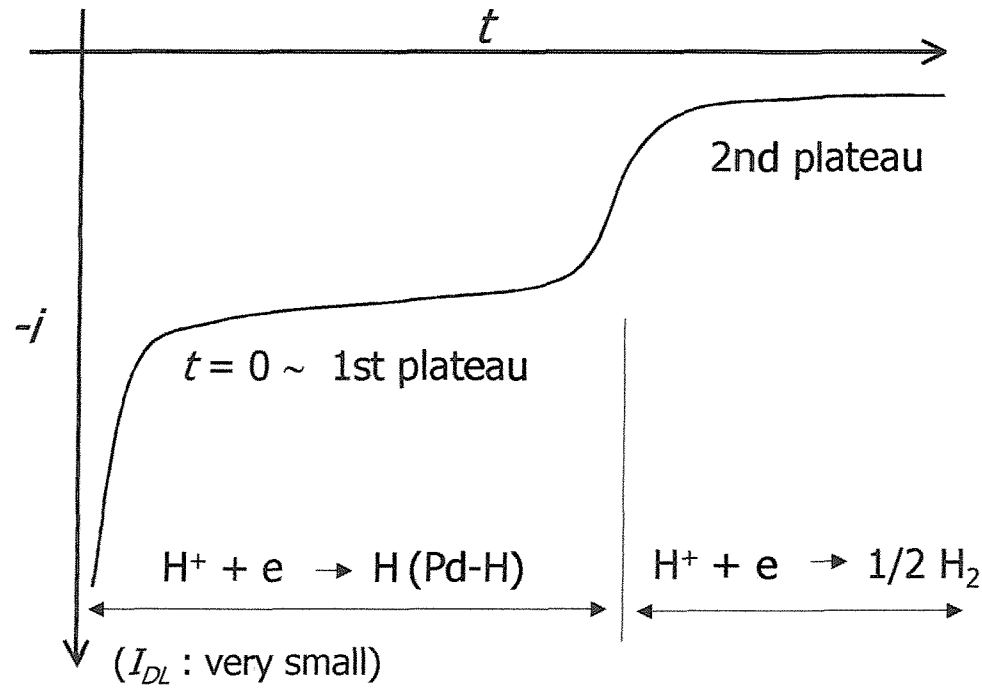

Figure 4.13. Schematic diagram of the hydrogen reactions taking place during loading hydrogen into H_1-e Pd (B) films on 25 μm diameter Pt microdisc electrodes in 0.5 M Na_2SO_4 + H_2SO_4 solutions (pH =1.88).

Two practically useful conclusions can be drawn from the results. Firstly, the H/Pd ratio of the H_1-e Pd films can be controlled by varying t_L. Secondly, the exact amount of hydrogen loaded to H_1-e Pd films can simply be estimated from the charge passed during loading, on the condition that t_L is in the first plateau region.

4-1-2-(3). Degradation of H_1-e Pd film

Bartlett et al[101] studied hydrogen evolution reaction on H_1-e Pd films deposited on Au electrodes (d= 1mm) and reported that the electrodes were stable towards repeated cycling to form the β phase. They concluded that the hydrogen

insertion and concomitant lattice expansion does not destroy the nanostructure. Similarly, in the present study, hydrogen absorption and desorption by H_1-e Pd films on Pt microdisc electrodes did not cause an abrupt change in electrochemical response. This confirms that the nanostructure of H_1-e Pd films is basically resistive to the lattice parameter expansion of about 3% (3.882 → 4.017)[47] caused by the insertion of hydrogen to form the β phase.

However, it was found in the present study that the repetitive absorption (β phase formation) / desorption of hydrogen causes a gradual decrease in the amount of hydrogen absorbed into the film (at a fixed E_L). For example, after repeatedly loading with hydrogen for 20 times (E_L = –0.75 V), an H_1-e Pd (B) film (Q_{Dep} = 11 μC) absorbed about 85 % of hydrogen compared to that before the repetitive loading. The electroactive area estimated from the surface oxide stripping charge was also found to decrease after the repetitive loading. These results suggest that Pd is lost gradually by repetitive absorption (β phase formation) / desorption of hydrogen. Hence, freshly prepared H_1-e Pd films were used for each experiment in the present study.

4-2. Hydrogen absorption behaviour in solutions containing other supporting electrolytes (pH ≈ 2)

Considering the application of H_1-e Pd hydride micro pH sensors to various solutions, the hydrogen absorption behaviour of H_1-e Pd films was studied in solutions (pH ≈ 2) containing KCl or $NaClO_4$ as supporting electrolytes. Hydrogen absorption behaviour in a solution without additional background electrolyte (only containing a proton source) was also studied briefly.

4-2-1. Fundamental electrochemical behaviour

Prior to the study on the hydrogen absorption behaviour, the fundamental electrochemistry of H_1-e Pd films in solutions (pH ≈ 2) containing KCl or $NaClO_4$ as supporting electrolytes was studied with cyclic voltammetry.

4-2-1-(1). 1 M KCl + HCl solution

The cyclic voltammogram for an H_1-e Pd film on a Pt microdisc in a deaerated 1 M KCl+ HCl solution (pH = 1.86) at 20 mV s^{-1} is shown in Figure 4.14.

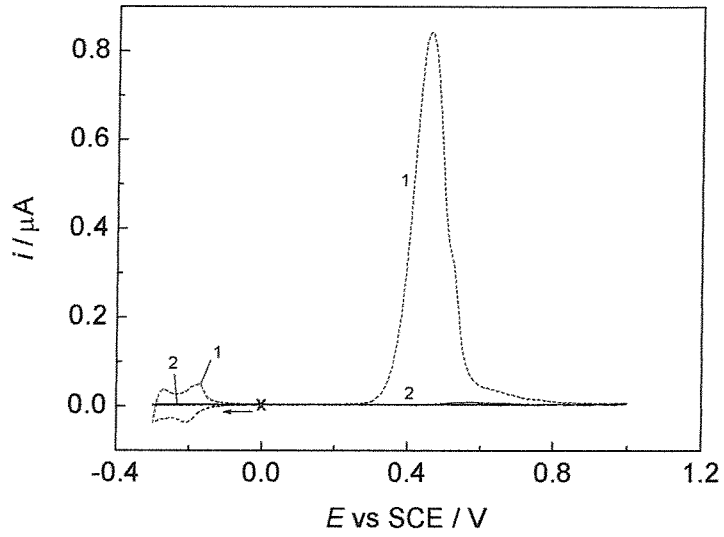

Figure 4.14. Cyclic voltammogram for an H_1-e Pd (B) film (Q_{Dep} = 5.5 μC) deposited on a Pt microdisc (d=25 μm) electrode in a 1 M KCl + HCl solution (pH = 1.86) at 20 mV s^{-1}. The voltammogram was first scanned negative from 0.0 V. (1) first cycle (2) second cycle.

In this experiment, the H_1-e Pd film was first cleaned by potential cycling in a 1 M H_2SO_4 as was done in other experiments. The electrode was then transferred to the 1 M KCl + HCl solution. The potential was scanned cathodically from 0.0 V vs SCE, to observe the cathodic currents for hydrogen reaction. On the following anodic scan, the corresponding anodic currents were also seen. After the double layer region, a massive anodic current was observed from about +0.3 V. The current showed a peak at around +0.46 V and decreased quickly. On the following cathodic scan, neither currents associated with the surface oxide nor with the hydrogen reactions were seen. This strongly suggests that the sharp anodic peak was associated with the anodic dissolution of Pd. The charge under the peak was 5.1 μC, which is close to the

charge passed for the H_1-e Pd film deposition (Q_{Dep} = 5.5 μC). From this result, we see that almost all the Pd was dissolved into the solution as a chloride complex such as $[PdCl_4]^{2-}$.

$$Pd + 4\ Cl^- \rightarrow [PdCl_4]^{2-} + 2\ e$$

Because of this anodic dissolution to form a chloride complex, care was taken not to scan the potential of H_1-e Pd films to anodic region (i.e. beyond 0.2 V vs SCE) in 1 M KCl + HCl solutions in the present study.

4-2-1-(2). 1 M $NaClO_4$ + $HClO_4$ solution

A cyclic voltammogram for an H_1-e Pd film on a Pt microdisc in a deaerated 1 M $NaClO_4$ + $HClO_4$ solution (pH = 2.02) at 20 mV s^{-1} is shown in Figure 4.14.

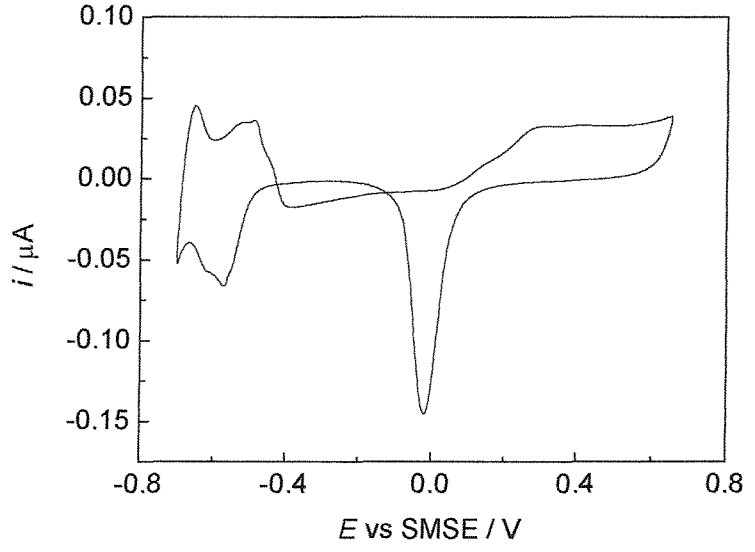

Figure 4.15. Cyclic voltammogram for an H_1-e Pd (B) film (Q_{Dep} = 11 μC) deposited on a Pt microdisc (d=25 μm) electrode in a deaerated 1 M $NaClO_4$ + $HClO_4$ (pH = 2.02) solution at 20 mV s^{-1}

On the cathodic scan, four waves of reduction currents corresponding to surface oxide stripping (–0.02 V), hydrogen adsorption (–0.57 V), the α phase

formation(–0.62 V) and the β phase formation (beginning from –0.67 V) are observed. In terms of the cathodic scan, the shape of the voltammogram is similar to that recorded in 0.5 M Na_2SO_4 + H_2SO_4 solutions (eg. Figure 4.1).
A difference is found on the anodic scan. In the 1 M $NaClO_4$ + $HClO_4$ solution, the desorption peak for adsorbed hydrogen (–0.49 V) is clearly smaller than the corresponding cathodic peak. Furthermore, a cathodic current is observed from –0.43 V to +0.09 V on the anodic scan. These phenomena were not observed in 0.5 M Na_2SO_4 + H_2SO_4 solutions. This difference must be attributable to the anions contained in the two solutions.

Perchloric acid and perchlorates are widely and frequently used as supporting electrolytes in electrochemical studies because of the low adsorbability of ClO_4^- ions[117]. It is an almost general view that ClO_4^- is stable in aqueous solutions. However, Horanyi et al[118, 119] have shown that an "unexpected" cathodic current appeared during some cyclic voltammetric measurements at platinized electrodes, in the presence of $HClO_4$ supporting electrolytes. They reported that the double layer region on the anodic sweep was distorted by the presence of the cathodic current, while the cathodic sweep behaved "normally". They explained this phenomenon by the reduction of ClO_4^- ions via loosely adsorbed ClO_4^- species :

$$ClO_4^- + 8\,H^+ + 8\,e \rightarrow Cl^- + 4\,H_2O, \qquad E^0 = 1.54\ V$$

They explained the reason why the reduction was only seen on the anodic sweep as follows. On the anodic scan, a clean surface is formed after the desorption of hydrogen, when ClO_4^- ions can loosely adsorb on the surface and the reduction of ClO_4^- ions can take place. As the adsorption of Cl^- (product of the reduction) and impurities proceeds, the surface is blocked and the rate of the process decreases. These adsorbates inhibit the adsorption of ClO_4^-, until they are eliminated from the surface by the adsorption of hydrogen.

Horanyii et al[120] later stated that a similar cathodic current was observed for a palladium electrode (data was not shown). Hence, the cathodic current observed on the anodic scan in the present study (Figure 4.15) is thought to result from the reduction of ClO_4^-. To verify if this is the case with the present

study, cyclic voltammetry was performed with different cathodic potential limits and the role of hydrogen adsorption on the negative current on the anodic sweep was studied. The resulting voltammograms are shown in Figure 4.16.

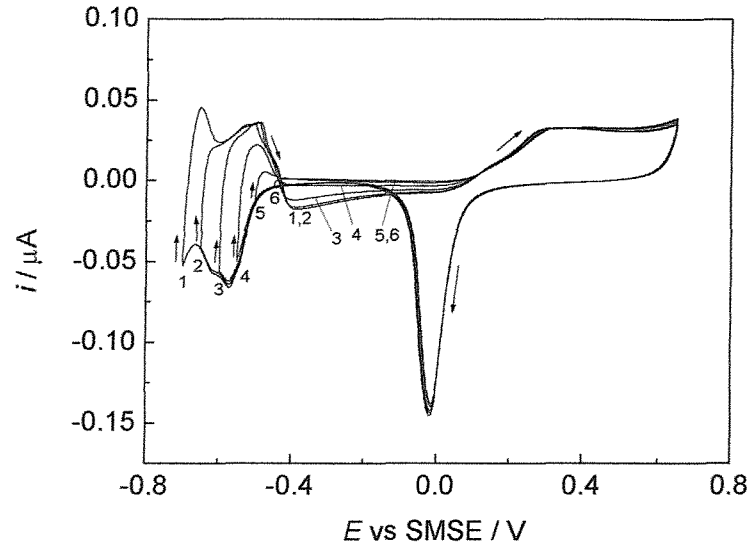

Figure 4.16. Cyclic voltammograms for an H_1-e Pd (B) film (Q_{Dep} = 11 μC) deposited on a Pt microdisc (d=25 μm) electrode in a deaerated 1.0 M $NaClO_4$ + 0.0126 M $HClO_4$ solution at 20 mV s^{-1}. Cathodic limits : (1) –0.70 V; (2) –0.65 V; (3) –0.60 V; (4) –0.55 V; (5) –0.50 V; (6) –0.45 V.

On the voltammograms with the cathodic limit of –0.70, -0.65 and –0.60 V, appreciable cathodic currents are observed in the double layer region on the anodic scan. In these cases, the adsorbates (Cl^-, impurities etc.) were expected to be almost completely replaced by the hydrogen on the preceding cathodic scan. When the cathodic limit is –0.55 V, the cathodic current on the anodic sweep is much smaller, presumably because only part of the adsorbates was removed on the cathodic scan. With the cathodic limit of –0.50 and –0.45 V, no negative section was found on the anodic scan. This can be explained by the blockage of the ClO_4^- adsorption by the adsorbed Cl^- and / or impurities, which were not removed on the preceding cathodic scan. These results are consistent with the behaviour reported for Pt by Horanyii et al and hence, the cathodic current

observed on the anodic sweep in the present study is attributable to the reduction of ClO_4^-.

4-2-2. Hydrogen absorption behaviour

Attempts were made to load H_1-e Pd films with hydrogen potentiostatically, in 1 M KCl+ HCl (pH = 1.86) and 1 M $NaClO_4$ + $HClO_4$ (pH = 2.02) solutions. For the loading potential, –0.75 V vs SMSE (≈ –0.35 V vs SCE) was employed. This E_L is equivalent to about +0.01 V vs. RHE.

In the 1 M KCl+ HCl solution (pH = 1.86), an H_1-e Pd (B) film (Q_{Dep} = 11 μC) on Pt microdisc (d = 25 μm) was loaded with hydrogen at E_L = –0.35 V vs SCE. The potential was not cycled in this solution prior to the loading, since applying the positive potential causes the anodic dissolution of the film. The current transient recorded during loading hydrogen had similar shapes to those recorded in 0.5 M Na_2SO_4 + H_2SO_4 solution (pH =1.88), ie. two plateaus assumed to correspond to hydrogen absorption and hydrogen gas evolution were observed. The H/Pd ratio was estimated to be 0.60 from the stripping charge, which indicates that the H/Pd ratio reached the β phase region.

In the 1 M $NaClO_4$ + $HClO_4$ solution (pH = 2.02), an H_1-e Pd (B) film (Q_{Dep} = 11 μC) on Pt microdisc (d = 25 μm) was loaded with hydrogen at E_L = –0.75 V vs SMSE. Prior to the loading, the potential was cycled in the potential range of –0.70 ↔ +0.65 V in the loading solution to get reproducible results; the same approach as in 0.5 M Na_2SO_4 + H_2SO_4 solutions was followed. The current transient again showed a similar shape to those recorded in 0.5 M Na_2SO_4 + H_2SO_4 solutions. An accurate estimation of the amount of hydrogen loaded in the film from the stripping charge was impossible because of the presence of the cathodic current corresponding to ClO_4^- reduction on the anodic scan. However, from the charge calculated by integrating the current observed during loading (charge passed before reaching the second plateau), the H/Pd ratio was assumed to be about 0.61.

The results discussed above demonstrate that the potentiostatic hydrogen loading to H_1-e Pd films was possible in 1 M KCl+ HCl (pH = 1.86) and 1 M

$NaClO_4$ + $HClO_4$ (pH = 2.02) solutions by employing E_L of about +0.01 V vs. RHE, just as in 0.5 M Na_2SO_4 + H_2SO_4 solutions. The behaviour (current transient) was also very similar to that in 0.5 M Na_2SO_4 + H_2SO_4 solutions.

Lastly, hydrogen absorption behaviour in a solution without additional background electrolyte (only containing a proton source) was studied briefly with cyclic voltammetry. Figure 4.17 shows the cathodic section of a cyclic voltammogram for an H_1-e Pd (B) film (Q_{Dep} = 11 μC) on a 25 μm diameter Pt microdisc electrode, in a deaerated 0.013 M $HClO_4$ solution (pH = 1.89) at 20 mV s^{-1}. From the anodic charge (+3.65 μC) of the voltammogram, the H/Pd ratio appeared to have reached 0.63. From this result, it is also expected to be possible to load hydrogen into H_1-e Pd films potentiostatically in solutions without additional background electrolytes.

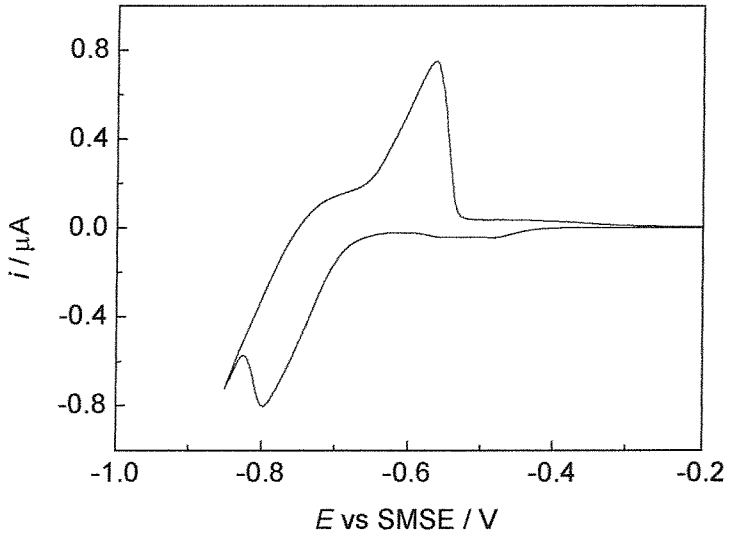

Figure 4.17. Cyclic voltammogram for an H_1-e Pd (B) film (Q_{Dep} = 11 μC) on a 25 μm diameter Pt microdisc electrode, in a deaerated 0.013 M $HClO_4$ solution (pH = 1.89) at 20 mV s^{-1}. A result for the potential range between –0.85 V and –0.2 V is shown, while the potential was scanned between –0.85 V and +0.7 V.

In the voltammogram shown in Figure 4.17, the cathodic peak for hydrogen absorption to form the β phase (peak at –0.8 V) is much more positive than that

recorded in a 0.5 M Na_2SO_4 + H_2SO_4 solution (Figure 4.4). This is thought to be attributed to the faster supply of protons into the pores due to the migration contribution[7] in the absence of additional background electrolyte. This can lessen the proton concentration change within the pores during hydrogen absorption, compared to 0.5 M Na_2SO_4 + H_2SO_4 solutions where the migration contribution is negligible.

4-3. Effect of pH on H absorption behaviour

The hydrogen absorption behaviour in solutions with pH higher than 2 is discussed in this section. As the pH gets higher, the rate of the absorption becomes limited by the concentration of the protons. Figure 4.18 shows cyclic voltammograms for an H_1-e Pd (B) film (Q_{Dep} = 11 μC) on a 25 μm diameter Pt microdisc electrode, in a deaerated 1 M $NaClO_4$ + 0.0035 M $HClO_4$ solution (pH = 2.5) at 20 mV s^{-1}. The cathodic current for hydrogen absorption to form the β phase can be seen below –0.71 V. This current reached a plateau of about –0.14 μA.

The diffusion limiting current for the proton reduction on microdisc electrodes can be calculated using the equation :

$$i_L = 4\,n\,F\,D\,c\,a$$

Where n is the number of electrons transferred, F is the Faraday constant, D is the diffusion coefficient, c is the concentration of protons, and a is the radius of the microdisc. Substituting $n = 1$, $D = 7.7 \times 10^{-5}$ cm^2 s^{-1} [121], $c = 0.0035$ M and a = 15 μm, the limiting current was estimated to be 0.156 μA, which is close to the plateau current value of –0.14 μA. Hence, rate of hydrogen absorption is thought to be limited by diffusion of protons in the solution, at potentials below –1.0 V.

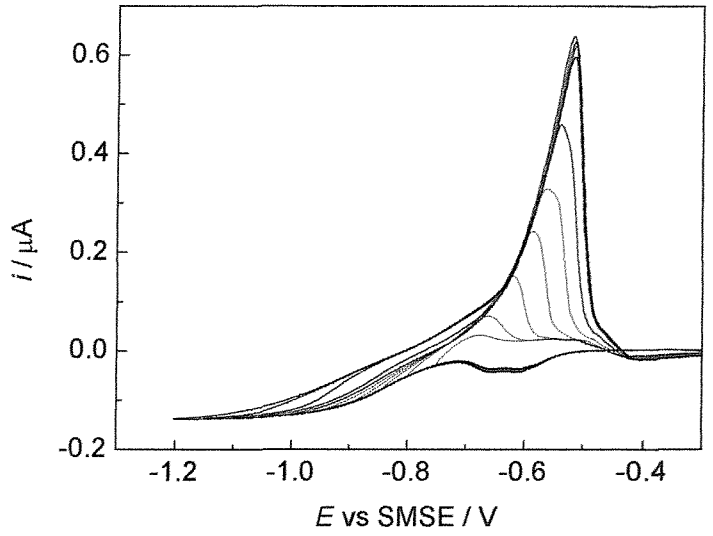

Figure 4.18. Cyclic voltammograms for an H_1-e Pd (B) film (Q_{Dep} = 11 μC) on a 25 μm diameter Pt microdisc electrode, in a deaerated 1 M $NaClO_4$ + 0.0035 M $HClO_4$ solution (pH = 2.5) at 20 mV s^{-1}. Results for the potential range between –1.2 V and –0.3 V are shown, while the potential was scanned between E_{C_Lim} and +0.7 V with E_{C_Lim} ranging from –1.20 ~ –0.75 V with 0.05 V increments.

In a solution with pH = 3, 4 and 5, the diffusion limiting current for proton reduction is expected to be around 50, 5 and 0.5 nA (assuming that $a_{H+} = [H^+]$). When the rate of hydrogen loading is limited by the diffusion of protons in the solution, the time required to load an H_1-e Pd film (Q_{Dep} = 11 μC) with hydrogen to H/Pd ratio of 0.6 is estimated to be about 1, 10 and 100 min respectively. Hence, to load hydrogen into H_1-e Pd films rapidly in solutions with a higher pHs (approx. pH > 3), the reduction of water has to be used instead of the reduction of protons.

$$H_2O + e \rightarrow H\ (Pd\text{-}H) + OH^-$$

In the case of solutions with higher pHs (e.g. pH > 3), a much more negative overpotential is needed in order to get the reduction of water to proceed and load hydrogen quickly into H_1-e Pd films.

Figure 4.19 shows cyclic voltammograms for an H_1-e Pd (B) film (Q_{Dep} = 11 μC)

on a 25 μm diameter Pt microdisc electrode in a deaerated 0.5 M Na_2SO_4 + NaOH solution (pH = 12.1) recorded at 20 mV s^{-1}. The reduction current peak at −1.55 V corresponds to the hydrogen absorption to form the β phase (the reduction of water). From these voltammograms, we see that the loading current of 0.1 μA (comparable to the current in pH = 2 solutions at E_L = +0.01 V vs. RHE) can be achieved by employing E_L = −1.45 V vs. SMSE (−0.10 V vs. RHE). Hence, by applying sufficient loading potentials, it is expected to be possible to load hydrogen into H_1-e Pd films quickly even in basic solutions.

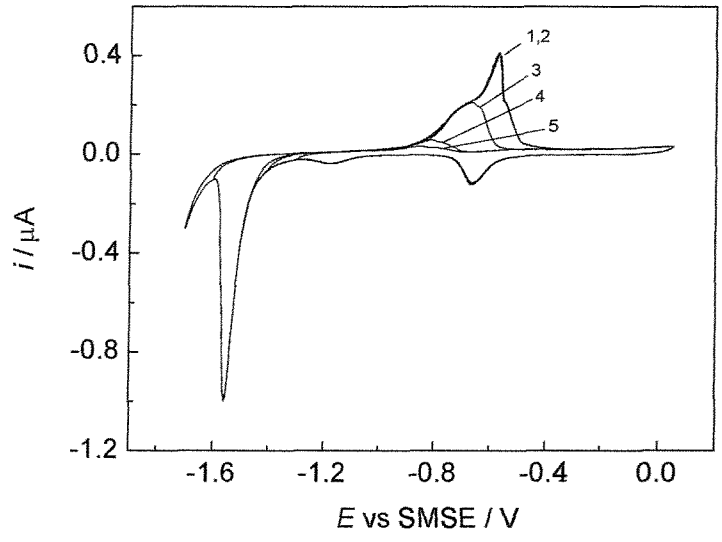

Figure 4.19. Cyclic voltammogram for an H_1-e Pd (B) film (QDep = 11 μC) deposited on a Pt microdisc (d=25 μm) electrode in a deaerated 0.5 M Na_2SO_4 + NaOH solution (pH = 12.1) at 20 mV s^{-1}. Cathodic limits : (1) −1.7 V; (2) −1.6 V; (3) −1.5 V; (4) −1.4 V; (5) −1.3 V.

4-4. Summary

Overview

In the present study, cathodic electrolysis is employed for loading H_1-e Pd films with hydrogen to prepare H_1-e Pd-hydride micro pH sensors. In this chapter, considering the application of the sensors to experiments in 0.5 M Na_2SO_4 + H_2SO_4 (pH ≈ 2), fundamental electrochemistry and hydrogen absorption

behaviour of H_1-e Pd-hydride films were studied in the solution. The study was extended to solutions (pH ≈ 2) containing KCl or $NaClO_4$ as supporting electrolytes and solutions containing no additional background electrolytes. The effect of pH on hydrogen absorption behaviour was also discussed.

0.5 M Na_2SO_4 + H_2SO_4 solutions (pH ≈ 2)

In cyclic voltammetry, peaks on the voltammograms were broadened and shifted as the scan rate was increased. This result is thought to be related to the change in proton concentration within the pores of the nanostructure.

The current transients recorded while loading hydrogen potentiostatically showed two plateau regions, which were found to correspond to hydrogen absorption and hydrogen gas evolution. It was found possible to control the H/Pd ratio of the films by varying the loading potential and / or the loading time. The amount of hydrogen loaded to the films can be monitored by the charge passed during loading, on the condition that the loading time is in the first plateau region.

Solutions containing other supporting electrolytes (pH ≈ 2)

The potentiostatic hydrogen loading of H_1-e Pd films was possible in 1 M KCl + HCl (pH = 1.86) and 1 M $NaClO_4$ + $HClO_4$ (pH = 2.02) solutions by applying the loading potential of +0.01 V vs. RHE, just as in 0.5 M Na_2SO_4 + H_2SO_4 (pH = 1.88) solutions. The behaviour (current transient) was almost identical to that in 0.5 M Na_2SO_4 + H_2SO_4 solutions, suggesting that the H/Pd ratio of the film can be controlled in the same way as mentioned above. It is important to note that the potential should not be scanned to the surface oxide region in solutions containing Cl^- ions, since it causes anodic dissolution of Pd and loss of the film.

Effect of pH

In solutions with higher pHs (approx. pH > 3), rapid loading of hydrogen into H_1-e Pd films can be achieved by using the reduction of water instead of the reduction of protons, but this generally requires more negative overpotential. In a solution with pH = 12.1, it is expected to be possible to load H_1-e Pd (B) films (Q_{Dep} = 11 μC) to β phase region within 1 minute, by applying the loading potential of –1.45 V vs. SMSE (–0.10 V vs. RHE).

Potentiostatic loading of hydrogen

In the following chapter, the potentiometric response of H_1-e Pd-hydride microelectrodes will be discussed. Before the potentiometric measurement, H_1-e Pd films were loaded with hydrogen potentiostatically in various solutions with pH ≈ 2. A loading potential equivalent to +0.01 V vs. RHE (E_L = –0.75 V vs. SMSE or –0.35 V vs SCE) was mainly used and the H/Pd ratio was controlled by varying the loading time. The loading potential was determined as such for two reasons; (1) at more positive potential, longer loading time is required (ie. >1 min), (2) at more negative potential, the loading is so rapid that precise control of the H/Pd ratio (via the loading time) becomes difficult.

Chapter 5. Potentiometric response of H_1-e Pd-hydride microelectrodes

5-1. Potential – time curves after hydrogen loading

5-1-1. 0.5 M Na_2SO_4 + H_2SO_4 (pH ≈ 2) solution

The potential of H_1-e Pd-hydride microelectrodes was monitored in deaerated 0.5 M Na_2SO_4 + 0.05 M H_2SO_4 (pH = 1.88) solutions at 25°C. First, H_1-e Pd films on Pt microdisc electrodes were loaded with hydrogen at –0.75 V to the β phase region. The electric circuit was then opened and the potential ($E_{Pd\text{-}H}$) with respect to the SMSE was monitored in the same solution. While monitoring the $E_{Pd\text{-}H}$, a blanket of argon was maintained above the solution to prevent air from entering the solution throughout the measurement.

A typical $E_{Pd\text{-}H}$ – time curve for an H_1-e Pd (B) film (Q_{Dep} : 11 μC) loaded with hydrogen is shown in *Figure 5.1.*

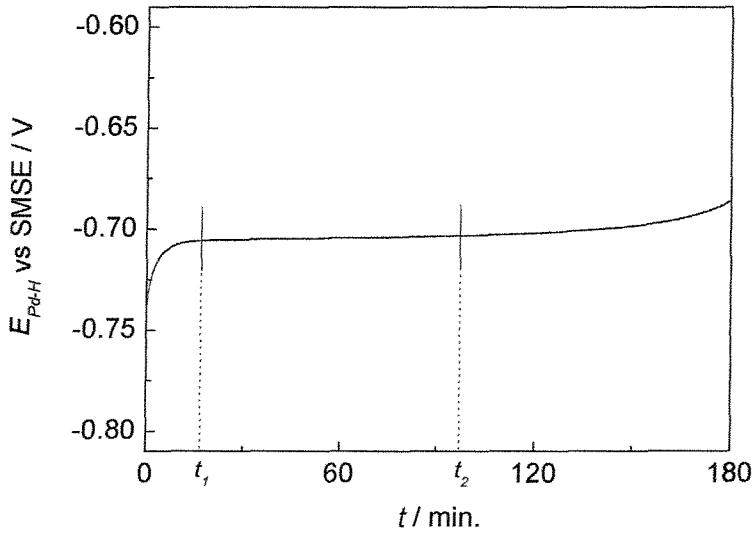

Figure 5.1. Open circuit potential of an H_1-e Pd (B) film (Q_{Dep} : 11 μC) on a 25 μm diameter Pt microelectrode in a deaerated 0.5 M Na_2SO_4, 0.05 M H_2SO_4 solution immediately after hydrogen was loaded at -0.75 V for 60 s. (H/Pd = 0.62).

The potential rose slowly from the loading potential of –0.75 V to reach a plateau at $t = t_1$ minutes. The potential was stable at –0.7033 ± 0.0012 V from $t = t_1$ to t_2 and started to rise again.

5-1-1-(1). Removal of hydrogen under open circuit conditions

The shape of the potential - time curve shown in Figure 5.1 was similar to those previously reported by Jasinski[64] for palladium black plated bulk palladium electrodes, loaded with hydrogen electrolytically. In his study, the electrode was loaded in deaerated 1 N H_2SO_4 solutions and the potential was monitored in various aerated solutions. The rise in potential after the plateau was explained by a decrease in H/Pd ratio to reach the α phase region, due to oxidation of sorbed hydrogen by dissolved oxygen.

To check if hydrogen absorbed in the H_1-e Pd film was lost while monitoring the potential in the present study (Figure 5.1), the amount of hydrogen remaining in the film was estimated from the stripping charge of an anodic potential sweep. The voltammogram conducted after the potential measurement (180 min.) is shown in Figure 5.2. A typical anodic sweep immediately after the loading procedure (without the potential measurement) is also shown for comparison. It is clear from the figure that most of the hydrogen absorbed in the H_1-e Pd film was lost during the potential measurement. The H/Pd ratio after the potential measurement was estimated to be about 0.03 from the stripping charge. This indicates that the potential began to slowly shift positively as the H/ Pd ratio approached the α phase region.

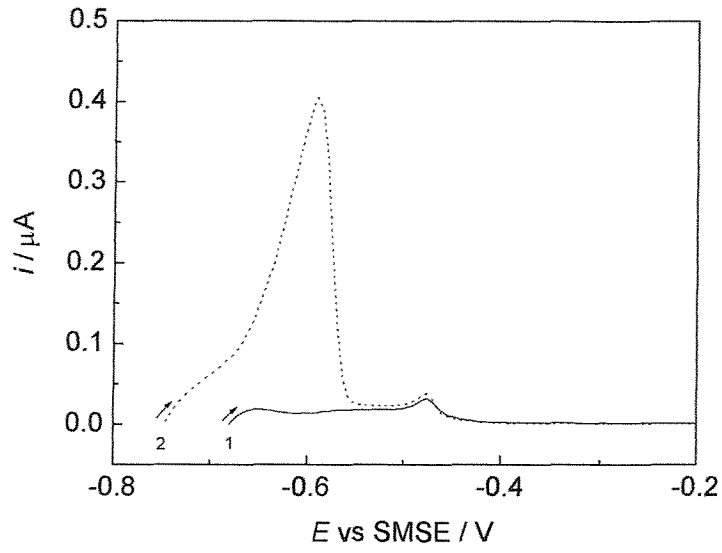

Figure 5.2. Voltammograms for the stripping of hydrogen absorbed in and adsorbed on H_1-e Pd (B) films (Q_{Dep} = 11 μC) on 25 μm diameter Pt microelectrodes in 0.5 M Na_2SO_4, 0.05 M H_2SO_4 solution, recorded at 10 mV s^{-1}. The anodic scans were started immediately after : (1) the measurement of the open circuit potential (shown in Figure 5.1). (2) the film was loaded with H. Loading conditions : Q_L = −0.75 V, t_L = 60 s, H/Pd = 0.62.

The results shown above prove that hydrogen was removed while monitoring the potential, despite operating under open circuit conditions. There are two possible pathways for hydrogen removal which can take place in parallel: namely the oxidation and the recombination processes.

In the present study (Figure 5.1), the solution was deaerated thoroughly and extremely pure reagents were used to prepare the test solutions. Trace quantities of impurities (oxidizing species) or oxygen, however, could still cause the oxidation process :

$$H(Pd-H) \rightarrow H^+ + e \qquad \textit{Equation 5.1}$$

On the other hand, hydrogen absorbed in palladium has a tendency[48] to leave

the metal under open circuit conditions even in the absence of oxidizing agents, by the recombination process[85, 86]. This can be explained by considering the equilibrium :

$$2H\,(Pd-H) \rightleftarrows H_2 \qquad \textit{Equation 5.2}$$

As discussed in Chapter 1, the pressure of hydrogen when the reaction described by Equation 5.2 is in equilibrium is about 0.02 atm[66] at 25 °C. Under the present experimental conditions, the equilibrium is shifted towards the right because of the absence of hydrogen outside the palladium (the solution was deaerated with Ar).

5-1-1-(2). Plateau region

The potential was very stable at about –0.703 V vs. SMSE between $t = t_1$ and t_2. This was assumed to correspond to the potential for α+β phase Pd-hydride. To compare this potential with the reported values for conventional Pd-hydride electrodes, the potential was converted to that with respect to RHE (Reversible hydrogen electrode). The potential of the RHE at 25 °C can be described by :

$$E_{RHE} = -0.05916\ \text{pH} \quad / \text{V vs. SHE}$$

Hence, in a 0.5 M Na_2SO_4 + 0.05 M H_2SO_4 solution (pH=1.88) at 25 °C,

$$\begin{aligned} E_{SMSE} &= +0.640 \quad / \text{V vs. SHE}^1 \\ &= +0.640 + 0.05916\ \text{pH} \quad / \text{V vs. RHE} \\ &= +0.751 \quad / \text{V vs. RHE (pH = 1.88)} \end{aligned}$$

The stable potential of about –0.703 V vs. SMSE observed in Figure 5.1 is, therefore, equivalent to +0.048 V vs. RHE. This reasonably agrees with the reported values[1, 45, 47, 49, 50, 52, 55] (around +0.050 mV vs. RHE) for conventional α+β phase Pd-hydride electrodes in various solutions. As was discussed in Chapter 1, the potential determining reaction for Pd-hydride electrodes is :

$$H^+ + e \rightleftarrows H(Pd-H) \qquad \textit{Equation 5.3}$$

$$E_{Pd-H}\,(\text{vs.SHE}) = E^{\circ}_{Pd-H} + \frac{RT}{F}\ln\frac{a_{H^+}}{a_{H(Pd-H)}} \qquad \textit{Equation 5.4}$$

In the α+β region, the potential ($E_{Pd\text{-}H}$) solely depends on pH (at a fixed temperature), since the activity of hydrogen in the palladium hydride lattice ($a_{H(Pd\text{-}H)}$) is independent of H/Pd ratio in this region, as discussed in Chapter 1.

5-1-1-(3). $0 < t < t_1$

In Figure 5.1 the rise in potential ($0 < t < t_1$) before reaching the stable potential for α+β phase is thought to correspond to the β phase. In the β phase region, $E_{Pd\text{-}H}$ is known to depend on the H/Pd ratio[45, 52, 64]. The rise in potential is associated with the decrease in H/Pd ratio due to the removal of hydrogen by the oxidation and/or recombination processes.

The time, t_1, required for reaching the plateau depends on the initial H/Pd value of the H_1-e Pd-hydride films. Figure 5.3 shows $E_{Pd\text{-}H}$ - time curves for H_1-e Pd-hydride electrodes with various initial H/Pd ratios. The H/Pd ratio was controlled by varying the loading time. For the films with H/Pd of 0.59 and 0.51, about fifteen and ten minutes respectively were needed for the potential to stabilize. In the case of H_1-e Pd films with H/Pd ratio of 0.42 and 0.28, the stable potential for α+β phase was reached almost instantly. For the H_1-e Pd film with H/Pd = 0.10, the potential began to rise slowly from the potential of α+β phase soon after the beginning of the measurement. It can be concluded from these results that H_1-e Pd-hydride microelectrodes show the stable potential for α+β phase when the H/Pd ratio is about 0.1 ~ 0.5. It is noteworthy that the stable potential can be obtained immediately after loading hydrogen to H_1-e Pd films by controlling the H/Pd ratio to ≈0.5 or lower. The H/Pd ratio can be controlled by varying the loading potential and the loading time, as discussed in the preceding chapter.

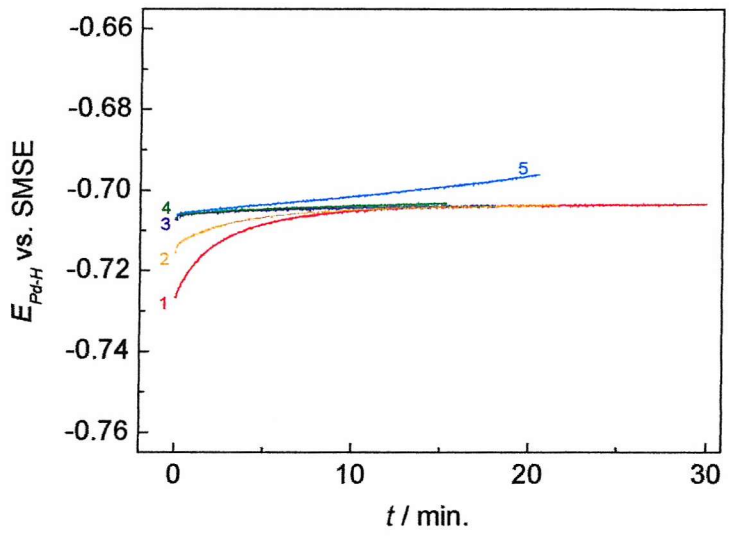

Figure 5.3. Open circuit potential of H_1-e Pd (A) films (Q_{Dep} : 11 μC) on a 25 μm diameter Pt microelectrode in a deaerated 0.5 M Na_2SO_4, 0.05 M H_2SO_4 solution immediately after loading H at E_L = –0.73 V. The H/Pd ratio was controlled by the loading time (t_L). H/Pd = (1) 0.59; (2) 0.51; (3) 0.42; (4) 0.28; (5) 0.10.

It has been reported for conventional palladium electrodes that electrolytic loading of hydrogen leads to higher hydrogen concentrations at the surface than in the bulk palladium, which result in a long t_1 (time to reach the plateau). To minimize this concentration gradient, anodization procedures were employed by several workers[52, 53]. The anodization procedures involve reversing the current for a short time after terminating the cathodic loading current; this is then followed by the measurement of the open circuit potential. In the case of H_1-e Pd films, however, the time taken for an H atom to diffuse through the wall (2.0~2.5 nm) of the nanostructure is calculated to be of the order of 50 nanoseconds (the diffusion coefficients of H in the α and β phases are around 2×10^{-7} and 2×10^{-6} cm^2 s^{-1} respectively). Thus immediately after cathodization the concentration of hydrogen can be assumed to be constant throughout the thickness of the pore wall, and for this reason anodization was not employed in the present study.

5-1-1-(4). $t_1 < t < t_2$

After showing the stable potential for α+β phase, the $E_{Pd\text{-}H}$ began to rise slowly. This is consistent with an increase of H/Pd ratio, as it approaches the α-phase region, the potential has been reported to depend on the H/Pd ratio[45, 52].

5-1-1-(5). Plateau potential and lifetime of H_1-e Pd hydride microelectrodes

In this section, the effects of the film thickness (controlled by Q_{Dep}), the geometric diameter and the nanostructure (dependent on the surfactant contained in the plating mixture) on the plateau potential for α+β phase and the lifetime (the length of the plateau) are discussed. Open circuit potential – time curves for various H_1-e Pd films on Pt microdisc electrodes are studied, using the same experimental procedure as that described in 5-1-1.

The overall shape of the resulting curve for each electrode was similar to that shown in Figure 5.1. The plateau potential (E_{PL}), t_1, t_2, and the lifetime ($t_2 - t_1$) for each case are listed in Table 5.1. Here, the potential at the time when $dE_{Pd\text{-}H}/dt$ is minimum (typically, 1 mV h^{-1}) in the plateau region was taken as E_{PL}, and the length of time where $E_{Pd\text{-}H} - E_{PL} \leq \pm 0.0012$ V (equivalent to ±0.02 in pH unit at 25 °C) was taken as the lifetime ($t_2 - t_1$).

Variation in E_{PL} found among ten different H_1-e Pd films was very small. E_{PL} ranged from −0.7049 V to −0.7032 V vs. SMSE (approx. +0.046 ~ +0.048 V vs RHE). The diameter, the Q_{Dep} and the surfactant added in the plating mixture did not show appreciable effect on the E_{PL} value.

Table 5.1. Estimated values of the plateau potential (E_{Pl}) and the lifetime for various H_1-e Pd-hydride electrodes. E_L = –0.75 V, H/Pd = 0.60 ~ 0.63. Test solution : deaerated 0.5 M Na_2SO_4, 0.05 M H_2SO_4 (pH = 1.88)

Electrode type	Substrate		Deposition of films			Results			
	Material	Nominal diameter / μm	Surfactant	Charge Q_{dep} / μC	Charge density / C cm^{-2}	Plateau potential E_{Pl} / V	t_1 / min.	t_2 / min.	Lifetime $t_2 - t_1$ / min.
H1-e Pd(A)	Pt	25	$C_{16}EO_8$	11	2.2	-0.7045	13	77	64
						-0.7049	15	76	61
H1-e Pd(B)	Pt	25	Brij® 56	5.5	1.1	-0.7032	20	51	31
						-0.7033	10	49	39
	Pt	25	Brij® 56	11	2.2	-0.7033	17	97	80
						-0.7037	28	94	66
	Pt	25	Brij® 56	22	4.5	-0.7040	31	210	179
						-0.7035	54	185	131
	Pt	10	Brij® 56	1.8	2.2	-0.7034	13	50	37
						-0.7037	6	33	27

H_1-e Pd-hydride microelectrodes had limited lifetime because of the removal of hydrogen loaded in the film under the open circuit condition. Comparing H_1-e Pd (B) films on 25 μm diameter Pt microdiscs with different Q_{Dep} (5.5, 11 and 22 μC) in Table 5.1, the lifetime ($t_2 - t_1$) as well as t_1 and t_2 was approximately proportional to Q_{Dep}. This suggests that the removal rate of hydrogen is independent of Q_{Dep}, when the H_1-e Pd films have the same nanostructure and close geometric diameters.

The effect of the diameter on the lifetime can be discussed by comparing H_1-e Pd (B) films with the same charge density (2.2 C m^{-2}) on Pt microdisc electrodes with different diameters (25 and 10 μm). The H_1-e Pd (B) films on 25 μm microdiscs showed greater t_1, t_2 and lifetime ($t_2 - t_1$) than those on 10 μm diameter microdiscs by a factor of 2~3 times, although they had the same thickness of the H_1-e Pd film. This suggests that hydrogen removal was accelerated by reducing the geometric diameter.

Comparison between H_1-e Pd (A) and H_1-e Pd (B) films reveals that H_1-e Pd (B) showed slightly greater values for t_1, t_2 and the lifetime. As discussed in Chapter 3, the electroactive area of H_1-e Pd (A) films is nearly twice that of H_1-e Pd (B) films with the same Q_{Dep}. Considering that the difference in the lifetime between two H_1-e Pd films was small, the effect of the electroactive area on the

rate of hydrogen removal is thought to be small.

To summarize the results discussed above, the rate of hydrogen removal was appreciably faster for the H_1-e Pd films with smaller diameter, while the effect of the electroactive area on the rate was relatively small. This may suggest that the removal rate of hydrogen from H_1-e Pd-hydride films under open circuit potential conditions is controlled by diffusion of oxidizing species (impurities or oxygen), considering that the diffusion of species in the solution to a microelectrode is faster for smaller electrodes.

The lifetimes of H_1-e Pd-hydride electrodes on 25 μm diameter Pt microdiscs were about 1 ~ 1.5 hours (Q_{Dep} = 11 μC) and 2 ~ 3 hours (Q_{Dep} = 22 μC), which are sufficient for typical SECM experiments although they are too short for continuous process monitoring. In the case of H_1-e Pd films on 10 μm diameter Pt microdiscs, a charge density of 4.5 C m^{-2} (Q_{Dep} = 3.6 μC) or more is needed to take the lifetime beyond one hour.
It was difficult to achieve a lifetime longer than an hour using an H_1-e Pd microelectrode with a diameter still smaller than 10 μm. To obtain a useful lifetime (>1 hr), a further increase in the thickness (Pd deposition charge density > 4.5 C m^{-2}) is required, which is believed to cause a significant enlargement of the diameter, as discussed in Chapter 3. Recessing the Pt microdisc electrode before H_1-e Pd film deposition could be a solution for preventing the increase in diameter. Using this method, it is expected to be possible to increase the Pd deposition charge density to get sufficient lifetime for SECM experiments, without causing the enlargement of the diameter. Well established procedures[122, 123] (repetitive potential pulsing in a solution containing $CaCl_2$, H_2O and HCl) to etch Platinum microdisc electrodes have been reported.

5-1-2. Solutions containing other supporting electrolytes

In order to study the effect of supporting electrolytes on the open circuit potential of H_1-e Pd-hydride microelectrodes, $E_{Pd\text{-}H}$ was monitored in solutions (pH ~ 2) containing 1 M KCl + HCl or 1 M $NaClO_4$ + $HClO_4$, after the film was loaded with hydrogen in each solution.

5-1-2-(1). 1 M KCl + HCl (pH ≈ 2) solution

An H_1-e Pd (B) film (Q_{Dep} = 11 μC) was loaded with hydrogen at –0.35 V vs. SCE to H/Pd = 0.61 in a 1 M KCl + HCl (pH = 1.86) solution, and its potential ($E_{Pd\text{-}H}$) was monitored in the same solution. The overall shape of the $E_{Pd\text{-}H}$ – time curve was almost identical to those obtained for 0.5 M Na_2SO_4 + H_2SO_4 solutions (Figure 5.1). The lifetime in the 1 M KCl + HCl (pH = 1.86) solution was 65 minutes, which is comparable to that in 0.5 M Na_2SO_4 + H_2SO_4 solutions (shown in Table 5.1). It has to be noted, however, that the lifetimes observed in different solutions cannot be compared directly, since impurities contained in the reagents used to prepare the solutions are expected to be different, which may affect the oxidation rate of hydrogen loaded in the H_1-e Pd films.
The plateau potential (E_{PL}) in the 1 M KCl + HCl solution (pH = 1.86) was –0.2987 V SCE. Taking into account the relationship of potential between SCE and RHE;

$$E_{SCE} = +0.2412 + 0.05916\ \mathrm{pH} \quad / \text{V vs. RHE}^{1}$$
$$= +0.351 \quad / \text{V vs. RHE (pH = 1.86)}$$

the plateau potential in the solution is equivalent to +0.052 V vs. RHE.

5-1-2-(2). 1 M $NaClO_4$ + $HClO_4$ (pH ≈ 2) solution

The open circuit potential of an H_1-e Pd-hydride microelectrode was monitored in a 1 M $NaClO_4$ + $HClO_4$ (pH = 2.02) solution. Before the measurement, the electrode (H_1-e Pd (B) film; Q_{Dep} = 11 μC) was loaded with hydrogen at –0.75 V vs. SMCE to H/Pd = 0.61, in the same solution. Overall the $E_{Pd\text{-}H}$ – time curve had a similar shape to those obtained in 0.5 M Na_2SO_4 + H_2SO_4 and 1 M KCl + HCl solutions, although a difference was found after t_2. As shown in Figure 5.4, at about t = 80 min, the $E_{Pd\text{-}H}$ began to rise rather quickly then rose very sharply at about t = 100 min. The steep rise in potential was in contrast to the results obtained in 0.5 M Na_2SO_4 + H_2SO_4 and 1 M KCl + HCl solutions, where the

potential rise after $t = t_2$ was much slower.

As discussed in the preceding chapter, reduction of ClO_4^- can take place at H_1-e Pd films in the absence of adsorbed species. The sharp rise in potential after $t = t_2$ is presumably due to the ClO_4^- reduction, which may accelerate the oxidation of hydrogen.

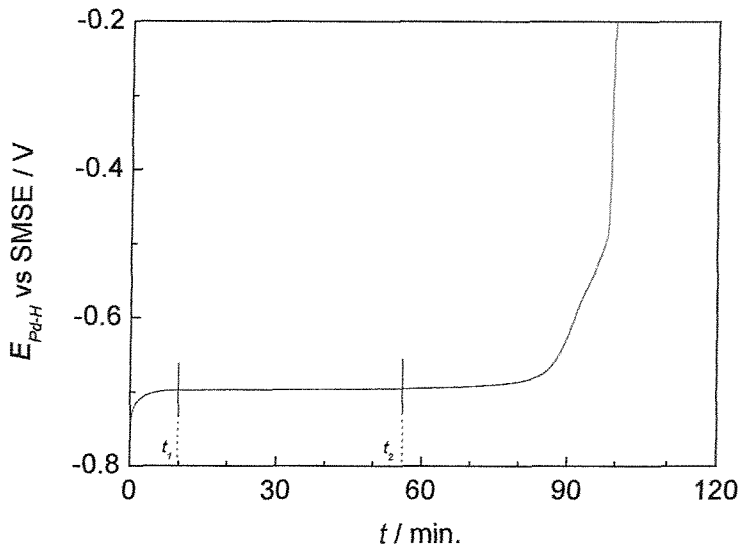

Figure 5.4. Open circuit potential of an H_1-e Pd (B) film (Q_{Dep} : 11 μC) on a 25 μm diameter Pt microelectrode in a deaerated 1 M $NaClO_4$ + $HClO_4$ solution (pH = 2.02) immediately after loading H at –0.75 V (H/Pd = 0.61).

The lifetime in the 1 M $NaClO_4$ + $HClO_4$ solution (pH = 2.02) was 46 minutes, which is shorter than those in Na_2SO_4 + H_2SO_4 and KCl + HCl solutions. Oxidation of hydrogen at the surface by ClO_4^- might have accelerated the removal of hydrogen, although the difference in lifetime between various solutions cannot be attributed directly to the effect of anions, because of the difference in impurities contained in the reagents.

The plateau potential (E_{PL}) in the 1 M $NaClO_4$ + $HClO_4$ solution (pH = 2.02) was –0.697 V SMSE, which is equivalent to about +0.063 V vs. RHE (E_{SMSE} = +0.760 V vs. RHE at this pH). Slight variations were found for the plateau potential values in different solutions, 1 M $NaClO_4$ + $HClO_4$, Na_2SO_4 + H_2SO_4 and KCl +

HCl solutions (+0.046 ~ +0.063 V vs. RHE). However, it is difficult to discuss this difference in detail, because of the uncertainty in the liquid junction potential (E_{LJ}) between the test solution and the reference electrode solution. E_{LJ} will be discussed in detail in 5-2-1.

5-2. Potential in solutions with different pH

5-2-1. Calibration curves

5-2-1-(1). 0.5 M Na_2SO_4 solutions

To study the potentiometric pH response of H_1-e Pd-hydride microelectrodes, titrations were performed in solutions containing 0.5 M Na_2SO_4. In each experiment, an H_1-e (B) Pd film on a Pt microdisc electrode was loaded with hydrogen cathodically at –0.75 V, in a 0.5 M Na_2SO_4 + 0.05 M H_2SO_4 solution. The open circuit potential ($E_{Pd\text{-}H}$) was monitored in the same solution, and the titration was started after the $E_{Pd\text{-}H}$ reached the stable value corresponding to the α+β phase. Diluted NaOH was added to raise the pH and diluted H_2SO_4 to lower the pH. Ar was bubbled continuously during the titration for two purposes, to deaerate and to stir the solution. During the titration, $E_{Pd\text{-}H}$ and the output of a combination glass pH electrode were monitored simultaneously. An example of the result of titrations is shown in Figure 5.5 The $E_{Pd\text{-}H}$ responded quickly when the pH was changed, and $E_{Pd\text{-}H}$ was very stable after each addition of NaOH or H_2SO_4. The response time will be discussed in section 5-2-2.

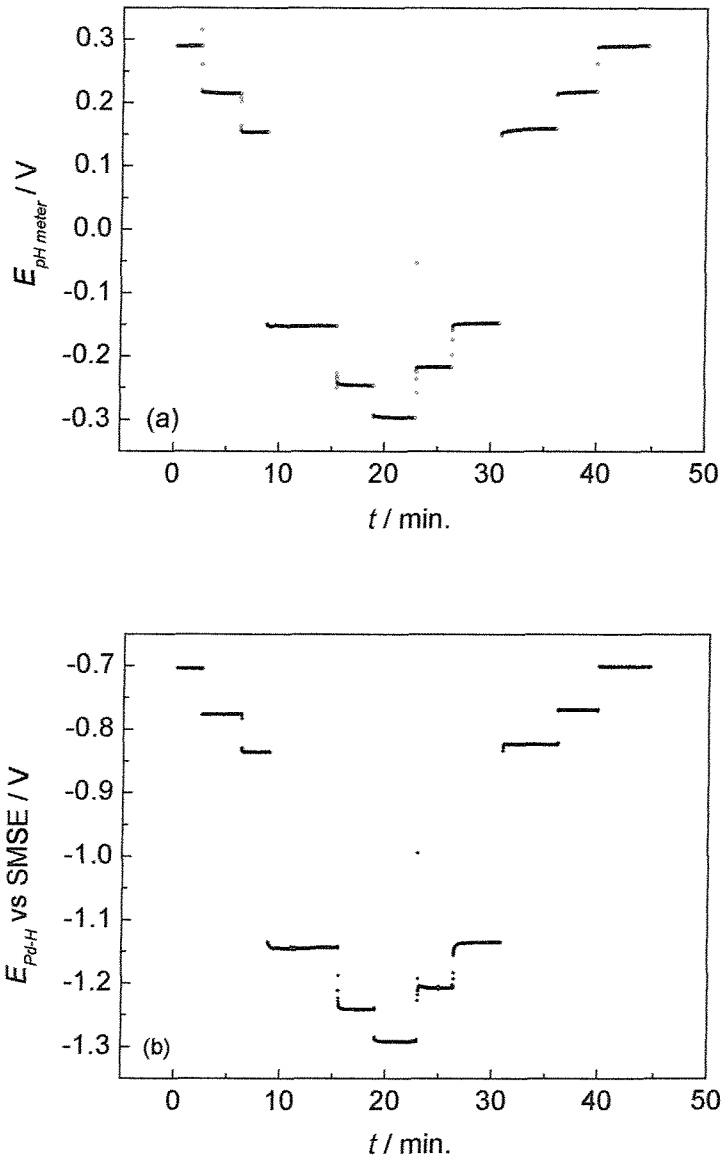

Figure 5.5. (a) Output of a pH meter connected to a combination glass pH electrode and (b) Open circuit potential of an H_1-e Pd (B) film (Q_{Dep} : 11 μC) loaded with H, during titration. The H loading conditions were : E_L = –0.75 V, t_L = 60 sec. The titration was started in a deaerated 0.5 M Na_2SO_4, 0.05 M H_2SO_4 solution after the E_{Pd-H} had stabilized. The solution was kept deaerated by continuous bubbling of Ar. Aliquots of 1 M NaOH and 1 M H_2SO_4 were used to control the pH.

For each plateau in Figure 5.5, $E_{Pd\text{-}H}$ was read and plotted as a function of pH, as shown in Figure 5.6. Here, the output of the combination pH electrode (in V) was converted to pH using a calibration curve obtained before the titration. In addition, the $E_{Pd\text{-}H}$ and the pH were measured in a buffer solution (0.5 M Na_2SO_4 + 0.025 M NaH_2PO_4 + 0.025 M Na_2HPO_4) before and after the titration and also plotted on the graph. The excellent linearity of the $E_{Pd\text{-}H}$ vs. pH relationship can be seen from the graph. All the plots for both forward and reverse titrations are on a straight line, which proves that the potentiometric pH response of the H_1-e Pd-hydride microelectrode is highly reversible.

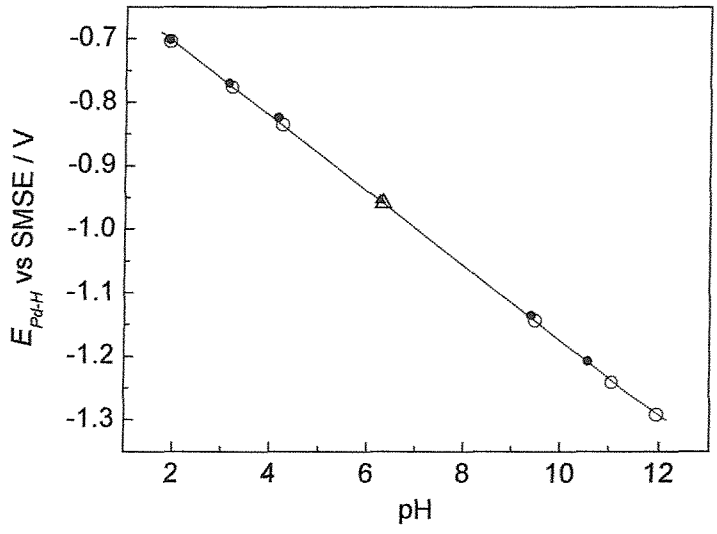

Figure 5.6. $E_{Pd\text{-}H}$ vs pH calibration curve obtained from the titration shown in Figure 5.5 in a deaerated 0.5 M Na_2SO_4 solution. ○, forward titration (NaOH was added); ●, reverse titration (H_2SO_4 was added); △, in 0.5 M Na_2SO_4 + 0.05 M phosphate buffer (before the titration); ▲, 0.5 M Na_2SO_4 + 0.05 M phosphate buffer (after the titration).

To assess the reproducibility of the potentiometric pH response of H_1-e Pd-hydride microelectrodes, two further titrations were performed using two different electrodes (Q_{Dep} = 22 and 44 μC). The plateau $E_{Pd\text{-}H}$ and pH values are plotted in Figure 5.7, together with the results shown in Figure 5.6. All the plots from three different electrodes are on a straight line with very small dispersion, which proves the excellent reproducibility of potentiometric pH

response among different electrodes.

By linear regression, correlation between E_{Pd-H} and pH in 0.5 M Na_2SO_4 solutions was calculated to be :

$$E_{Pd-H} = -0.5891 - 0.0587\,\mathrm{pH} \quad / \mathrm{vs.SMSE}$$
$$r^2 = 0.99986 \qquad \textit{Equation 5.5}$$

The slope (–0.0587 V/pH) is in good agreement with the theoretical value (–2.303 RT/nF = –0.0592 V/pH for 25 °C and n=1). The intercept was –0.05891 V vs. SMSE, which is equivalent to about +0.051 V vs. SHE. This reasonably agrees with previous works for conventional Pd-hydride electrodes, where the plateau potentials for α+β phase were reported to be about +0.050 V vs. RHE in various solutions. However, discussion of the absolute values measured in the present study requires the consideration of liquid junction potentials (E_L) between the reference electrode solution and the test solution.

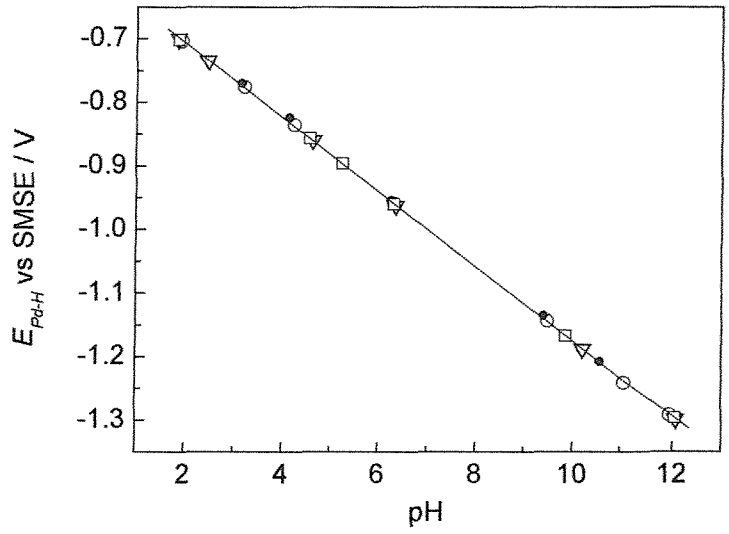

Figure 5.7. E_{Pd-H} vs pH calibration curve obtained from titrations in deaerated 0.5 M Na_2SO_4 solutions, using 3 different H1-e Pd (B) films on 25 mm diameter Pt microdisc electrodes. H_1-e Pd films were loaded with hydrogen at E_L = –0.75 V in deaerated 0.5 M Na_2SO_4, 0.05 M H_2SO_4 solutions where the titrations were started. ○/●, Q_{Dep} = 11 μC, forward / reverse titration; □, Q_{Dep} = 22 μC, forward titration; ▽, Q_{Dep} = 44 μC, forward titration.

Liquid junction potential (E_{LJ})

Concentration gradients exist between two different solutions (liquid junction). The liquid junction is not at equilibrium, because net flows of mass occur continuously across the junction. However, a mass transport steady state is reached ultimately when the effects of diffusion and migration are balanced out. Liquid junction potentials can be classified into three types[124] :

(a) Two solutions of the same electrolyte at different concentrations; e.g. 0.01 M HCl / 0.1 M HCl.
(b) Two solutions at the same concentration with different electrolytes having an ion in common; e.g. 0.1 M HCl / 0.1 M KCl.
(c) Two solutions not satisfying conditions (a) or (b); e.g. 0.1 M HCl / 0.05 M KNO_3.

While the E_{LJ} for type (a) junctions can be determined by calculation independent of the method of forming the junction, type (b) and (c) junctions have potentials that depend on the technique of junction formation and can be treated only in an approximate manner.

Liquid junctions between the reference electrode solution and the test solution in the present study all belong to type (c). Approximate values for E_{LJ} for type (b) and (c) junctions can be obtained by making assumptions that the concentrations of ions everywhere in the junction are equivalent to activities, that ionic mobilities are independent of concentration, and that the concentration of each ion follows a linear transition between the two phases. Then, E_{LJ} for type (b) and (c) junctions can be estimated by the Henderson equation[125] :

$$E_{LJ} = \frac{\sum_i \frac{|z_i| u_i}{z_i} \left[C_i(\beta) - C_i(\alpha)\right]}{\sum_i |z_i| u_i \left[C_i(\beta) - C_i(\alpha)\right]} \frac{RT}{F} \ln \frac{\sum_i |z_i| u_i C_i(\alpha)}{\sum_i |z_i| u_i C_i(\beta)} \qquad \textit{Equation 5.6}$$

where u_i is the mobility, z_i the charge, C_i the molar concentration of species i.

It is impossible to estimate the liquid junction potential for the junction;

$$K_2SO_4 \text{ (sat.)} \quad / \quad 0.5 \text{ M } Na_2SO_4 + H_2SO_4 \text{ (+ NaOH)}$$

since the activity coefficients for the species in the solution is far from unity, ie. the mean activity coefficients, $\gamma_{\pm}$, for saturated K_2SO_4 ($\approx$ 0.7 M) and 0.5 M Na_2SO_4 are 0.23 and 0.24 respectively[126].

5-2-1-(2). Buffer solutions

To assess the absolute values of the potential of H_1-e Pd-hydride microelectrodes and compare them with reported values more precisely, potentiometric measurements were performed using systems designed to reduce the liquid junction potential. Dilute buffer solutions were employed as test solutions, together with an SCE as the reference electrode. In these systems, ionic transport at the junction is dominated by KCl (saturated), whose concentration is much higher than salts in the test solutions. Owing to the nearly equal mobility of K^+ and Cl^-, the liquid junction potential can be minimized, although accurate values of E_{LJ} still cannot be calculated. Reported values[2] of E_{LJ} for the junction between saturated KCl solution and buffer solutions used in the present study are summarized in Table 5.2. They ranged from –0.0018 V to –0.0030 V.

Table 5.2. Reported values[2] of the liquid junction potential.

Liquid junction		Liquid junction potential
Reference electrode solution	Test solution	E_{LJ} / V
KCl (sat.) approx. 4.2 M	0.01 M HCl	-0.0030
	0.05 M KH phthalate	-0.0026
	0.025 M NaH_2PO_4 + 0.025 M Na_2HPO_4	-0.0019
	0.025 M $NaHCO_3$ + 0.025 M Na_2CO_3	-0.0018
	0.01 M NaOH	-0.0023

The open circuit potential of H_1-e Pd-hydride microelectrodes was measured in the solutions shown in Table 5.2 in the following manner. First, an H_1-e Pd (B) film (Q_{Dep} = 22μC) on a 25 μm diameter Pt microdisc electrode was loaded with hydrogen cathodically at –0.75 V in a deaerated 0.5 M Na_2SO_4 + 0.05 M H_2SO_4 solution. After the $E_{Pd\text{-}H}$ reached the stable value corresponding to the α+β phase, the electrode was rinsed with purified water and transferred to a test solution (also deaerated), thermostated at 25 °C. The potential was monitored with respect to SCE for about 3 minutes. The electrode was then rinsed and immersed in a deaerated 0.5 M Na_2SO_4 + 0.05 M H_2SO_4 solution. The potential was monitored again in this solution to make sure that the electrode was still showing the stable potential for α+β phase. The electrode was then rinsed and transferred to the next test solution where the potential was monitored. By repeating this procedure, the potential of an H_1-e Pd microelectrode was measured in five different solutions listed in Table 5.2.

Two sets of measurements were conducted and the resulting values of $E_{Pd\text{-}H}$ were plotted as a function of pH in Figure 5.8.

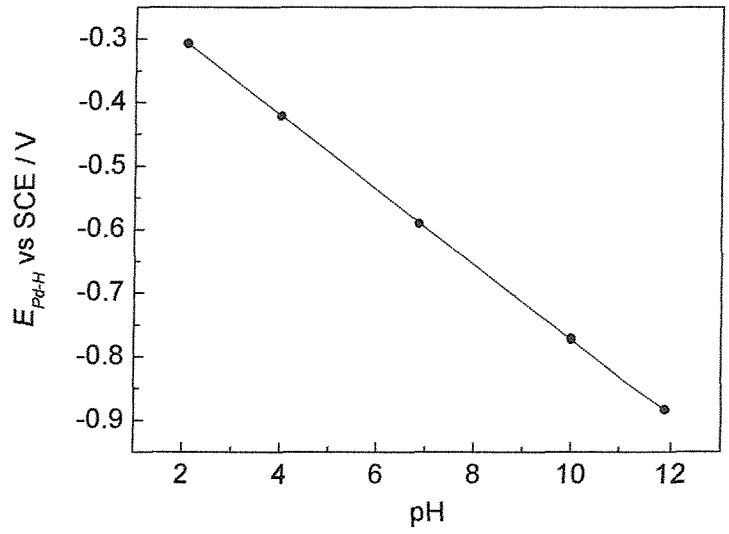

Figure 5.8. $E_{Pd\text{-}H}$ vs pH calibration curve obtained in deaerated buffer solutions. An H_1-e Pd (B) film (Q_{Dep} = 22 μC) on 25 μm diameter Pt microdisc was loaded with hydrogen at E_L = –0.75 V in a deaerated 0.5 M Na_2SO_4, 0.05 M H_2SO_4 solution. The electrode was transferred to the buffer solutions after the potential stabilized.

Excellent linearity and reproducibility are found for the relationship between the E_{Pd-H} and the pH. The relationship can be described by :

$$E_{Pd-H} = -0.1871 - 0.0586\,\mathrm{pH} \quad / \mathrm{vs.SCE}$$
$$r^2 = 0.99997 \qquad \textit{Equation 5.7}$$

The slope (–0.0586 V/pH) is in good agreement with the theoretical value. The intercept was –0.1871 V vs. SCE, which is equivalent to about +0.054 V vs. SHE. . To compare the calibration curve with the predicted line (slope : 2.303 RT/F = 0.05916 V/pH, intercept : +0.050 V vs. SHE), the potentials of the calibration curve were converted to the value with respect to SHE. The resulting calibration curve is shown in Figure 5.9, together with the predicted line.

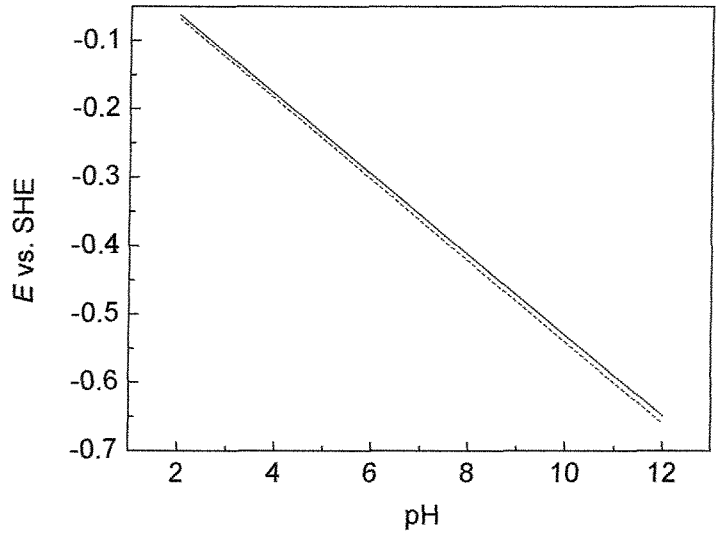

Figure 5.9. E_{Pd-H} vs pH calibration curve obtained in deaerated dilute buffer solutions (solid line). Results shown in Figure 5.8 are converted to the potential with respect to SHE. The predicted line (slope : –0.05916 V/pH, intercept : +0.050 V) is shown for comparison (solid line).

Potentials were not corrected for variations in the liquid junction potential, since the values shown in Table 5.2 can only be used for reference purposes. It can be seen from the graph that the difference in potential between the calibration curve and the predicted line is small in the whole pH range investigated in the present study. The differences were about 0.005 V at pH = 2 and about 0.011 V at pH = 12. Considering the expected experimental errors;

(a) Change in $E_{Pd\text{-}H}$ with time: ~ ±1.2mV.
(b) Potential of SCE: ~ ±1mV
(c) Temperature control of the experimental cell: ~ ±1 °C; corresponding to ~ ±0.7 mV[52] ($E_{Pd\text{-}H}$), ~ ±0.7 mV[1] (SCE).
(d) Liquid junction potential: ~ ±3 mV

it can be concluded that the potentiometric pH response of H_1-e Pd-hydride electrodes was almost theoretical and ideal.

5-2-1-(3). Discussion

From the results shown above, H_1-e Pd-hydride microelectrodes are shown to be excellent potentiometric micro pH sensors, on the condition that a calibration has been performed using the same system (the test solution and the reference electrode). The potential vs. pH calibration curves for H_1-e Pd-hydride microelectrodes appear to possess excellent linearity. Furthermore, the potentiometric pH response is highly reversible for forward and reverse titration, and results from three different electrodes show an excellent reproducibility. Once calibration is conducted using an electrode, further calibration (for each electrode, or before and after the experiments) is believed to be unnecessary, thanks to the excellent reproducibility.

The reproducibility and linearity are a clear advantage over other potentiometric micro pH sensors, whose potentiometric response often varies from one electrode to another. For most potentiometric micro pH sensors, calibration before and after performing the pH measurement experiments is required and if the two calibrations show significant differences, the experiment has to be discarded and repeated[127].

From the sources of errors discussed above (a~d), the expected error is less than ~ ±0.003 V (corresponding to 0.05 pH units), on the condition that a calibration has been performed using the same test solution and the reference electrode (by performing a calibration using the same system, the liquid junction potential is incorporated in the calibration curve).
It is noteworthy that a care has to be taken to the error in pH values of solutions used for calibration. For example, if a combination pH electrode is used, the error can be caused by the potential of the pH electrode (temperature dependence etc.) and the liquid junction potential between the test solution and the solution of the built-in reference electrode.

The slope and the intercept of the calibration curve obtained in the dilute buffer solutions agreed reasonably with the previous reports where the potentials of α+β phase Pd-hydride electrodes were +0.050 V vs RHE. It proves that the potentiometric pH response of the H_1-e Pd-hydride microelectrodes is almost theoretical. Hence, using systems where the liquid junction potential is small (ie. < 0.003 V), an approximate measurement (accuracy ~ ± 0.2 pH unit) is possible using the predicted line instead of a calibration curve.

5-2-2. Response Time

The potentials monitored for 30 s. from the time when an H_1-e Pd-hydride electrode was placed ($t = 0$) in solutions with different pH are shown in Figure 5.10. The electrode was loaded with hydrogen in a 0.5 M Na_2SO_4 + 0.05 M H_2SO_4 solution and rinsed with purified water before being transferred to each solution.
As can be seen from the graph, the potential responded quickly when the electrode was placed in each solution, i.e. the potential reached a stable value within 1 s. In order to evaluate the response time quantitatively in more detail, however, further investigation is necessary.

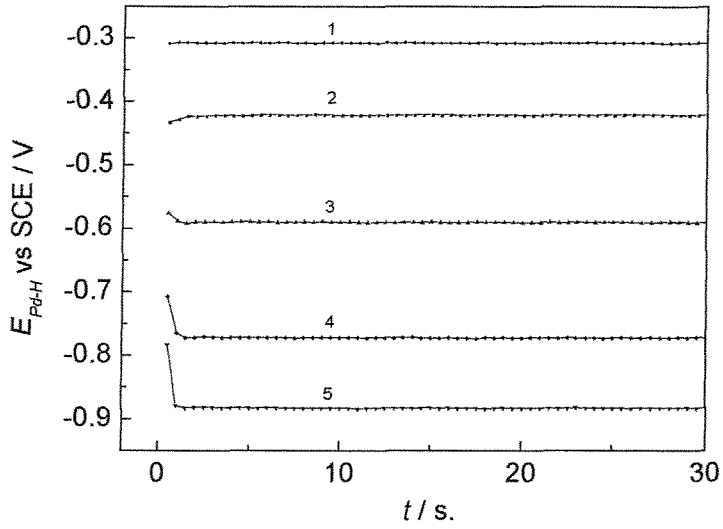

Figure 5.10. Potentiometric pH response of an H_1-e Pd (B) film (Q_{Dep} : 22 μC) loaded with hydrogen. The electrode was loaded with hydrogen at E_L = –0.75 V for t_L = 70 s. in a deaerated 0.5 M Na_2SO_4, 0.05 M H_2SO_4 solution. After its potential stabilized, the electrode was transferred to each buffer solution at t=0. (1) pH 2.06 (2) pH 4.00 (3) pH 6.86 (4) pH 10.00 (5) pH11.88

5-3. Influence of dissolved oxygen

5-3-1. Current transient while loading hydrogen in an aerated solution

To assess the possibility of applying H_1-e Pd-hydride microelectrodes as micro pH sensors in aerated solutions, an H_1-e Pd (B) film was loaded with hydrogen in an aerated 0.5 M Na_2SO_4 + 0.05 M H_2SO_4 solution and the potential was monitored in the same solution. A current transient recorded while loading hydrogen into the film is shown in Figure 5.11. The shape of the current transient is similar to that obtained in a deaerated solution which is also shown in Figure 5.11. The cathodic current was larger in a deaerated solution, owing to the presence of the reduction current for dissolved oxygen. The difference was constant at about 9 nA throughout the measurement, suggesting that the

oxygen reduction current was independent of hydrogen content of the H_1-e Pd film, at this potential.

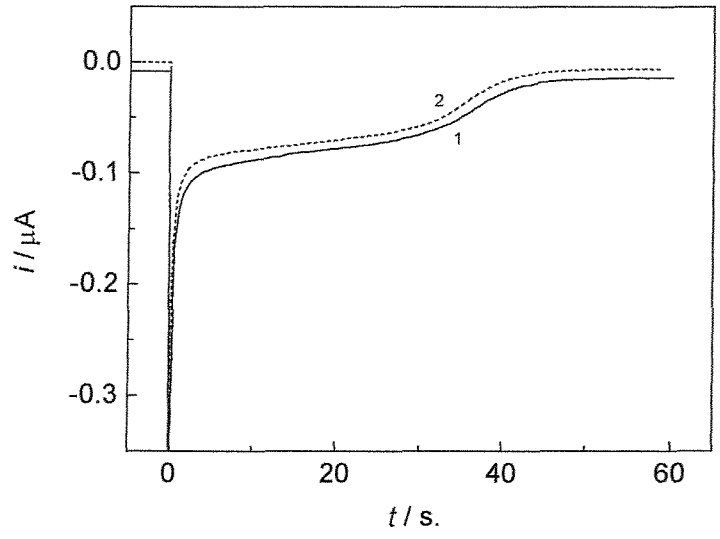

Figure 5.11. Current transient while loading hydrogen into an H_1-e Pd (B) film (Q_{Dep} : 9.0 μC) on a 25 μm diameter Pt microelectrode in a 0.5 M Na_2SO_4 + 0.05 M H_2SO_4 solution at –0.75 V. (1) aerated (2) deaerated

5-3-2. Potential in an aerated solution

The potential monitored after the loading procedure in the aerated solution is shown in Figure 5.12. The potential reached a plateau in 1 minute, and the length of the plateau corresponding to the α+β phase was about 3 minutes. After the plateau, $E_{Pd\text{-}H}$ rose rather quickly and at around 5.7 min., $E_{Pd\text{-}H}$ rose sharply to stabilize at around +0.2 V.

Compared to deaerated conditions, the length of the plateau is significantly shorter, which clearly indicates that the removal of hydrogen is accelerated by the presence of oxygen. In contrast to the length of the plateau which is affected drastically by the presence of oxygen, the plateau potential value (–0.697 V) is only slightly shifted positive (6~7 mV) from the potential in deaerated solutions (see Table 5.1).

The H_1-e Pd-hydride is thought to be in the β phase between $t = 0$ and 1min., in the α+β phase at the plateau potential, and in the α phase from around $t = 5$ to 5.7 min. The final potential value of +0.2 V (circa +0.80 V vs. SHE at pH = 2) is thought to be the corrosion potential with oxygen reduction and Pd dissolution as the cathodic and anodic components[128]. It is assumed, therefore, that removal of sorbed hydrogen was completed at around t = 5.7 min.

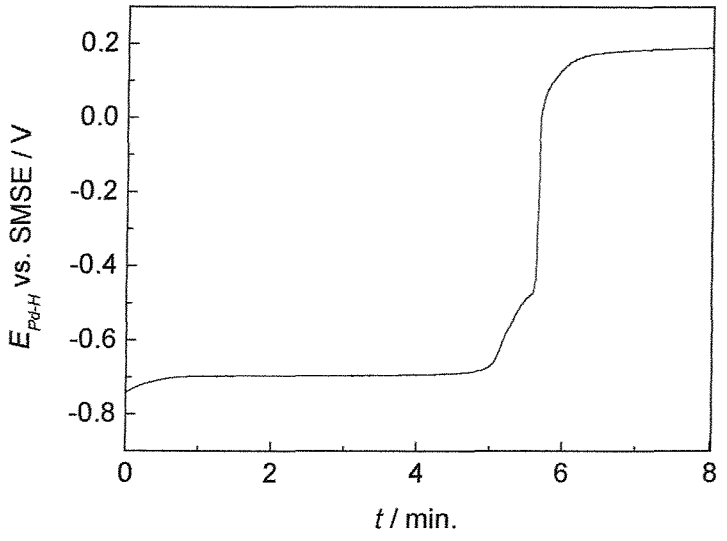

Figure 5.12. Open circuit potential of an H_1-e Pd (B) film (Q_{Dep} : 9.0 μC) on a 25 μm diameter Pt microelectrode in an aerated 0.5 M Na_2SO_4, 0.05 M H_2SO_4 solution immediately after loading H at −0.75 V for 60 s. (expected H/Pd = 0.62).

At the plateau potential, three electrode reactions are believed to be taking place (excluding the reactions associated with impurities) :

Anodic reaction

(a) Oxidation of sorbed H ; $H\ (Pd\text{-}H) \rightarrow H^+ + e$

Cathodic reactions

(c-1) Reduction of protons in the solution; $H^+ + e \rightarrow H(Pd\text{-}H)$

(c-2) Reduction of oxygen dissolved in the solution

In a deaerated solution, reaction (a) and (c-1) proceed at the same rate (exchange current density), since reaction (c-2) does not take place. In an aerated solution, the rate of reaction (a) and the total rate of reactions (c-1) and (c-2) balance. Hence, reaction (a) proceeds faster than reaction (c-1) to compensate the electron transfer corresponding to the reaction (c-2). This accounts for the very short length of the plateau potential. The plateau potential is assumed to be a mixed potential due to the reactions (a), (c-1) and (c-2). The potential shift caused by the presence of oxygen will be discussed later (in Figure 5.14).

5-3-3. Oxygen reduction on H_1-e Pd (-hydride) electrodes

Figure 5.13 shows cyclic voltammograms for the H_1-e Pd (B) film used for the experiments shown above, obtained in aerated and deaerated solutions. Below –0.1 V on the cathodic scan and below +0.2 V on the anodic scan, the voltammogram recorded in the aerated solution is shifted towards negative currents, which is explained by presence of the reduction current for dissolved oxygen. Oxygen reduction does not seem to take place when surface oxide is present, since the oxygen reduction current in the cathodic scan was observed only below –0.1 V. Similar behaviour has been reported[129] for Pd thin layers on Au electrodes. Below –0.2 V, the difference in current between aerated and deaerated solutions was constant at about 9 nA, which is assumed to be the diffusion limiting current for oxygen reduction. This value is approximately equal to the oxygen reduction current observed during the hydrogen loading process at –0.75 V (Figure 5.11). This again confirms that the oxygen reduction current on H_1-e Pd (-hydride) is independent of hydrogen content in the film.

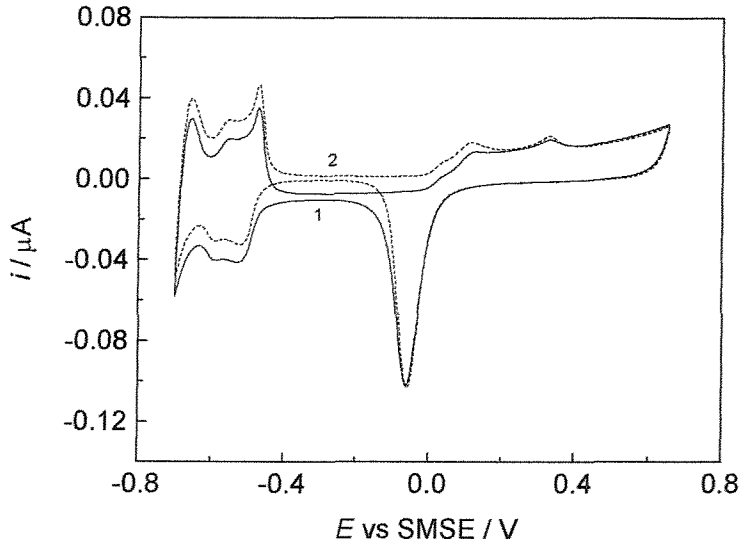

Figure 5.13. Cyclic voltammograms for an H_1-e Pd (B) film (Q_{Dep} = 9.0 μC) deposited on a Pt microdisc (d=25 μm) electrode in a 0.5 M Na_2SO_4 + 0.05 M Na_2SO_4 solution at 20 mV s^{-1}. (1) aerated (2) deaerated

Assuming that the electrode reaction (c-2) was taking place between t = 0 and 5.7 minutes during the $E_{Pd\text{-}H}$ measurement (Figure 5.12) at the constant rate limited by the diffusion of oxygen, the charge associated with the reaction (c-2) passed during this period is :

$$Q_{O2,red} = 9 \times 10^{-9}\,(\text{A}) \times 5.7 \times 60\,(\text{s.}) = 3.1 \times 10^{-6}\,(\text{C})$$

This value is close to 2.9 μC, the charge required for oxidation of hydrogen loaded in the H_1-e Pd-hydride film (Q_{Dep} = 9.0 μC, H/Pd = 0.61). This result therefore suggests that the extremely short lifetime of H_1-e Pd –hydride electrode in the aerated solution is caused by the oxidation of sorbed hydrogen in combination with the reduction of oxygen, whose rate was controlled by the diffusion of oxygen.

On Pd, there are two possible pathways for the reduction of dissolved oxygen, ie. the four electron reduction to form H_2O ($O_2 + 4H^+ + 4e \rightarrow 2H_2O$) and the two electron reduction leading to the formation of H_2O_2 ($O_2 + 2H^+ + 2e \rightarrow H_2O_2$).

Difference in the pathway has been reported to arise from adsorption[130] of anions or hydrogen (affected by anions in the supporting electrolyte and the electrode potential). Adsorption of ions reduced the number of electrons from 4. In the case of Pt microdisc electrodes[131], high rates of mass transfer (small geometric size) have been reported to force the number of electrons to fall below 4, because H_2O_2 escapes by diffusion before it can be further reduced to H_2O. Birkin et al[106] reported that plating H_1-e Pt layer to Pt microdisc electrodes increased the number of electrons involved in the reaction to ~4, because H_2O_2 can be reduced straightaway to H_2O.

The effective number of electrons involved in the oxygen reduction on H_1-e Pd (-hydride) can be estimated from the limiting current, using the formula :

$$i_L = 4nFDca$$

$$n = \frac{i_L}{4FDca} \qquad \textit{Equation 5.8}$$

where i_L is the limiting current (= 9 nA), F is the Faraday constant (=96485 C mol^{-1}), D is the diffusion coefficient of oxygen in the solution, c is the concentration of oxygen and a is the geometric radius of the electrode (≈ 15 μm). The diffusion coefficient and the solubilitiy of oxygen in 0.5 M Na_2SO_4 were not found in the literature. A diffusion coefficient of 2×10^{-5} cm^2 s^{-1} was used considering that the reported D-values are 1.79×10^{-5} cm^2 s^{-1} (in 1 M H_2SO_4)[132], 2.02×10^{-5} cm^2 s^{-1} (in 1 M NaOH)[132], 2.45×10^{-5} cm^2 s^{-1} (in 0.1 M NaOH)[131] and 2.29×10^{-5} cm^2 s^{-1} (in 0.1 M NaCl)[131]. On the other hand, reported values for oxygen solubilities[132] (oxygen saturated, 1 atm, 25 °C) are : 1.25 mmol dm^{-3} (in water), 1.05 mmol dm^{-3} (in 1 M H_2SO_4), 0.845 mmol dm^{-3} (in 1 M NaOH). Taking these data into account, the oxygen concentration (air saturated) of 0.2 mmol dm^{-3} was used in the calculation.

The number of electrons involved in the reduction of oxygen was estimated to be 3.9 by approximate calculation using Equation 5.8. The oxygen reduction observed on the H_1-e Pd (-hydride) electrode was, therefore, assumed to be the four electron reduction ($O_2 + 4H^+ + 4e \rightarrow 2H_2O$) regardless of H/Pd ratio or the presence of adsorbed hydrogen on the surface.

The influence of dissolved oxygen is summarized in Figure 5.14. In an aerated solution, the lifetime was very short because of the reaction (c-2). However, the shift in the potential was small, which can be explained by the large exchange current for the reaction $H^+ + e \rightleftarrows H(Pd\text{-}H)$ compared to the current for the reaction (c-2). The exchange current was estimated to be about 70 nA for an H_1-e Pd (B) film with $Q_{Dep} = 11$ μC. The estimation of the exchange current will be discussed in the following chapter, in the context of the comparison between normal Pd films and H_1-e Pd films.

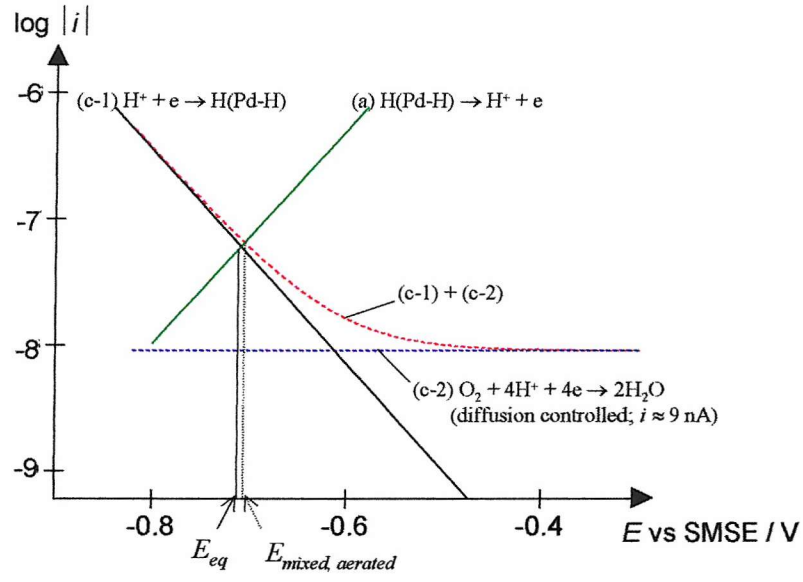

Figure 5.14. Explanation of the open circuit potentials in deaerated and aerated solutions. E_{eq} : Equilibrium potential of the reaction $H^+ + e \rightleftarrows H(Pd\text{-}H)$, which is the potential in deaerated solutions. $E_{mixed,\ aerated}$: Mixed potential of reactions (a), (c-1) and (c-2), which is the potential in aerated solutions. Lines (a) and (c-1) were drawn using Tafel equations, on the assumption that $\alpha = 0.5$, $n = 1$ and $i_0 = 70$ nA.

5-3-4. Influence of other oxidizing agents

The influence of oxidizing agents present in the solution can be discussed in the same way as in Figure 5.14. The effect of the oxidizing agents can be assessed by their limiting current which reflects the concentration of the agents.

The H_I-e (B) Pd-hydride microelectrode lost all the hydrogen in about 5.7 minutes in the aerated solution while the limiting current for oxygen reduction was about 9 nA. In order to extend the time by a factor of ten, the limiting current needs to be smaller than 1 nA. Assuming $n = 1$, $D = 10^{-5}$ cm^2 s^{-1}, and $a =$ 15 μm, the concentration of the oxidizing agent which corresponds to $i_L = 1$ nA is estimated to be about 0.2 mM by calculation using Equation 5.8. From this approximate calculation, the concentration of an oxidizing agent, in general, has to be lower than around 0.2 mM to get sufficient length of lifetime. Under this condition, shift in the potential is expected to be negligible.

The lifetime can be lengthened by increasing the thickness of H_I-e Pd deposits. Increasing the deposition charge density over 4.5 C cm^{-2}, however, is not ideal considering the increase in the diameter and the projection height. As discussed previously in this chapter, etching the Pt microdisc electrode before H_I-e Pd film deposition can be a solution for preventing the diameter enlargement. On the other hand, applying a protective film on the electrode can be a measure to prevent the influence of oxidizing agents, and it is an interesting topic for future work.

5-4. Summary

Overview

In this chapter, the potentiometric response of H_I-e Pd-hydride microelectrodes was studied. H_I-e Pd films were loaded with hydrogen cathodically under the condition discussed in the preceding chapter. The potentiometric pH response was found to be stable, reversible, reproducible and almost theoretical in deaerated solutions. From the results, H_I-e Pd-hydride microelectrodes are believed to be excellent potentiometric micro pH sensors.

Potential – time curves in deaerated solutions (pH ≈ 2)

The potential corresponding to the α+β phase was shown to be very stable (e.g. ± 0.0012 V for 1 ~ 1.5 hours in the case of H_I-e Pd films with $Q_{Dep} = 11$ μC, $d = 25$ μm). The potential was close to the reported values for conventional Pd-hydride electrodes, and was reproducible among different electrodes. H_I-e Pd-hydride microelectrodes had limited lifetime because of the removal of

hydrogen loaded in the film under the open circuit condition, by oxidation and/or recombination processes. The lifetime was roughly proportional to the geometric diameter and the thickness (Pd film deposition charge density) of H_I-e Pd films. It is expected to be possible to fabricate H_I-e Pd-hydride electrodes possessing sufficient lifetime (>1 Hour) with the diameter down to 10 μm, without causing a significant enlargement of the geometric size. No appreciable difference in the lifetime and the constant potential value for the α+β phase was observed between 0.5 M Na_2SO_4 + H_2SO_4, 1 M KCl + HCl and 1 M $NaClO_4$ + $HClO_4$, solutions (pH ≈ 2), considering the experimental errors and the liquid junction potential.

Potentiometric pH response in deaerated solutions

The potential of H_I-e Pd-hydride electrodes responded to the pH changes quickly (response time < 1 second). The relation between the potential and pH was found to be linear with a slope of circa –0.059 V / pH over a wide pH range (2 ~ 12). The potentiometric pH response was reversible for forward and reverse titrations and was reproducible among different H_I-e Pd-hydride electrodes. Excellent reproducibility of the response makes it possible to conduct pH measurements without calibration before and after the measurements, a procedure normally essential for most potentiometric micro pH sensors. The calibration curve obtained in dilute buffer solutions was very close to the predicted line (slope : 2.303 RT/F = 0.05916 V/pH, intercept : +0.050 V vs. SHE). Considering the experimental errors and the liquid junction potential, it can be concluded that the potentiometric pH response of H_I-e Pd-hydride electrodes is almost theoretical.

Influence of dissolved oxygen

On H_I-e Pd (-hydride) microelectrodes, the diffusion limiting current for oxygen reduction (assumed to be $O_2 + 4H^+ + 4e \rightarrow 2H_2O$) was observed in the potential range below –0.2 V, regardless of the surface coverage of adsorbed hydrogen or the H/Pd ratio of the H_I-e Pd film. Since this reaction leads to the oxidation of sorbed hydrogen, the lifetime of H_I-e Pd-hydride microelectrodes was so short in aerated solutions that they cannot be applied as potentiometric micro pH sensors. However, influence of oxygen on the potential was small, which can be explained by the large exchange current for the reaction $H^+ + e \rightleftarrows H(Pd\text{-}H)$

compared to the current for the oxygen reduction.

Influence of oxidizing species other than oxygen

Any oxidizing species, in general, is expected to have similar effect to oxygen. From an approximate calculation (assuming $n = 1$, $D = 10^{-5}$ cm^2 s^{-1}, and $a = 15$ μm), the concentration has to be lower than circa 0.2 mM to get sufficient lifetime. Under this condition, shift in the potential is expected to be negligible. It is needless to say that a small amount of noble metal ions is expected to affect the response seriously, not only by accelerating the removal of hydrogen but also depositing a solid on the surface.

Chapter 6. Advantage of the nanostructure

In Chapter 4, the hydrogen absorption behaviour of H_I-e Pd films on Pt microdisc elecrodes was discussed. It was shown that the films can be loaded with hydrogen quickly (~ 1 minute) and that the H/Pd ratio can be controlled by varying the loading potential and the loading time. In Chapter 5, the potentiometric pH response of H_I-e Pd-hydride microelectrodes was shown to be rapid, reproducible and almost theoretical in deaerated solutions.
In this chapter, these outstanding properties will first be compared with the properties of "plain Pd films" (Pd film without the nanostructure) on Pt microdisc electrodes in order to clarify the role of the nanostructure. Properties of "polished Pd microdisc" (Pd microwire sealed in a glass pipette) electrodes will then be discussed to see primarily the effect of hydrogen diffusion into the bulk of the microwire. At the end of this chapter, the advantages of the nanostructure will be discussed and summarized.

6-1. Properties of plain Pd films on Pt microdisc electrodes

6-1-1. H absorption behaviour

Cyclic voltammetry was performed to study the basic electrochemical behaviour of plain Pd films deposited on 25 μm diameter Pt microdiscs in a deaerated 0.5 M Na_2SO_4 + 0.05 M H_2SO_4 solution (pH = 1.88). A typical cyclic voltammogram recorded in a potential range between –0.70 and +0.65 V is shown in Figure 6.1. In contrast to the voltammograms for H_I-e Pd films in the same solution (e.g. Figure 4.1), the currents associated with the hydrogen reactions (adsorption/desorption and absorption/desorption) cannot be distinguished, although a shoulder is observed on each wave for cathodic and anodic scans for the plain Pd film. Unresolved peaks on the voltammogram for plain Pd films can be attributed to the small current associated with adsorbed hydrogen compared to the massive current associated with absorbed hydrogen. The peaks corresponding to absorbed and adsorbed hydrogen were not clearly resolved also in the case of 1 M H_2SO_4 solution (Figure 3.17, line 1). These

results are consistent with the reports on conventional palladium electrodes[133].

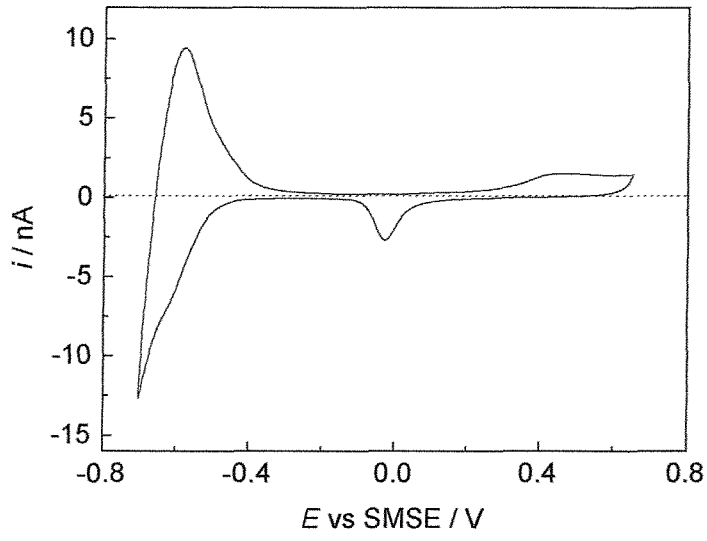

Figure 6.1. Cyclic voltammogram for a plain Pd film (Q_{Dep} = 11 μC) on a 25 μm diameter Pt microdisc electrode at 20 mV s^{-1} in a 0.5 M Na_2SO_4, 0.05 M H_2SO_4 solution.

To study the hydrogen reactions on the plain Pd films in more detail, the potential was scanned to further negative values. The resulting voltammogram for a plain Pd film is shown in Figure 6.2, together with that for an H_1-e Pd (B) film with the same deposition charge (Q_{Dep}).

In the cathodic scan, the current corresponding to the hydrogen absorption into the plain Pd film (below –0.70 V) was found to be much smaller than that of the H_1-e Pd (B) film. This proves that the rate of hydrogen absorption is greatly enhanced by the presence of the nanostructure, in which no point within the metal is more than a few nanometres from the surface. In the case of H_1-e Pd films, the time taken for an H atom to diffuse through the wall (2 ~ 2.5 nm) is estimated to be of the order of 50 nanoseconds (the diffudsion coefficients of H in the α and β phases are around 2×10^{-7} and 2×10^{-6} cm^2 s^{-1} repectively). Diffusion of hydrogen through the lattice is expected to be so fast as not to be rate limiting. Because of the difference in the rate of hydrogen absorption, it is expected that a more negative loading potential and / or a longer loading time have to be

employed to load hydrogen to the desired H/Pd ratio in plain Pd films compared to H_1-e Pd films.

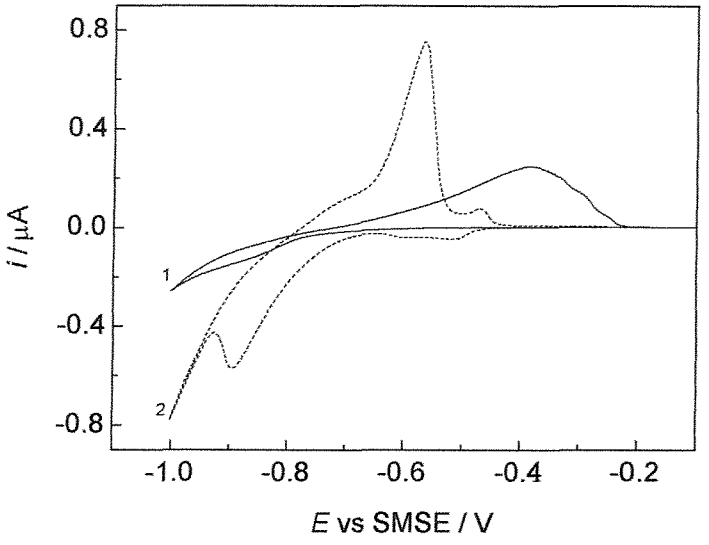

Figure 6.2. Cyclic voltammograms showing hydrogen reactions for Pd films (Q_{Dep} = 11 μC) on Pt microdisc (d=25 μm) electrodes at 20 mV s^{-1} in a 0.5 M Na_2SO_4, 0.05 M H_2SO_4 solution. (1) a plain Pd film; (2) an H_1-e Pd (B) film.

On the anodic scan, the stripping peak for sorbed hydrogen is more drawn out for the plain Pd film than the H_1-e Pd film and the current on the plain Pd film continued to flow until about –0.2 V. Charges passed below –0.2 V was almost the same for cathodic and anodic scans (–3.12 μC and +3.16 μC respectively). This suggests that the cathodic current observed with the plain Pd film was associated solely with adsorption and absorption of hydrogen, not with hydrogen gas evolution. From the stripping charge, the plain Pd film is assumed to have reached the H/Pd ratio of 0.59.

To find the optimum conditions to load plain Pd films with hydrogen, the effects of the loading potential and loading time on the H/Pd ratio of the films were studied. In this experiment, the potential was stepped from –0.20 V, where the current was zero, to the loading potential, E_L. The potential was held at E_L for the loading time, t_L. To estimate the amount of hydrogen loaded into the film,

the potential was swept back at 10 mV s^{-1} and the anodic charge passed during the sweep was calculated. The H/Pd ratios were calculated assuming the Pd film deposition efficiency of 98 %. These potentiometric loading experiments were conducted after a stable cyclic voltammogram similar to Figure 6.1 was obtained, in order to get reproducible results. The applied charge, stripping charge and calculated H/Pd value for each loading conditions are listed in Table 6.1.

Table 6.1. Hydrogen absorption behaviour of plain Pd films (Q_{Dep} = 11 μC) on 25 μm diameter Pt microdisc electrodes. Results are averages for two electrodes.

H Loading conditions		Results		
Potential E_L / V	Time t_L / s.	Applied charge Q_L / μC	Stripping charge Q_{Str} / μC	H/Pd atomic ratio
-0.75	180	1.49	1.44	0.27
	600	3.74	3.37	0.63
	1800	5.70	3.27	0.61
-0.80	180	2.25	2.19	0.41
-0.85	180	4.12	3.79	0.70
	300	5.82	3.66	0.68

As expected from the voltammogram shown in Figure 6.2, a more negative E_L and / or longer t_L was required for plain Pd films than H_I-e Pd (B) films, to achieve the H/Pd ratio in the β phase region. For instance, about 600 seconds (about 15 times longer than for H_I-e Pd (B)) was needed at E_L = –0.75 V. By applying a more negative E_L, –0.85 V, 180 seconds was sufficient to achieve an H/Pd ratio larger than 0.6. It is interesting to note that the maximum H/Pd ratio for plain Pd films at E_L = –0.75 V was about 0.62, which is comparable to that for H_I-e Pd films. This is consistent with the previous work[102] in which H_I-e Pd films are reported to possess the same crystal structure as bulk palladium. It has to be noted, however, that the same Faradaic efficiency was assumed for the deposition of the two different Pd films. Certain error can arise from slight difference in the Faradaic efficiency. A current transient

recorded during loading hydrogen at E_L = –0.75 V is shown in Figure 6.3, together with a current transient for an H_1-e Pd film.

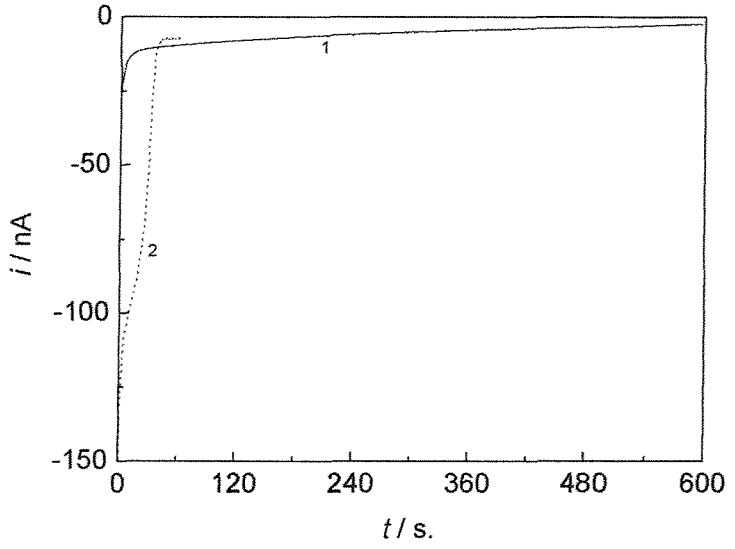

Figure 6.3. Current transients recorded while loading hydrogen into Pd films (Q_{Dep} = 11 μC) on 25 μm diameter Pt microdisc electrodes in deaerated 0.5 M Na_2SO_4, 0.05 M H_2SO_4 solutions. The potential was stepped from –0.20 V to –0.75 V at t = 0. (1) A plain Pd film. (2) An H_1-e Pd (B) film.

The differences between the two transients are quite clear. First, the current is much smaller for the plain Pd film; this is the reason for the longer t_L (by about 15 times). Secondly, a plateau corresponding to the absorption of hydrogen is not observed on the transient for the plain Pd film, although the hydrogen absorption was completed before t = 600 s. The current near t = 600 s is thought to correspond to hydrogen gas evolution. Similarly, the hydrogen absorption plateau was not observed on the transient at E_L = –0.85 V.

6-1-2. Potentiometric response

The potential of plain Pd films deposited on Pt microdisc electrodes loaded with

hydrogen was monitored in deaerated 0.5 M Na_2SO_4 + 0.05 M H_2SO_4 solutions (pH = 1.88). The monitoring of potential was started immediately after the hydrogen loading procedure. The following loading conditions, E_L = –0.75 V, t_L = 600 s (expected H/Pd ≈ 0.62) and E_L = -0.85 V, t_L = 180 s. (expected H/Pd ≈ 0.69) were employed.

Resulting potential – time curves for plain Pd films (Q_{Dep} = 11 μC) are shown in Figure 6.4, together with a potential – time curve for an H_1-e Pd (B) film with the same Q_{Dep}.

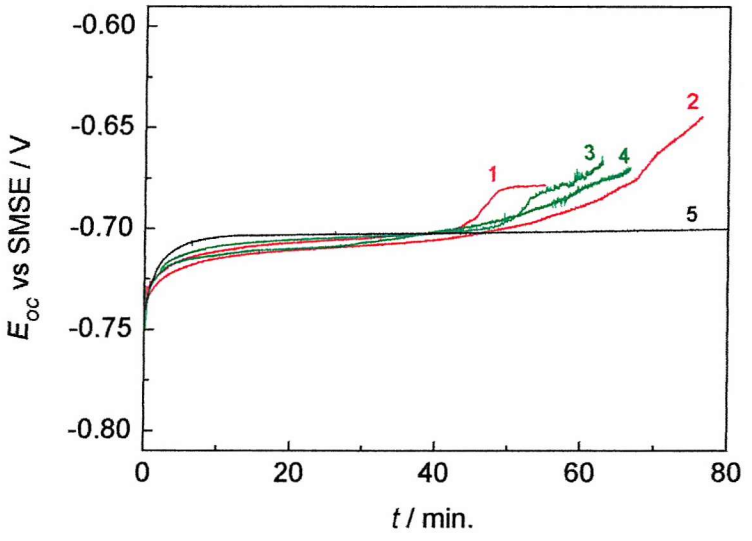

Figure 6.4. Open circuit potentials of Pd films (Q_{Dep} = 11 μC) on 25 μm diameter Pt microelectrodes in deaerated 0.5 M Na_2SO_4, 0.05 M H_2SO_4 solutions immediately after loading hydrogen. (1), (2) Plain Pd films loaded with hydrogen at E_L = –0.75 V for t_L = 600 s. (3),(4) Plain Pd films; E_L = –0.85 V, t_L = 180 s. (5) an H_1-e Pd (B) film; E_L = –0.75 V, t_L = 60 s.

The potential of plain Pd-hydride films rose quickly from E_L and tended to reach a plateau. However, the potential in this plateau region was not as stable as that for the H_1-e Pd-hydride microelectrode, and an appreciable slope was still observed. Furthermore, the reproducibility of the plateau potential was poor and the difference in the plateau potential among four different electrodes was as large as 0.006 V (in the case of H_1-e Pd-hydride films, the difference was less

than 0.002 V among 10 different electrodes).

After about $t = 30 \sim 45$ min, the potential of plain Pd-hydride films began to rise quickly. This short plateau length, compared to H_I-e Pd films, cannot be attributed to the complete removal of absorbed hydrogen, since neither the oxidation process nor the recombination process is expected to be faster on plain Pd-hydride films than on H_I-e Pd-hydride films. Hence, in order to estimate the amount of hydrogen remaining in the film, an anodic sweep was performed after the potential monitoring, to strip hydrogen from the film. The voltammogram obtained after monitoring potential is shown in Figure 6.5. For comparison, a voltammogram of an anodic sweep recorded just after loading the same film with hydrogen (without a potential monitoring) is also shown in the graph.

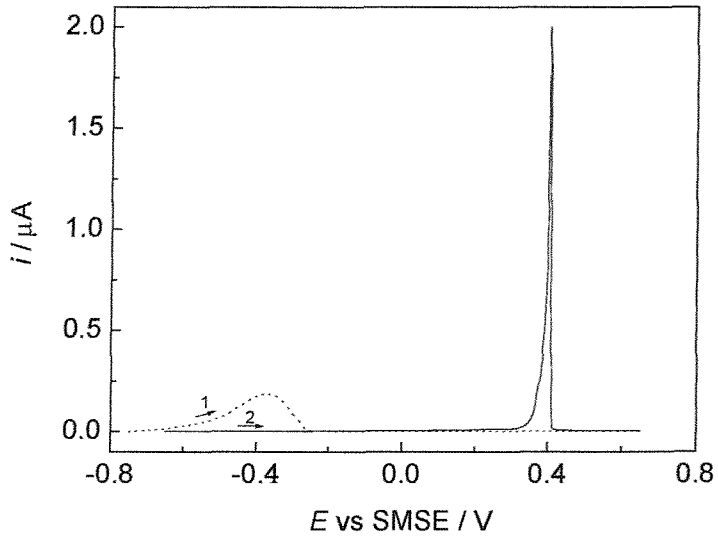

Figure 6.5. Voltammograms for the stripping of hydrogen loaded in plain Pd films (Q_{Dep} = 11 μC) in 0.5 M Na_2SO_4, 0.05 M H_2SO_4 solution, recorded at 10 mV s^{-1}. The anodic scans were started immediately after : (1) the film was loaded with H, (2) the measurement of the open circuit potential (Figure 6.4; line 2). Loading conditions : E_L = –0.75 V, t_L = 600 s.

In the case of the voltammogram taken immediately after loading, stripping of hydrogen was completed at about –0.2 V and the hydrogen stripping charge was 3.43 μC (corresponding to H/Pd = 0.64). In contrast, anodic current was not observed in this potential range (< –0.2 V) on the voltammogram recorded after the potential monitoring. Instead, very sharp anodic peak was observed at about +0.4 V, whose charge was 2.65 μC. Assuming that all the charge (2.65 μC) was associated with the oxidation of hydrogen absorbed in the film, the H/Pd ratio is estimated to be 0.49. It suggests that at the end of the potential monitoring, the plain Pd-hydride film was in the α+β phase, which should still give the stable potential. Hence, in contrast to H_1-e Pd-hydride films, the lifetime of plain Pd films is found to be not limited by the removal of hydrogen.

In the open circuit measurements shown in Figure 6.4, the H/Pd ratios of the plain Pd-hydride films were in the β phase region at $t = 0$ and the ratios were still as high as around 0.49 (from the results for line 2) at the end of the measurement. The plain Pd-hydride films are thought to have lost their surface activity soon after the H/Pd ratio reached around 0.50 (approximate maximum H/Pd ratio at which H_1-e Pd showed the stable potential corresponding to α+β phase). Hence, in order to verify the open circuit potential of plain Pd-hydride microelectrodes when H/Pd ratio is near the middle of the α+β phase, a plain Pd film was loaded with hydrogen at E_L = –0.80 V for t_L = 180 s (Q_L = 2.23 μC, estimated H/Pd = 0.41) and its open circuit potential was monitored. The resulting potential – time curve is shown in Figure 6.6. The potential was close to the plateau potential of H_1-e Pd films (corresponding to the α+β phase) at around t = 10 ~ 30 min. However, the potential was not very stable and an appreciable slope was still observed. The potential began to rise rather rapidly (at around t = 30 min), just as in the case of plain Pd-hydride films with the initial Pd/H ratio in the β phase (shown in Figure 6.4).

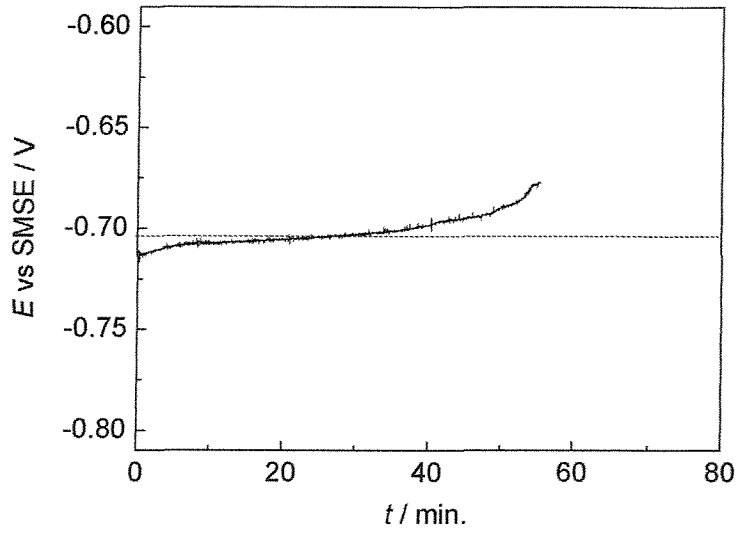

Figure 6.6. Open circuit potential of a plain Pd film (Q_{Dep} = 11 μC) on a 25 μm diameter Pt microelectrode in a deaerated 0.5 M Na_2SO_4, 0.05 M H_2SO_4 solution immediately after loading hydrogen at E_L = –0.80 V for t_L = 180 s. (estimated H/Pd = 0.41). Dotted line shows the plateau potential value of H_1-e Pd films which corresponds to the α+β phase.

To investigate the surface state of the plain Pd-hydride film after potential monitoring, cyclic voltammetry was performed after the potential measurement shown in Figure 6.6. The resulting cyclic voltammograms are shown in Figure 6.7.

The voltammetry was started from the open circuit potential after the potential measurement (≈ –0.65V), and the potential was first scanned to –0.70 V. The current value was almost zero on this scan. The potential was then scanned to +0.65 V. In this scan, current was almost zero until about –0.2 V, where a very small anodic current started to flow. The anodic current increased slowly, and a massive anodic peak appeared at about +0.4 V. This behaviour is very similar to that observed on the voltammogram shown in Figure 6.5. The anodic charge passed during this anodic scan was 1.73 μC, which is believed to be chiefly due to the oxidation of absorbed hydrogen (surface oxide formation charge is negligibly small). The H/Pd ratio was estimated to be 0.32 from the charge, which indicates that the plain Pd-hydride film was still in the α+β phase when the

potential started to rise at around t = 30 minutes in Figure 6.6.

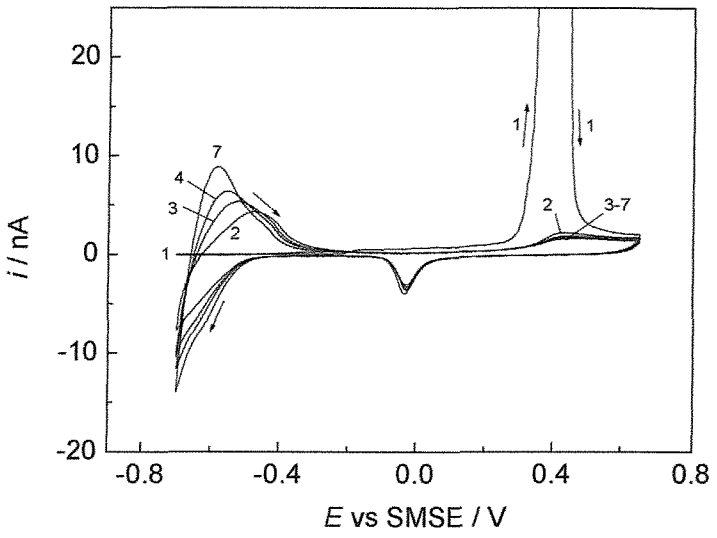

Figure 6.7. Cyclic voltammograms for a plain Pd film (Q_{Dep} = 11 μC) loaded with hydrogen in 0.5 M Na_2SO_4, 0.05 M H_2SO_4 solution, recorded at 20 mV s^{-1}. The scan was started at –0.2 V after the measurement of the open circuit potential (Figure 6.6)

The potential was then cycled between +0.65 and –0.70 V continuously (curves 2~7 in Figure 6.7). In these cycles, the currents for hydrogen reactions (below –0.3 V) were observed. These results suggest that the surface of the plain Pd-hydride film was blocked at the end of the potential monitoring, and that the cause of the surface blockage was eliminated by the anodic scan. The magnitude of the currents for hydrogen reactions increased gradually with the number of cycles.

From the results discussed in this section, the potentiometric response of plain Pd-hydride microelectrodes in 0.5 M Na_2SO_4 + H_2SO_4 solutions (pH 1.88) can be summarized as follows. When in the α+β phase, plain Pd-hydride electrodes show the potential close to the plateau potential observed for H_I-e Pd-hydride films. However, the potential is not very stable, and an appreciable slope is observed. The plateau does not last as long as that of H_I-e Pd-hydride film and

the potential begins to rise quickly quite soon. This may be attributed to a surface blockage caused under the open circuit condition. Owing to the surface blockage, the potential determining reaction ($H^+ + e \rightleftarrows H$ (Pd-H)) is extremely slow at this stage. The surface activity can be recovered by applying the positive potential in the oxide formation region, where hydrogen remaining in the film is released.

6-1-3. Surface blockage

In the preceding section, plain Pd-hydride films appeared to lose their surface activity under open circuit conditions. To verify the role of cycling the potential to the surface oxide region, cyclic voltammetry was performed without taking the potential to the oxide region (potential range –0.70 ~ –0.15 V), and the result is shown in Figure 6.8.

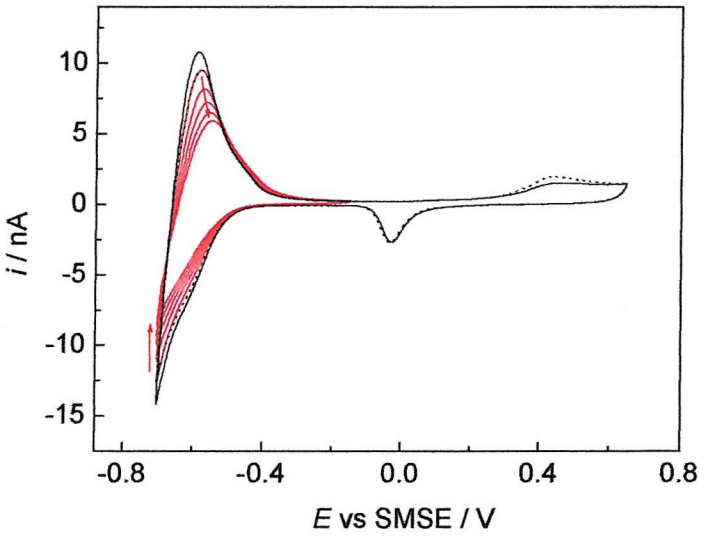

Figure 6.8. Cyclic voltammograms for a plain Pd film (Q_{Dep} = 11 μC) in 0.5 M Na_2SO_4, 0.05 M H_2SO_4 solution, recorded at 20 mV s^{-1}. Procedures of the experiment are as follows: (1) a cycle (–0.70V ⇔ +0.65 V) shown by a solid black line, (2) five cycles (–0.70 ⇔ –0.15 V) shown by red lines, (3) a cycle (–0.70V ⇔ +0.65 V) shown by a dotted black line.

During 5 cycles (shown by the red line in the graph), the magnitude of the currents for hydrogen reactions was found to decrease gradually. However, almost the same magnitude of current as that observed before cycling between –0.70 and –0.15 was recovered by scanning the potential to the oxide formation region, as shown in Figure 6.8 (see solid and dotted black lines). This result shows that the plain Pd film gradually lost its surface activity when the potential was cycled in the potential range more negative than oxide region. To regain the surface activity, the potential had to be scanned to the oxide formation region.

Next, in order to investigate whether the surface blockage is an event unique to the potential in the hydrogen reaction region, the potential was held at the double layer region (–0.20 V) for 10 minutes in a 0.5 M Na_2SO_4 + H_2SO_4 solution (pH = 1.88) and cyclic voltammograms were recorded before and after the potentiostatic experiment.

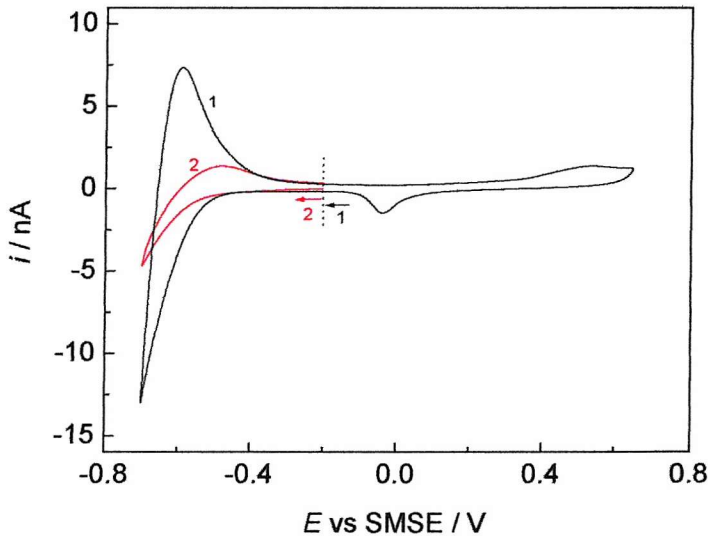

Figure 6.9. Cyclic voltammograms for a plain Pd film (Q_{Dep} = 11 μC) in 0.5 M Na_2SO_4, 0.05 M H_2SO_4 solution, recorded at 20 mV s^{-1}. The voltammograms were taken before and after the potential was kept at –0.20 V for 600 s. (1) a cycle (–0.70 V ⇔ +0.65 V) before the potentiostatic experiment. (2) a scan (–0.20 V → –0.70 V → –0.20 V) after the potentiostatic experiment.

As shown in Figure 6.9, the currents for hydrogen reactions were appreciably smaller for the voltammogram after holding the potential at –0.20 V, than that before. The result of this experiment shows that a plain Pd film loses its surface activity even if the potential is not scanned to the hydrogen reaction region. It suggests that plain Pd films have a tendency to lose the surface activity automatically in the 0.5 M Na_2SO_4 + H_2SO_4 solution, unless the potential is taken to the surface oxide region.

It has been reported that the surface activity of Pd is not reproducible and tends to decay[1, 45]. The cause of the decay in surface activity was thought to be adsorption of traces of a poisoning species, which has not been identified. To obtain electrodes with a high activity, several surface activation methods have been suggested, ie. (1) oxidation of the surface[51] (by either heating in oxygen or electrolytic anodization) followed by electrolytic reduction of the oxide or (2) electroplating a layer of Pd black[51, 134].
The gradual loss of surface activity of plain Pd films in the present study is also likely to be caused by adsorption of traces of impurities in the solution, although the adsorbates were not identified. Since the decay of surface activity took place both at –0.2 V and under the open circuit condition (potential : –0.72 ~ –0.70 V), it is assumed that the impurity can adsorb on the Pd surface in the wide potential range; –0.72 ~ –0.2 V. Considering this potential range, cathodic deposition of a metal impurity is unlikely to be the cause of the surface activity decay. The surface activity of plain Pd films was recovered by scanning the potential to the surface oxide formation region, which is consistent with the activation method (1) discussed above.

Conventional size Palladium-hydride electrodes have been employed as reference electrodes[52, 54-60] and pH electrodes[53, 61-68] by a number of workers. In each case, to attain a surface with high activity, palladium electrodes were subjected to an activation step (e.g. cycling the potential several times between oxide formation and hydrogen evolution region), before the hydrogen loading step. For the same reason, a majority of them used palladized electrodes. However, 'bright' Pd-hydride electrodes have also been employed as reference and pH electrodes. Typically, Pd wires (d ≈ 100 ~ 200 μm)[55, 57] or Pd plates[63]

were first activated by pre-anodization and then fully charged with hydrogen cathodically. Thus prepared Pd-hydride electrodes were reported to be serviceable up to 24 hours.

In the present study, plain Pd films on 25 μm diameter Pt microelectrode lost their surface activity almost completely in less than an hour, which was thought to be caused by adsorption of traces of impurities in the solution. The difference in serviceable period between the present study on microelectrodes and previous works on relatively large electrodes is assumed to be attributed to the size, i.e. :

(1) When the rate of the adsorption of traces of impurities is diffusion controlled (because of the extremely low concentration), the surface active sites of a microelectrode are believed to be covered in a shorter time than those of a conventional size electrode, since diffusion is faster in the case of microelectrodes.

(2) Microelctrodes have very small surface areas, in other words, a small number of surface active sites. Because of the large number of original active sites, conventional size electrodes are assumed to be capable of sustaining the stable potential longer than microelectrodes even if the same percentage of active sites are covered.

(3) Diffusion of oxidizing species (traces of impurities) which can shift the potential positive is also faster for microelectrodes.

The surface activity of Pd electrodes was reported to decay rapidly particularly in dilute sulphuric acid solutions[45, 51], and adsorption of poisoning impurities was suggested as the probable cause. In the present study, the usage of 0.5 M Na_2SO_4 + 0.05 M H_2SO_4 solution, which contains a high concentration of sulphate, might therefore have played a role in the fast decay of the surface activity.

6-2. Properties of polished Pd microdisc electrodes

Polished Pd microdisc electrodes are expected to have behaviour similar to plain Pd films, ie. much slower hydrogen absorption rate than H_I-e Pd films and

automatic loss of surface activity. A main drawback expected for polished Pd microdisc electrodes is the difficulty in achieving the stable potential corresponding to the α+β phase because of the diffusion of absorbed hydrogen into the bulk of the Pd microwire. To get the sufficient H/Pd ratio near the surface of the tip of Pd wires sealed in insulating material, Fleischmann[55] loaded bare Pd wires (d > 100 μm) with hydrogen cathodically and afterwards coated the curved part of the cylindrical surface with Lacomit varnish, care being taken that the tip remained exposed. This preparation method, however, is obviously unsuitable for microsensors for SECM.

In the present study, attempts were made to load polished Pd microdisc electrodes with hydrogen cathodically (from the tip). In this section, the hydrogen absorption behaviour and the potentiometric response will be discussed chiefly in comparison with plain Pd films.

6-2-1. H absorption behaviour

Figure 6.10 shows a cyclic voltammogram for a polished Pd microdisc electrode in a deaerated 0.5 M Na_2SO_4 + 0.05 M H_2SO_4 solution (pH = 1.88).

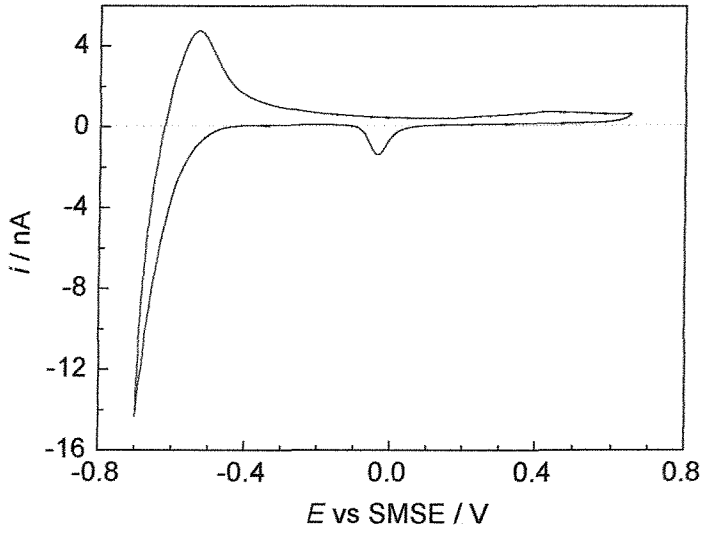

Figure 6.10. Cyclic voltammogram for a polished Pd microdisc (d=25 μm) electrode at 20 mV s^{-1} in a 0.5 M Na_2SO_4, 0.05 M H_2SO_4 solution.

The currents associated with the absorbed and adsorbed hydrogen cannot be distinguished, just as with plain Pd films. Unresolved peaks can again be attributed to the small adsorption/desorption currents compared to the massive absorption/desorption currents.

On the cathodic scan of the voltammogram shown in Figure 6.10, small anodic currents are observed in the potential ranges of the surface oxide (+0.10 ~ +0.65 V) and the double layer charging (–0.45 ~ –0.10 V). This anodic current is thought to correspond to the oxidation of absorbed hydrogen atoms which diffuse back to the surface from the bulk of the Pd electrode. This phenomenon was clearly seen when more hydrogen was loaded into the film by scanning the potential to further negative values. In the experiment shown in Figure 6.11, after a voltammogram recorded in the potential range –0.60 V ~ +0.65 V (curve 1), the potential was cycled from +0.65 V to –1.00 V then +0.65 V (curve 2).

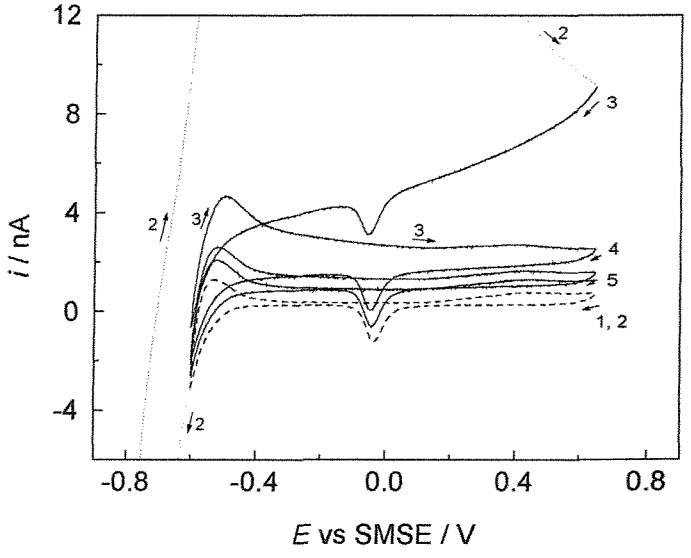

Figure 6.11. Cyclic voltammograms for a Pd microdisc (d=25 μm) electrode at 20 mV s^{-1} in a 0.5 M Na_2SO_4, 0.05 M H_2SO_4 solution. The numbers in the graph shows the order of the scans. (1) +0.65 V → –0.65 V → +0.65 V (2) +0.65 V → –1.00 V → +0.65 V (3)~(5) +0.65 V → –0.65 V → +0.65 V, 3 cycles.

On the anodic scan from –1.00 V, a large current for oxidation of absorbed hydrogen was observed, and an appreciable anodic current was still observed on the next cathodic scan and subsequent cycles (curve 3~5). This can be explained as follows. When the potential was scanned to –1.00 V, hydrogen was absorbed in the electrode and diffused into the bulk of the microwire. The hydrogen atoms which remained near the surface were oxidized by the following anodic scan. During the subsequent cycles (curve 3~5), absorbed hydrogen atoms diffused back from the bulk to the surface and were oxidized continuously.

To study the hydrogen reactions on the polished Pd microdisc electrode in more detail, the potential range of –1.00 ~ +0.10 V of the voltammogram shown in Figure 6.11 (curve 2) is redrawn and shown in Figure 6.12.
As expected from the results for plain Pd films, the current corresponding to the hydrogen absorption (below –0.65 V on the cathodic scan) on the Pd microdisc was much smaller than on the H_I-e Pd film. Hence, in order to load hydrogen, more negative potential and / or longer time is expected to be required for Pd microdisc electrodes than for H_I-e Pd films.

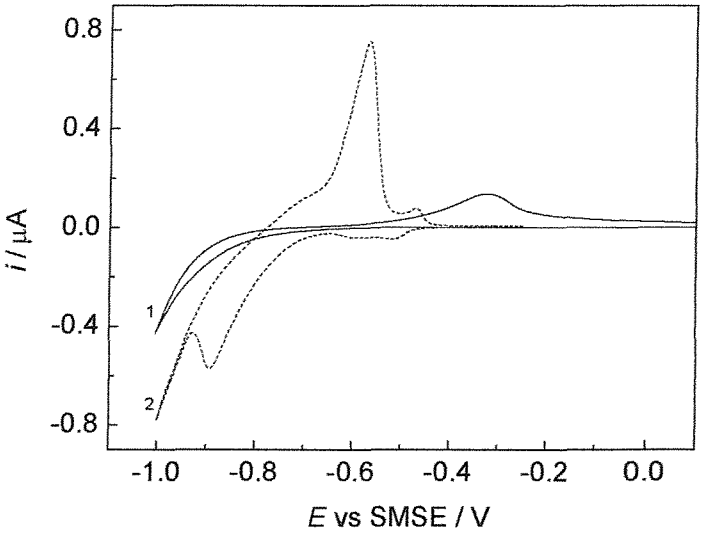

Figure 6.12. Cyclic voltammograms for Pd microelectrodes at 20 mV s^{-1} in a 0.5 M Na_2SO_4, 0.05 M H_2SO_4 solution, showing hydrogen reactions. (1) a polished Pd microdisc (d=25 μm) electrode; (2) an H_I-e Pd (B) film (Q_{Dep} = 11 μC) on a Pt microdisc (d=25 μm) electrode.

Polished Pd microdisc electrodes were loaded at various loading potentials (E_L = −0.75, −0.80, −0.90, −1.00 V) for t_L = 1800 s. The charges passed while loading hydrogen are listed in Table 6.2, and the current transients recorded for each case are shown in Figure 6.13.

Table 6.2. Conditions and applied charges for loading hydrogen into Pd microdisc electrodes (d=25 μm), in deaerated 0.5 M Na_2SO_4, 0.05 M H_2SO_4 solutions.

No.	H Loading		
	Potential E_L / V	Time t_L / s.	Applied charge Q_L / μC
1	-0.75	1800	3.4
2	-0.80	1800	6.4
3	-0.90	1800	16.3
4	-1.00	1800	69.9

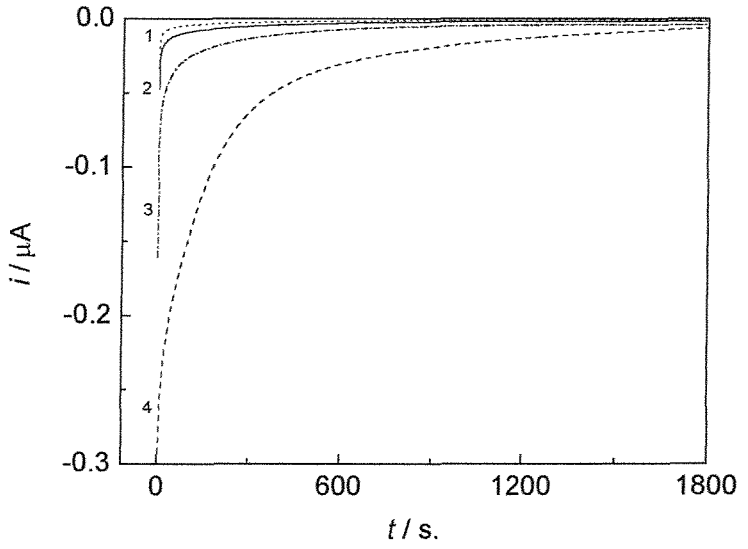

Figure 6.13. Current transients recorded while loading Pd microdisc electrodes with hydrogen in deaerated 0.5 M Na_2SO_4, 0.05 M H_2SO_4 solutions. The potential was stepped from –0.20 V to E_L at t = 0. Numbers in the graph correspond to the loading conditions in Table 6.2.

In each case the current simply decayed gradually. The current at E_L = −0.75 V

is confirmed to be much smaller than that for H_I-e Pd films at the same E_L (around –0.1 μA). At this potential, 1800 s (30 min) was needed to pass a loading charge of 3.4 μC; this can be achieved within a minute in the case of H_I-e Pd films. By applying loading potentials more negative than –0.75 V, the current increased and so did the charge passed during the loading procedure. The charge passed at E_L = –1.00 V was about twenty times greater than that at E_L = –0.75 V.

6-2-2. Potentiometric response

The potential – time curves for Pd microdisc electrodes loaded with hydrogen under the conditions listed in Table 6.2 are shown in Figure 6.14 (curves 1~4). A potential – time curve for an H_I-e Pd (B) film (Q_{Dep} = 11 μC) on a 25 μm diameter Pt microdisc electrode loaded with hydrogen is also shown in the graph for comparison.

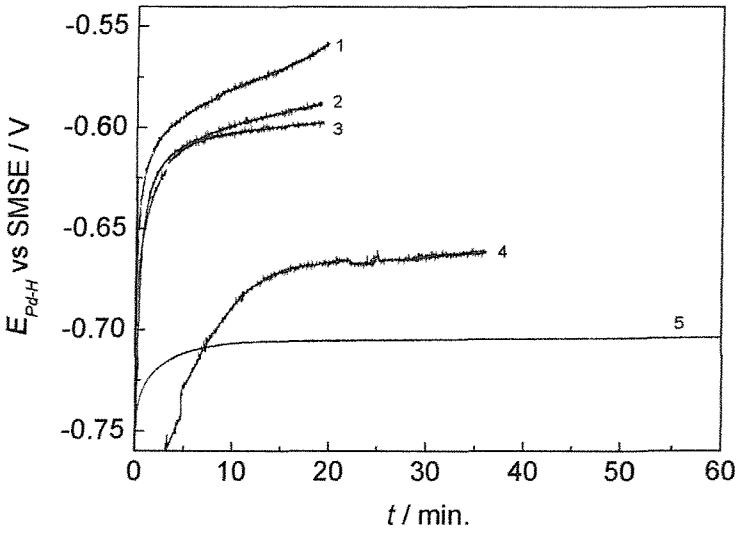

Figure 6.14. Open circuit potentials of Pd electrodes in deaerated 0.5 M Na_2SO_4, 0.05 M H_2SO_4 solutions immediately after loading hydrogen. (1) ~ (4) polished Pd microdisc electrodes (d = 25 μm). Numbers correspond to the loading conditions in Table 6.2. (5) an H_I-e Pd (B) film (Q_{Dep} = 11 μC) on a 25 μm diameter Pt microdisc electrode; E_L = –0.75 V, t_L = 60 s.

None of the hydrogen-loaded Pd microdisc electrodes showed the plateau potential corresponding to the α+β phase. The potential rose continuously beyond the expected plateau potential (≈ –0.70 V). In the case of the film loaded at –1.00 V (line 4), the potential rose rather slowly, but did not show even a short plateau at the potential corresponding to the α+β phase. This indicates that the potential rise beyond the expected plateau potential was not caused by the continuous decrease in the H/Pd ratio near the surface. The potential rise is likely to be attributed to the surface blockage, observed with plain Pd films. In the case of polished Pd microdiscs, the surface is thought to have already lost its activity when the potential monitoring was started at $t = 0$. This is possible because of the longer loading time (30 min) compared with those for plain Pd films (3 or 10 min), during which adsorption of traces of impurities can occur. Furthermore, the time required for the complete coverage of the surface active sites is assumed to be shorter for polished microdiscs than plain Pd films, because of the smaller electroactive area of polished Pd microdiscs (The estimated roughness factors were 2.1 for polished Pd microdiscs and 5.2 for plain Pd films; Chapter 3).

There still is a possibility that the plateau potential can be obtained with polished Pd microdiscs by employing more negative E_L and shorter t_L. However, it is not believed to be possible to achieve more stable potential than with plain Pd films on Pt microdiscs, because of the diffusion of absorbed hydrogen into the bulk. Furthermore, such a negative E_L is not ideal since it raises the possibility of the cathodic deposition of impurities. Hence further attempts to load polished Pd microdisc electrodes with hydrogen were not made in this study.

6-3. Advantage of the nanostructure

In this section, the advantages of the nanostructure will be discussed from two aspects, ie. hydrogen loading into H_I-e Pd films, and potentiometric response of H_I-e Pd-hydride films. To focus on the effect of the nanostructure, the experimental results for H_I-e Pd films (shown in Chapter 4 and 5) were compared with those for plain Pd films (shown in this chapter), rather than

polished Pd microdisc electrodes.

6-3-1. Advantage to hydrogen loading

6-3-1-(1). Rapid hydrogen absorption

The rate of hydrogen absorption is greatly enhanced by the presence of the nanostructure, in which no point within the metal is more than a few nanometres from the surface. Diffusion of hydrogen through the lattice is expected to be so fast as not to be rate limiting. Therefore, shorter loading time and less negative potentials are required to load H_I-e Pd films with hydrogen. Thanks to the short loading time (< 1 min), H_I-e Pd films can be loaded with hydrogen quickly just before pH measurements. It is expected to be possible to conduct a series of SECM experiments (typically, 1 hour/experiment) consecutively with a few minute intervals for the hydrogen charging. In addition, less negative loading potentials lower the possibility of depositing impurities (e.g. metal ions) onto the film. The rapid absorption of hydrogen also opens the possibility of continuous pH monitoring with reloading at regular intervals in situ.

6-3-2. Advantage to potentiometric response

The potentiometric pH response of H_I-e Pd-hydride films was found to be rapid, stable, reproducible and almost theoretical. The contribution of the nanostructure to the excellent potentiometric response is now discussed by comparing H_I-e Pd films with plain Pd films.

6-3-2-(1). Large electroactive area

The plateau potential corresponding to the $\alpha+\beta$ phase was not very stable for plain Pd-hydride films, where an appreciable slope was observed. In addition, the reproducibility of the plateau potential among different electrodes was found to be poor. The less stable and less reproducible potentiometric response of plain Pd-hydride microelectrodes appeared to be chiefly due to the gradual loss

of surface activity under the open circuit condition. When the potential determining reaction ($H^+ + e \rightleftarrows H(Pd\text{-}H)$) is almost completely blocked, the potential rises sharply. This phenomenon was not observed during the potential monitoring of H_1-e Pd films.

It was found that plain Pd films have a tendency to lose the surface activity gradually in the 0.5 M Na_2SO_4 + H_2SO_4 solution unless the potential is taken to the surface oxide formation region. To check if this is also the case with H_1-e Pd films, the same experiment as shown in Figure 6.8 was performed (cyclic voltammetry between –0.70 V and –0.15 V) for an H_1-e Pd film and the change in hydrogen currents was studied. The resulting voltammogram is shown in Figure 6.15.

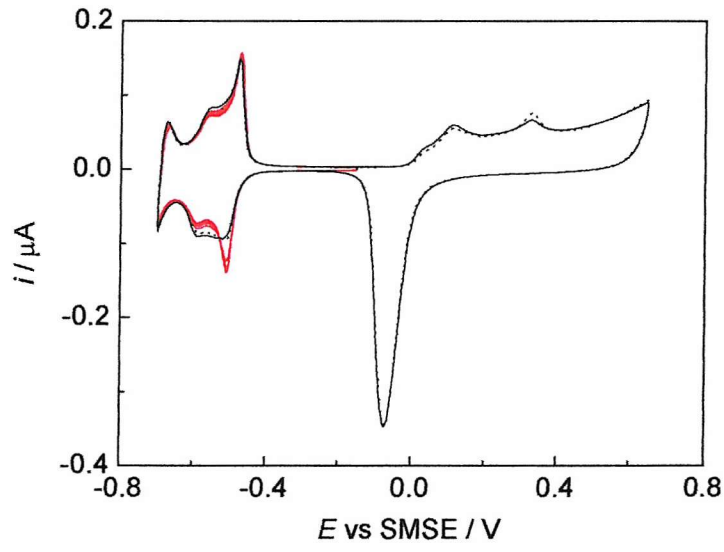

Figure 6.15. Cyclic voltammograms for an H_1-e Pd (A) film (Q_{Dep} = 11 μC) in 0.5 M Na_2SO_4, 0.05 M H_2SO_4 solution, recorded at 20 mV s^{-1}. Procedures of the experiment were as follows (the same as Figure 6.8) : (1) a cycle (–0.70V ⇔ +0.65 V) shown by a solid black line (2) five cycles (–0.70 ⇔ –0.15 V) shown by red lines (3) a cycle (–0.70V ⇔ +0.65 V) shown by a dotted black line

During the five cycles between –0.70 V and –0.15 V (shown by red lines), no

appreciable change was observed in terms of the magnitude of the current, in contrast to the result for a plain Pd film (Figure 6.8) where hydrogen reaction currents decreased with the number of cycles.

As discussed previously, the decay in the surface activity seen for plain Pd films might be attributed to adsorption of traces of impurities in the solution. The adsorption of impurities is also expected to occur on H_1-e Pd films. However, thanks to the large electroactive areas, the rate of the surface activity decline is assumed to be much slower for H_1-e Pd films than plain Pd films. In fact, a close look at the red lines in Figure 6.15 reveals a slight decrease in the hydrogen currents, which presumably shows that the loss of surface activity is taking place slowly.

In general, impurities which can adsorb upon the active centres (compounds of sulphur and arsenic, etc.) and those which can be reduced and deposit a solid upon the electrode (Pt, Ag, Cu, etc.) will clearly hinder the potentiometric response of Pd-hydride microelectrodes. A trace quantity of these impurities will settle on the electrode surface gradually and eventually cover all the active sites. When the rate of the settling is diffusion controlled (because of the extremely low concentration), the rate on microelectrodes should be higher than on conventional size electrodes, because of the quasi-hemispherical diffusion. This explains the fast loss of surface activity observed for plain Pd-hydride microelectrodes. For microelectrodes of the same radius, the time taken for the complete coverage of impurities is expected to be proportional to the roughness factor (R_F), assuming that the rate of the adsorption is diffusion controlled. From this discussion, H_1-e Pd films, which possess much greater R_F than plain Pd films by factor of 50 ~ 100, are believed to be capable of retaining the stable potential much longer, in the presence of trace quantity of impurities of these kinds in the solution.

6-3-2-(2). Fast potential determining reaction

In this section, the rate of the potential determining reaction ($H^+ + e \rightleftarrows H$ (Pd-H)) will be discussed. To compare H_1-e Pd-hydride and plain Pd-hydride films both in the $\alpha+\beta$ phase, they were loaded with hydrogen to H/Pd ratio of about 0.35 at $E_L = -0.75$ V and anodic sweep voltammograms were performed

from E_L. In this experiment, hydrogen reactions on the plain Pd film were not blocked since the voltammograms were recorded immediately after the loading procedure. Resulting anodic sweep voltammograms are shown in Figure 6.16.

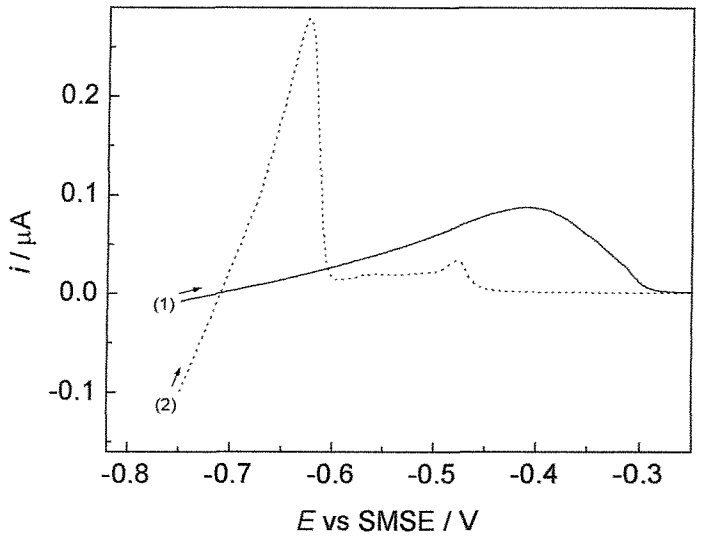

Figure 6.16. Voltammograms for the stripping of hydrogen from Pd films (Q_{Dep} = 11 μC) loaded with hydrogen. Solution : 0.5 M Na_2SO_4, 0.05 M H_2SO_4 , scan rate : 10 mV s^{-1}. The anodic scan was started immediately after the Pd films had been loaded with hydrogen at –0.75 V for t_L s to H/Pd = 0.35. (1) a plain Pd film on a Pt microdisc (d=25 μm) electrode; t_L = 180 s. (2) an H_1-e Pd (B) film on a Pt microdisc (d=25 μm) electrode; t_L = 10 s.

The H_1-e Pd-hydride showed higher currents for both absorption of hydrogen (below –0.7 V) and desorption of absorbed hydrogen (–0.7 ~ –0.6 V for H_1-e Pd-hydride, –0.7 ~ –0.3 V for plain Pd-hydride) than the plain Pd film. The voltammograms close to the equilibrium potential were enlarged and shown in Figure 6.17

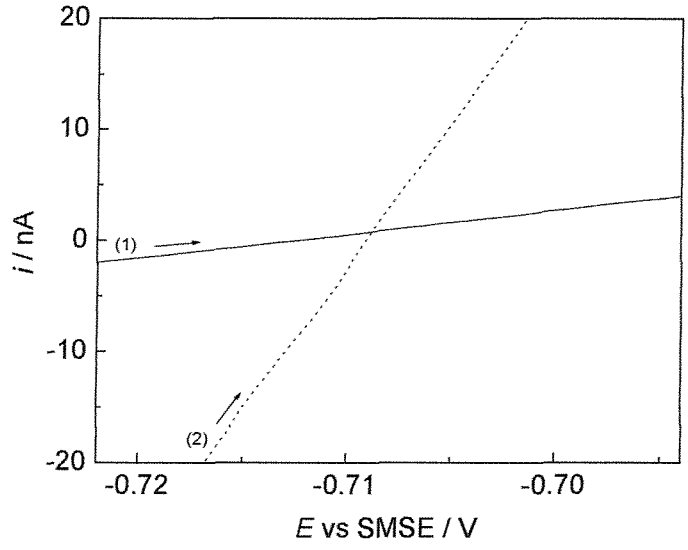

Figure 6.17. Voltammograms for Pd films (Q_{Dep} = 11 μC) loaded with hydrogen. The region near the potential where the current is zero of the voltammmogram shown in Figure 6.16 was enlarged. Experimental conditions are shown in the legend of Figure 6.16.

The slope of the current close to the equilibrium potential for the H_1-e Pd-hydride film is much larger than that for the plain Pd-hydride film, which shows that the rate of the potential determining reaction :

$$H^+ + e \rightleftarrows H\ (Pd\text{-}H) \qquad \textit{Equation 6.1}$$

is much greater on the H_1-e Pd-hydride film.

A limiting form of the Butler Volmer equation applies at very low values of the overpotential ($\eta << 2RT/nF$, ie. η < 10 mV). Assuming $\alpha_A = \alpha_C = 0.5$, the Butler Volmer equation reduces to :

$$I = I_0 \frac{nF}{RT}\eta \qquad \textit{Equation 6.2}$$

where α_A and α_C are the anodic and cathodic transfer coefficients, I is the

current density and I_0 is the exchange current density. Using this equation and the slope read from the voltammogram (Figure 6.17), the exchange current density, I_0, can be estimated. The calculated values for the H_1-e Pd (B) and plain Pd films are listed in Table 6.3, together with a result for H_1-e Pd (A) film, which was estimated from an experiment identical to that shown in Figure 6.17.

Table 6.3. Exchange current densities for $H^+ + e \rightleftarrows H$ (Pd-H) on Pd-hydride microelectrodes in 0.5 M Na_2SO_4 + 0.05 M H_2SO_4 (pH = 1.88) solutions, estimated from Equation 6.2 and the i/E slopes obtained from voltammograms.

Pd film	Substrate		Deposition of films		Experimental result	Calculated parameters	
	Material	Nominal diameter / μm	Surfactant	Charge Q_{Dep} / μC	slope i/E / 10^{-6} A V^{-1}	Exchange current i_0 / nA	Exchange current density I_0 [1] / A m^{-2}
H1-e Pd (A)	Pt	25	$C_{16}EO_8$	11	3.7	94	133
H1-e Pd (B)	Pt	25	Brij	11	2.6	67	95
Plain Pd	Pt	25	-	11	0.22	6	8

1) In the calculation of I_0, the geometric surface area was used, ie. $I_0 = i_0 / S$ ($S = \pi r^2$, $r = 15$ μm).

The estimated exchange current densities of the equilibrium (described by Equation 6.1) for H_1-e Pd (A) and H_1-e Pd (B) films are greater than that for the plain Pd film by a factor of about 11 and 16, respectively. This high exchange current density (high rate of the potential determining reaction) is a significant advantage in terms of the potentiometric response of Pd-hydride microelectrodes for several aspects considered below.

(a) Influence of impurities (oxidizing species)

The oxidizing agents which are reduced at the electrode but do not deposit a solid on the electrode (e.g. gaseous oxygen, Fe^{3+}, CrO_4^{2-} etc) can potentially shift the potential positively. Generally, the rate of electrode reactions of traces of impurities (oxidizing species) on Pd-hydride microelectrodes is expected to be controlled by the diffusion of the species to the surface of the electrodes. If the

exchange current density for the potential determining equilibrium is much greater than the rate of the electrode reaction of an impurity (in most case diffusion limited) in terms of the current, the influence of the impurity on the potential can be minimized. Hence, the potential of H_I-e Pd films is expected to be much less sensitive to oxidizing impurities.

(b) Influence of input bias current

In potentiometric measurements, an input bias current (or leakage current) flows through the circuit, whose magnitude depends on the potential measuring apparatus. In the case of microelectrodes, the potential value is very sensitive to the bias current, since even a few pA correspond to a significant Faradaic process. Moreover, any other current driven through the potential measurement circuit (e.g. electrical noise) can also affect the potential. Thanks to the large exchange current density, the influence of the bias current on the potential is expected to be much smaller for H_I-e Pd-hydride microelectrodes than for plain Pd microelectrodes.

(c) Rapid establishment of the equilibrium

With high rate of the potential determining reaction, it can be expected that the potential of Pd-hydride attains its thermodynamic equilibrium value rapidly[1, 3, 59]. If the rate of the potential determining reaction is sluggish, establishing the desired potential cannot be guaranteed.

According to the three aspects discussed above, the high rate of the potential determining reaction (high exchange current density) is believed to contribute to the stability, reproducibility, accuracy (theoretical response) and short response time of the potentiometric response of H_I-e Pd hydride microelectrodes.

6-4. Summary

Overview

In Chapter 4, it was found that H_I-e Pd films on Pt microdisc can be loaded with hydrogen quickly (~ 1 min) and that the H/Pd ratio can be controlled by varying the loading potential and the loading time. In Chapter 5, the potentiometric response of H_I-e Pd-hydride films was found to be rapid, stable, reproducible and almost theoretical in solutions not containing oxidizing species. The contribution of the nanostructure to the excellent properties was discussed by comparing the experimental results for H_I-e Pd films with those for Pd microelectrodes without the nanostructure (plain Pd films and polished Pd microdiscs).

Plain Pd films on Pt microdisc

From the cyclic voltammetry, the current corresponding to hydrogen absorption was much smaller than that of H_I-e Pd films. Accordingly, to load the Pd films with hydrogen to the desired H/Pd ratio (near β phase region) potentiostatically, a more negative E_L and / or a longer t_L was needed for plain Pd films than H_I-e Pd films.

When in the α+β phase, plain Pd-hydride films showed the potential close to the plateau potential for the α+β phase observed for H_I-e Pd-hydride films. However, the potential is not very stable, where an appreciable slope is observed. Furthermore, the plateau (with a slight slope) was much shorter than the stable plateau observed for H_I-e Pd-hydride films. This was found to be caused by a surface blockage occurring under the open circuit condition. Owing to the surface blockage, the rate of potential determining reaction is believed to be extremely slow at the end of the plateau. The cause of the surface blockage is not clear. One possibility is adsorption of traces of poisoning impurities, although adsorbates have not been identified. The surface activity of plain Pd films was recovered by scanning the potential to the surface oxide region.

Polished Pd microdisc

As expected, polished Pd microdisc electrodes showed behaviour similar to plain Pd films, ie. slower hydrogen absorption rate than H_I-e Pd films and automatic

loss of surface activity. In conjunction with the diffusion of absorbed hydrogen from the surface to the bulk of the microwires, it was even more difficult to achieve the stable potential for α+β phase than with plain Pd microdisc electrodes.

Difficulty in attaining stable potential using Pd-hydride microelectrodes

From the results for plain Pd films and polished Pd microelectrodes, it was found to be difficult to produce the stable potential corresponding to the α+β phase using microelectrodes. The reason for this was thought to be a gradual loss of surface activity due to: (1) fast diffusion of traces of adsorbable impurities and (2) small initial active surface area. When the adsorption rate of traces of adsorbable impurities is diffusion controlled, the adsorption is expected to proceed faster than with conventional size electrodes, which can reduce the electroactive areas and hence the rate (exchange current density) of the potential determining reaction. When the exchange current density decreases, the potential of Pd microelectrodes can drift towards anodic values rather readily because of the potentially small active surface area and the fast diffusion of oxidizing impurities to the microelectrodes.

Advantage of the nanostructure

In the case of H_I-e Pd films, the rate of cathodic absorption of hydrogen was much greater than with Pd electrodes without the nanostructure. This can be explained by the fast diffusion of hydrogen through the lattice. Hence, a much shorter loading time (< 1 min) is necessary to load H_I-e Pd films with hydrogen to the desired H/Pd ratios, which makes it possible to conduct a series of experiments consecutively with a few minute intervals for the hydrogen charging.

The adsorption rate of traces of impurities is expected to be controlled by diffusion in the most cases (because of the extremely low concentration), which is fast in the case of microelectrodes. This is presumably the main reason why Pd microelectrodes lost their surface activity quite soon (30 ~ 45 min). H_I-e Pd films, which possess much greater R_F than plain Pd films by a factor of 50 ~ 100, are believed to be capable of retaining the stable potential much longer. This lower sensitivity to the adsorption of impurities is believed to contribute to the

stability, reproducibility and accuracy of the potentiometric response of H_I-e Pd-hydride microelectrodes.

The rate of the potential determining reaction was found to be much faster on H_I-e Pd films than on Pd microelectrodes without the nanostructure. The estimated exchange current density was larger for H_I-e Pd films by a factor of 11 ~ 16. The high rate of the potential determining reaction is believed to contribute to the stability, reproducibility, accuracy (theoretical response) and short response time of the potentiometric response of H_I-e Pd-hydride microelectrodes by : (1) reduced influence of oxidizing impurities and input bias current resulting from the high exchange current density and (2) rapid establishment of the equilibrium.

Chapter 7. Conclusions and further work

7-1. Conclusions

There have been no practical and reliable micro pH sensors with a wide pH range, although a number of microsensors to measure local pH have been studied. The extremely small size of microelectrodes is clearly a disadvantage in obtaining a stable and reproducible potential, especially in the case of potentiometric sensors.

The α+β Pd-hydride phase has been known to show almost theoretical potential dependance on pH. However, this has not been applied to microelectrodes, probably because of the difficulty in loading hydrogen into the electrodes. In the present study, taking advantage of the stable and reproducible potential of α+β phase, an attempt was made to fabricate Pd-hydride micro pH sensors for the first time.

Aiming for truly reliable potentiometric response, nanostructured films (H_1-e Pd films) were employed in the present study. H_1 nanostructured films had been shown to possess massive surface areas and good catalytic activity. Hence the potential determining process was expected to be rapid (high exchange current density) when H_1 nanostructured films were applied to the potentiometric sensors.

To overcome the difficulty in loading hydrogen into Pd microelectrodes, we deposited H_1-e Pd films on Pt (not Pd) microdisc electrodes. In this way, it was possible to prevent hydrogen from diffusing deep into the bulk of the microwire.

The main goal of this research was to fabricate reliable potentiometric pH sensors with a wide effective pH range, taking advantage of the properties of the α+β Pd-hydride phase and the H_1 nanostructure.

H_1-e Pd films were electrodeposited on Pt microdisc electrodes from plating mixtures containing non-ionic surfactants. The roughness factors of H_1-e Pd films were estimated to be typically 300 from the oxide stripping peak of cyclic voltammograms in 1 M H_2SO_4. The hydrogen absorption behaviour of H_1-e Pd films was studied in detail chiefly in solutions with pH ≈ 2. Hydrogen

absorption was shown to be very fast for H_I-e Pd films and the films were readily loaded with hydrogen to form the β phase. A potentiostatic hydrogen loading procedure for H_I-e Pd films was established, where the H/Pd ratio of the film can be controlled by varying the loading potential and the loading time. Preliminary results indicate that rapid loading of hydrogen is also possible in solutions with higher pHs.

The prepared H_I-e Pd-hydride microelectrodes showed excellent potentiometric response over a wide range of pH (2 ~ 12). The potentiometric pH response was rapid, stable, reproducible and almost theoretical in deaerated solutions. The excellent potentiometric response is thought to arise from the very fast potential determining process ($H^+ + e \rightleftarrows H(Pd\text{-}H)$) on H_I-e Pd films. The estimated exchange current density for an H_I-e Pd film was larger than that for a plain Pd film by a factor of 11 ~ 16. This fast potential determining process is believed to contribute to the stability, reproducibility, accuracy and short response time of the potentiometric response by; (1) reducing the influence of traces of oxidizing impurities and that of any kind of input bias current including electrical noise and (2) rapidly establishing the equilibrium. In addition, the massive electroactive area (roughness factor) may contribute to reducing the effect of traces of adsorbable impurities.
The H_I-e Pd-hydride microelectrodes show such a reproducible potentiometric response that once a calibration is performed, it is possible to conduct pH measurements without calibration before and/or after the pH measurements, a procedure normally essential for potentiometric micro pH sensors.

The main drawback of H_I-e Pd-hydride microelectrodes is their limited lifetime. The longest lifetime, without causing significant enlargement of the diameter, was 2 ~ 3 hours for d = 25 μm electrodes (Q_{Dep} = 22 μC) in deaerated solutions. This is sufficient for many analytical experiments, although too short for continuous process monitoring. In aerated solutions, the lifetime of the H_I-e Pd-hydride microelectrodes was very short (e.g. about 3 min for H_I-e Pd films with Q_{Dep} = 11 μC, d = 25 μm) because of the oxidation of sorbed hydrogen by dissolved oxygen.

From the merits and demerits discussed above, H_1-e Pd-hydride microelectrodes can be a very powerful pH probes in SECM experiments. When used as an SECM tip for mapping pH distribution near a substrate, H_1-e Pd-hydride microelectrodes are believed to possess further advantages;

(a) The electrode can be reloaded with hydrogen quickly, which makes it possible to perform an SECM experiment repeatedly.
(b) The response time is short (confirmed to be < 1 s),
(c) Absolute tip-substrate distance determination is possible by recording an experimental approach curve (e.g. oxygen reduction) before loading hydrogen.
(d) The tip does not affect the concentration profile of the species generated or consumed at the substrate, since it is a passive sensor.

Below is an example of the procedure for applying H_1-e Pd-hydride microelectrodes to SECM experiments using a test solution in which the hydrogen absorption behaviour of the H_1-e pd films is unknown.

(1) Preparation of a Pt microdisc electrode.
(2) Deposition of an H_1-e Pd films on the Pt microdisc.
(3) Acid cleaning of the H_1-e Pd film (e.g. –0.65 V ↔ +0.70 V vs SMSE, in 1 M H_2SO_4)
(4) Optimization of hydrogen loading conditions (potential, time) in a solution with the same composition as the test solution.
(5) Hydrogen loading into the H_1-e Pd film in a solution with the same composition as the test solution.
(6) Potential-pH calibration in the test solution.
(7) SECM experiment (Figure 7.1). It is important to note that the test solution for SECM experiments should not contain oxidizing species and has to be deaerated before the loading procedure.

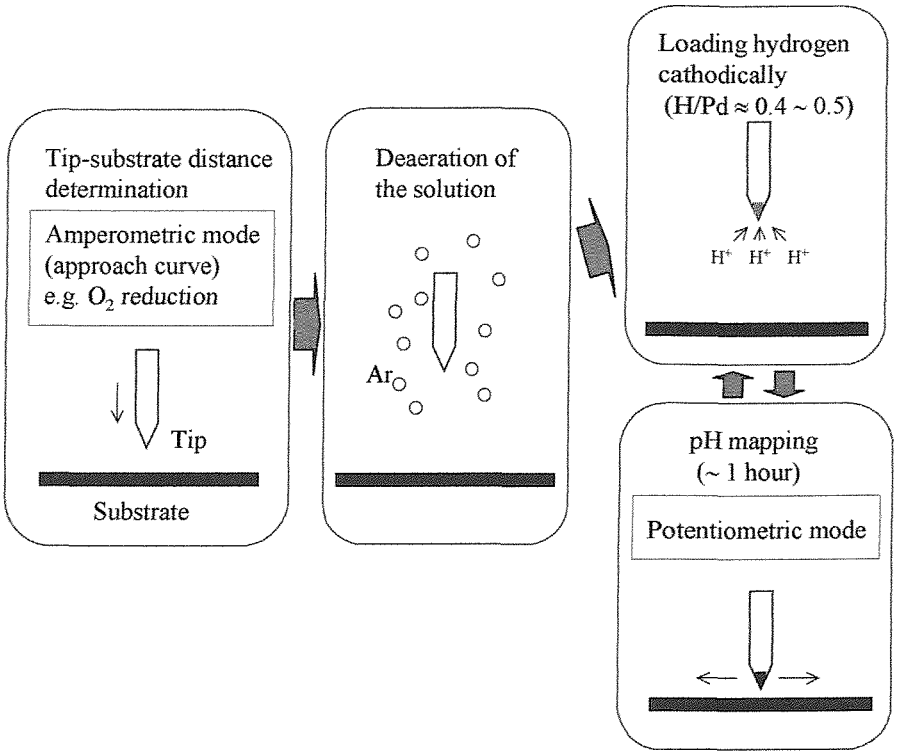

Figure 7.1. An example of application of H_1-e Pd-hydride microelectrodes to SECM experiments.

7-2. Further work

In aerated solutions, the lifetime of H_1-e Pd-hydride microelectrodes was very short, because of the presence of oxygen. Similar effect is expected with any oxidizing species. The field to which this sensor is applicable will be widened substantially if we can lengthen the lifetime in aerated solutions. One possible solution is recessing the Pt microdisc electrodes before H_1-e Pd film deposition. Well established procedures for etching Pt microdisc electrodes have been reported[122, 123]. It is believed to be possible to increase the thickness of the H_1-e Pd layer without enlarging the diameter. To achieve the lifetime of 1hour in aerated solutions, the minimum thickness is expected to be around 10 μm for d= 25 μm electrodes.

Another possible solution to lengthen the lifetime in the presence of oxidizing species is to coat a protective film over the H_I-e Pd film. By the use of proton permeable film, the potentiometric pH response is expected to remain. In fact, several workers coated potentiometric micro pH sensors (W / WOx[37], Ir / IrOx[35]) with Nafion resin to resist attacks of coexisting species in the solution. It is of course essential to retain the possibility of loading hydrogen through the protective film.

In the discussion up to now, typical SECM experiments ($\approx$ 1 hour) have been the main target. By taking a completely different approach, it can be possible to widen the application of H_I-e Pd-hydride electrodes further. Since hydrogen absorption is very rapid for H_I-e Pd films, it is expected to be possible to reload the films in situ more frequently. The H_I-e Pd-hydride electrodes will show the stable potential of the $\alpha+\beta$ phase as long as the H/Pd ratio is kept in the range 0.1 ~ 0.5. If we can keep the H/Pd ratio in this range by in situ frequent reloading, a continuous pH measurement will be possible. This approach may lead to the applicability of H_I-e Pd-hydride electrodes to solutions containing oxidizing species (including aerated solutions).

Another interesting topic for further work is the application of H_I nanostructured films to other potentiometric microsensors (e.g. metal / metal oxide). In general, the potentiometric response is worse for microelectrodes than for conventional size electrodes. Because of their massive surface areas, H_I nanostructured films are expected to show behaviour similar to conventional size electrodes. Furthermore, from the results obtained in the present study, the influence of traces of adsorbable impurities can be reduced, compared to microelectrodes without the nanostructure. In fact, in our preliminary study an H_I-e Pt / PtOx microelectrode showed much more stable potentials than a Pt / PtOx microelectrode without the nanostructure.
This study can be started with Pd / PdOx, since the deposition procedure of H_I-e Pd films is already established, and they can be oxidized by applying a combination of ac + dc potentials in sulphuric acid solutions[43]. On the other hand, the deposition methods for Sb[21] and IrOx[35] from aqueous media have been reported. Hence, it is expected to be possible to form H_I-e Sb or H_I-e IrOx films.

For these two films, further treatment (e.g. oxidation) is not necessary. Performing this study may also give some further information on the role of the nanostructure in achieving the good potentiometric response.

Chapter 8. References

(1) Ives, D.; Janz.G *Reference Electrodes*; Academic Press, Inc.: New York, 1961.

(2) Bates, R. G. *Determination of pH, Theory and practice*; John Wiley and Sons: New York, 1964.

(3) Compton, R. G.; Sanders, H. W. *Electrode Potentials*; Oxford University Press: Oxford, 1996.

(4) Yang, Y. F.; Denuault, G. *Journal of the Chemical Society-Faraday Transactions* **1996**, *92*, 3791-3798.

(5) Ciszkowska, M.; Stojek, Z.; Morris, S. E.; Osteryoung, J. G. *Analytical Chemistry* **1992**, *64*, 2372-2377.

(6) Frank, M. H. T.; Denuault, G. *Journal of Electroanalytical Chemistry* **1993**, *354*, 331.

(7) Frank, M. H. T.; Denuault, G. *Journal of Electroanalytical Chemistry* **1994**, *379*, 399-406.

(8) Baldo, M. A.; Daniele, S.; Mazzocchin, G. A. *Anal.Chim.Acta* **1993**, *272*, 191.

(9) Perdicakis, M.; Piatnicki, C.; Sadik, M.; Pasturaud, R.; Benzakour, B.; Bessiere, J. *Anal.Chim.Acta* **1993**, *273*, 81.

(10) Ciszkowska, M.; Stojek, Z.; Osteryoung, J. G. *Journal of Electroanalytical Chemistry* **1995**, *398*, 49.

(11) Abdelsalam, M. E.; Denuault, G.; Baldo, M. A.; Daniele, S. *Journal of Electroanalytical Chemistry* **1998**, *449*, 5-7.

(12) Abdelsalam, M. E.; Denuault, G.; Baldo, M. A.; Bragato, C.; Daniele, S. *Electroanalysis* **2001**, *13*, 289-294.

(13) Daniele, S.; Baldo, M. A.; Bragato, C.; Denuault, G.; Abdelsalam, M. E. *Analytical Chemistry* **1999**, *71*, 811-818.

(14) Thomas, R. C. *Ion-selective Intercellular Microelectrodes*; Academic Press, 1978.

(15) Klusmann, E.; Schultze, J. W. *Electrochimica Acta* **1997**, *42*, 3123-3134.

(16) Park, J. O.; Paik, C. H.; Alkire, R. C. *Journal of the Electrochemical Society* **1996**, *143*, L174-L176.

(17) Ogle, K.; Baudu, V.; Garrigues, L.; Philippe, X. *Journal of the Electrochemical Society* **2000**, *147*, 3654-3660.

(18) Ammann, D. *Ion-Selective microelectrodes*; Springer-Verlag, 1986.

(19) Murase, K.; Honda, T.; Hirato, T.; Awakura, Y. *Metallurgical and Materials Transactions B-Process Metallurgy and Materials Processing Science* **1998**, *29*, 1193-1198.

(20) Honda, T.; Murase, K.; Hirato, T.; Awakura, Y. *Journal of Applied Electrochemistry* **1998**, *28*, 617-622.

(21) Tsuru, Y.; Yamabe, K.; Hosokawa, K. *Hyoumen Gijutsu* **1989**, *40*, 345.

(22) Horrocks, B. R.; Mirkin, M. V.; Pierce, D. T.; Bard, A. J.; Nagy, G.; Toth, K. *Analytical Chemistry* **1993**, *65*, 1213-1224.

(23) Toth, K.; Nagy, G.; Horrocks, B. R.; Bard, A. J. *Analytica Chimica Acta* **1993**, *282*, 239-246.

(24) Remis, D.; Bulychev, A. A.; Kurella, G. A. *Biochimica Et Biophysica Acta* **1986**, *852*, 68-73.

(25) Toth, K.; Nagy, G.; Wei, C.; Bard, A. J. *Electroanalysis* **1995**, *7*, 801-810.

(26) Matulis, J.; Slizys, R. *Electrochimica Acta* **1964**, *9*, 1177.

(27) Higashi, K.; Fukushima, H.; Urakawa, T.; Adaniya, T. *Journal of the Electrochemical Society* **1981**, *128*, 2081.

(28) Lin, L.; Ohgai, T.; Akiyama, T.; Fukushima, H.; Yamauchi, Y. *Hyoumen Gijutsu* **1996**, *47*, 869.

(29) Noguchi, H.; Kotani, I.; Hashiba, H.; Suzuki, T. *Kinzoku Hyoumen Gijutsu* **1985**, *36*, 58.

(30) Antonenko, Y.; Bulychev, A. *Biochimica et Biophysica Acta* **1991**, *1070*, 474.

(31) Ogata, Y.; Uchiyama, S.; Hayashi, M.; Yasuda, M.; Hine, F. *Journal of Applied Electrochemistry* **1990**, *20*, 555-558.

(32) Vanhoudt, P.; Lewandowski, Z.; Little, B. *Biotechnology and Bioengineering* **1992**, *40*, 601-608.

(33) Tanabe, H.; Togashi, H.; Misawa, T.; Mudali, U. K. *Journal of Materials Science Letters* **1998**, *17*, 551.

(34) Wipf, D. O.; Ge, F. Y.; Spaine, T. W.; Bauer, J. E. *Analytical Chemistry* **2000**, *72*, 4921-4927.

(35) Bezbaruah, A. N.; Zhang, T. C. *Analytical Chemistry* **2002**, *74*, 5726-5733.

(36) Luo, J. L.; Lu, Y. C.; Ives, M. B. *Journal of Electroanalytical Chemistry* **1992**, *326*, 51-68.

(37) Yamamoto, K.; Shi, G.; Zhou, T.; Xu, F.; Zhu, M.; Liu, M.; Kato, T.; Jin, J.; Jin, L. *Analytica Chimica Acta* **2003**, *480*, 109-117.

(38) Liu, C. C.; Bocchicchio, B. C.; Overmyer, P. A.; Neuman, M. R. *Science*

1980, *207*, 188-189.

(39) Kim, J. Y.; Lee, Y. H. *Biotechnology and Bioengineering* **1989**, *34*, 131-136.

(40) Grubb, W. T.; King, L. H. *Analytical Chemistry* **1980**, *52*, 270-273.

(41) Kinoshita, E.; Ingman, F.; Edwall, G.; Thulin, S.; Glab, S. *Talanta* **1986**, *33*, 125-134.

(42) Kinoshita, E.; Ingman, F.; Edwall, G.; Glab, S. *Electrochimica Acta* **1986**, *31*, 29-38.

(43) Bloor, L. J.; Malcolmelawes, D. J. *Journal of Electroanalytical Chemistry* **1990**, *278*, 161-173.

(44) Graham, T. **1866**, *156*, 415.

(45) Lewis, F. *The palladium hydrogen system*; Academic Press: London, 1967.

(46) Lewis, F. A. **1995**, *20*, 587-592.

(47) Aben, P. C.; Burgers, W. G. *Trans. Faraday Soc.* **1962**, *58*, 1989-1992.

(48) Schuldiner, S.; Castellan, G. W.; Hoare, J. P. *The Journal of Chemical Physics* **1958**, *28*, 16-19.

(49) Hoare, J. P.; Schuldiner, S. *Journal of Physycal Chemistry* **1957**, *61*, 399-402.

(50) Flanagan, T. B.; Lewis, F. A. *Trans. Faraday Soc.* **1959**, *55*, 1409-1420.

(51) Flanagan, T. B.; Lewis, F. A. *Trans. Faraday Soc.* **1959**, *55*, 1400.

(52) Vasile, M. J.; Enke, C. G. *Journal of the Electrochemical Society* **1965**, *112*, 865-870.

(53) Macdonald, D. D.; Wentrcek, P. R.; Scott, A. C. *Journal of the Electrochemical Society* **1980**, *127*, 1745-1751.

(54) Bucur, R. V.; Stoicovici, L. *Journal of Electroanalytical Chemistry* **1966**, *11*, 152-154.

(55) Fleischmann, M.; Hiddleston, J. N. *Journal of Scientific Instruments* **1968**, *1*, 667-668.

(56) Dobson, J. V. *Journal of Electroanalytical Chemistry* **1972**, *35*, 129-135.

(57) Dobson, J. V.; Chapman, B. R.; Thirsk, H. R. In *HIGH TEMPERATURE, HIGH PRESSURE ELECTROCHEMISTRY IN AQUEOUS SOLUTIONS*; NACE PUBLICATION, 1976, pp 341-351.

(58) Goffe, R. A.; Tseung, A. C. *Medical & Biological Engineering & Computing* **1978**, *16*, 670-676.

(59) Tseung, A. C.; Goffe, R. A. *Medical & Biological Engineering & Computing* **1978**, *16*, 677-680.

(60) Kelly, J. F. D.; Goffe, R. A.; Tseung, A. C. *Medical & Biological*

Engineering & Computing **1981**, *19*, 333-339.

(61) Schwing, J. P.; Rogers, L. B. *Analytica Chimica Acta* **1956**, *15*, 379-388.

(62) Stock, J. T.; Purdy, W. C.; Williams, T. R. *Analytica Chimica Acta* **1959**, *20*, 73-78.

(63) Liteanu, C.; Haiduc, I. *Revue Roumaine de Chimie* **1970**, *15*, 1555-1561.

(64) Jasinski, R. *Journal of the Electrochemical Society* **1974**, *121*, 1579-1584.

(65) Kelly, J. F. D.; Goffe, R. A.; Tseung, A. C. C. *Medical & Biological Engineering & Computing* **1981**, *19*, 333-339.

(66) Tsuruta, T.; Macdonald, D. D. *Journal of the Electrochemical Society* **1981**, *128*, 1199-1203.

(67) Kihara, S.; Yoshida, Z.; Matsui, M. *Bull. Inst. Chem. Res., Kyoto Univ.* **1986**, *4*, 207-217.

(68) Dobson, J. V.; Brims, G. *Electrochimica Acta* **1987**, *32*, 149-153.

(69) Graham, T., *Proc. R. Soc.* **1868**, 422.

(70) Zhang, W. S.; Zhang, X. W.; Li, H. Q. *Journal of Electroanalytical Chemistry* **1997**, *434*, 31-36.

(71) Mengoli, G.; Bernardini, M.; Fabrizio, M.; Manduchi, C.; Zannoni, G. *Journal of Electroanalytical Chemistry* **1996**, *403*, 143-151.

(72) Lim, C.; Pyun, S. I. *Electrochimica Acta* **1994**, *39*, 363-373.

(73) Baldauf, M.; Kolb, D. M. *Electrochimica Acta* **1993**, *38*, 2145-2153.

(74) Takasu, Y.; Enami, E.; Matsuda, Y. *Chemistry Letters* **1986**, 1735-1738.

(75) Tateishi, N.; Yahikozawa, K.; Nishimura, K.; Suzuki, M.; Iwanaga, Y.; Watanabe, M.; Enami, E.; Matsuda, Y.; Takasu, Y. *Electrochimica Acta* **1991**, *36*, 1235-1240.

(76) Tateishi, N.; Yahikozawa, K.; Nishimura, K.; Takasu, Y. *Electrochimica Acta* **1992**, *37*, 2427-2432.

(77) Breiter, M. W. *Journal of Electroanalytical Chemistry* **1980**, *109*, 253-260.

(78) Conway, B. E.; Jerkiewicz, G. *Journal of Electroanalytical Chemistry* **1993**, *357*, 47-66.

(79) Bucur, R. V.; Bota, F. *Electrochimica Acta* **1982**, *27*, 521.

(80) Czerwinski, A.; Zamponi, S.; Marassi, R. *Journal of Electroanalytical Chemistry* **1991**, *304*, 233-239.

(81) Czerwinski, A.; Marassi, R.; Zamponi, S. *Journal of Electroanalytical Chemistry* **1991**, *316*, 211-221.

(82) Czerwinski, A.; Marassi, R. *Journal of Electroanalytical Chemistry* **1992**, *322*, 373-381.

(83) Czerwinski, A.; Maruszczak, G.; Zelazowska, M.; Lancucka, M.; Marassi, R.; Zamponi, S. *Journal of Electroanalytical Chemistry* **1995**, *386*, 207-211.

(84) Czerwinski, A.; Czauderna, M.; Maruszczak, G.; Kiersztyn, I.; Marassi, R.; Zamponi, S. *Electrochimica Acta* **1997**, *42*, 81-86.

(85) Czerwinski, A.; Kiersztyn, I.; Grden, M.; Czapla, J. *Journal of Electroanalytical Chemistry* **1999**, *471*, 190-195.

(86) Czerwinski, A.; Kiersztyn, I.; Grden, M. *Journal of Electroanalytical Chemistry* **2000**, *492*, 128-136.

(87) Czerwinski, A.; Kiersztyn, I.; Grden, M. *Journal of Solid State Electrochemistry* **2003**, *7*, 321-326.

(88) Szpak, S.; Mosierboss, P. A.; Gabriel, C. J.; Smith, J. J. *Journal of Electroanalytical Chemistry* **1994**, *365*, 275-281.

(89) Zhang, W. S.; Zhang, X. W.; Zhao, X. G. *Journal of Electroanalytical Chemistry* **1998**, *458*, 107-112.

(90) Attard, G. S.; Glyde, J. C.; Goltner, C. G. *Nature* **1995**, *378*, 366.

(91) Attard, G. S.; Bartlett, P. N.; Coleman, N. R. B.; Elliott, J. M.; Owen, J. R.; Wang, J. H. *Science* **1997**, *278*, 838-840.

(92) Attard, G. S.; Coleman, N. R. B.; Elliott, J. M. In *Mesoporous Molecular Sieves 1998*, 1998; Vol. 117, pp 89-94.

(93) Bartlett, P. N.; Birkin, P. N.; Ghanem, M. A.; de Groot, P.; Sawicki, M. *Journal of the Electrochemical Society* **2001**, *148*, C119-C123.

(94) Whitehead, A. H.; Elliott, J. M.; Owen, J. R. *Journal of Power Sources* **1999**, *82*, 33-38.

(95) Whitehead, A. H.; Elliott, J. M.; Owen, J. R.; Attard, G. S. *Chemical Communications* **1999**, 331-332.

(96) Attard, G. S.; Leclerc, S. A. A.; Maniguet, S.; Russell, A. E.; Nandhakumar, I.; Bartlett, P. N. *Chemistry of Materials* **2001**, *13*, 1444-+.

(97) Guerin, S.; Attard, G. S. *Electrochemistry Communications* **2001**, *3*, 544-548.

(98) Nelson, P. A.; Elliott, J. M.; Attard, G. S.; Owen, J. R. *Journal of New Materials for Electrochemical Systems* **2002**, *5*, 63-65.

(99) Nelson, P. A.; Elliott, J. M.; Attard, G. S.; Owen, J. R. *Chemistry of Materials* **2002**, *14*, 524-529.

(100) Guerin, S. PhD thesis, University of Southampton, 1999.

(101) Bartlett, P. N.; Gollas, B.; Guerin, S.; Marwan, J. *Physical Chemistry Chemical Physics* **2002**, *4*, 3835-3842

(102) Marwan, J. PhD thesis, University of Southampton, 2003.

(103) Nandhakumar, I.; Elliott, J. M.; Attard, G. S. *Chemistry of Materials* **2001**, *13*, 3840.

(104) Elliott, J. M.; Cabuche, L. M.; Bartlett, P. N. *Analytical Chemistry* **2001**, *73*, 2855-2861.

(105) Elliott, J. M.; Birkin, P. R.; Bartlett, P. N.; Attard, G. S. *Langmuir* **1999**, *15*, 7411-7415.

(106) Birkin, P. R.; Elliott, J. M.; Watson, Y. E. *Chemical Communications* **2000**, 1693-1694.

(107) Evans, S. A. G.; Elliott, J. M.; Andrews, L. M.; Bartlett, P. N.; Doyle, P. J.; Denuault, G. *Analytical Chemistry* **2002**, *74*, 1322-1326.

(108) Evans, S. A. G. PhD thesis, University of Southampton, 2002.

(109) Bartlett, P. N. In *Biosensors: A practical Approach*; Oxford University Press, 1990, pp 47.

(110) Denuault, G. *Chem. Ind.* **1996**, *18*, 678.

(111) Mitchell, D. J.; Tiddy, G. J. T.; Waring, L.; Bostock, T.; McDonald, M. P. *Journal of the Chemical Society., Faraday Trans. 1* **1983**, *79*, 975.

(112) Rand, D. A. J.; Woods, R. *Electroanalytical Chemistry* **1972**, *35*, 209-218.

(113) Burke, L. D.; Casey, J. K. *Journal of the Electrochemical Society* **1993**, *140*, 1284.

(114) Rand, D. A. J.; Woods, R. *Electroanalytical Chemistry* **1971**, *31*, 29-38.

(115) Brummer, S. B. *Journal of Physical Chemistry* **1965**, *69*, 562.

(116) Pyo, M.; Bard, A. J. *Electrochimica Acta* **1997**, *42*, 3077-3083.

(117) Lang, G.; Ujvari, M.; Horanyi, G. *Corosion Science* **2003**, *45*, 1-5.

(118) Horanyi, G.; Bakos, I. *Journal of Electroanalytical Chemistry* **1992**, *331*, 727-737.

(119) Bakos, I.; Horanyi, G. *Journal of Electroanalytical Chemistry* **1993**, *347*, 383-391.

(120) Horanyi, G.; Bakos, I. *Models in Chemistry* **1994**, *131*, 25-41.

(121) Mills, R.; Lobo, V. M. M. *Self Diffusion in Electrolyte Solutions, a Critical Examination of Data Compiled from the Literature, Physical Sciences Data*; Elsevier: Amsterdam, 1989.

(122) Liu, H. Y.; Fan, F. R. F.; Lin, C. W.; Bard, A. J. *Journal of the American Chemical Society* **1986**, *108*, 3838.

(123) Gewirth, A. A.; Crasto, D. H.; Bard, A. J. *Journal of Electroanalytical Chemistry* **1989**, *261*, 477.

(124) Lingane, J. J. *Electroanalytical Chemistry*; Wiley-Interscience: New York,

1958.

(125) Bard, A. J.; Faulkner, L. R. *Electrochemical Methods 2nd edition*; John Wiley & Sons: New York, 2001.

(126) Lobo, V. M. M. *Handbook of Electrolyte Solutions*; Elsevier, 1989.

(127) Bard, A. J.; Mirkin, M. V. *Scanning Electrochemical Microscopy*; Marcel Dekker: New York, 2001.

(128) Vracar, L. M.; Sepa, D. B. *Journal of the Electrochemical Society* **1987**, *134*, 1695-1697.

(129) Naohara, H.; Ye, S.; Uosaki, K. *Electrochimica Acta* **2000**, *45*, 3305-3309.

(130) Climent, V.; Markovic, N. M.; Ross, P. N. *Journal of Physical Chemistry* **2000**, *104*, 3116-3120.

(131) Pletcher, D.; Sotiropoulos, S. *Journal of Electroanalytical Chemistry* **1993**, *356*, 109-119.

(132) Lingane, J. J. *Journal of Electroanalytical Chemistry* **1961**, *2*, 296-309.

(133) Woods, R. *Chemisorption at electrodes*; Marcel Dekker inc.: New York, 1976.

(134) Barton, J. C.; Leitch, W. F. N.; Lewis, F. A. *Trans. Faraday Soc.* **1963**, *59*, 1208-1217.